Int. J. Electrochem. Sci., 6 **(2011)** 5830 - 5917

International Journal of ELECTROCHEMICAL SCIENCE
www.electrochemsci.org

Paving the Way to The Integration of Smart Nanostructures: Part II: Nanostructured Microdispersed Hydrated Metal Oxides for Electrochemical Energy Conversion and Storage Applications

Serge Rebouillat[1], *Michael E.G. Lyons*[2,*], *Michael P. Brandon*[2], *Richard L. Doyle*[2]

[1] DuPont International S.A., 2 Chemin du Pavillon, CH1218 Le Grand Saconnex, Geneva, Switzerland
[2] Physical and Materials Electrochemistry Laboratory, School of Chemistry, University of Dublin, Trinity College, Dublin 2, Ireland.
[*]E-mail: melyons@tcd.ie

Received: 25 August 2011 / *Accepted:* 2 October 2011 / *Published:* 1 November 2011

The use of hydrogen gas produced by the electrolysis of water is the basis of a long term energy conversion and storage option that has been and still continues to be the subject of considerable research. Alkaline water electrolysis, using electricity generated by renewable sources has been proposed as an environmentally inoffensive route to the production of the large volumes of hydrogen gas required by a possible hydrogen economy. The electrochemistry of oxygen has proved to be of perennial interest both from a fundamental and an applied perspective, especially in the important areas of energy conversion and storage. Despite the recent renewal in interest in the oxygen evolution reaction (OER) at transition metal oxide based electrodes in alkaline solution, the details of the mechanism remain controversial. In the present extended essay, the redox, charge storage and electrocatalytic behavior with respect to the OER of oxidized Ni, Fe and Co oxides in alkaline solution is discussed, the acid/base properties of the oxide is emphasized, and a plausible general reaction pathway involving the rate determining formation of a superoxy (-OOH) intermediate is proposed.

Keywords: oxygen evolution electrocatalysis, oxidized iron, nickel and cobalt electrodes, transition metal electrochemistry, oxygen evolution mechanisms

1. INTRODUCTION

Electrochemical science is a venerable discipline drawing its roots and inspiration from the work of Faraday. Yet the subject also forms the scientific basis for a feasible solution to the major issue of cheap sustainable energy production underpinning the future sustainability of 21st century

life. The quest for sustainable energy production has been described as the 'moonshot for our generation'. Electrochemical science provides the basis for the so called hydrogen economy which involves the production of molecular hydrogen from non fossil sources, its distribution and storage, and its cold combustion in a fuel cell to generate electricity (see figure 1). The use of hydrogen gas produced by the electrolysis of water is the basis of a long term energy conversion and storage option that has been and still continues to be the subject of considerable research and development, albeit occuring in fits and starts depending on current research funding priorities, fashions and directions. Alkaline water electrolysis, using electricity generated by renewable sources has been proposed as an environmentally inoffensive route to the production of the large volumes of hydrogen gas required by a possible hydrogen economy [1] as illustrated in figure 1.

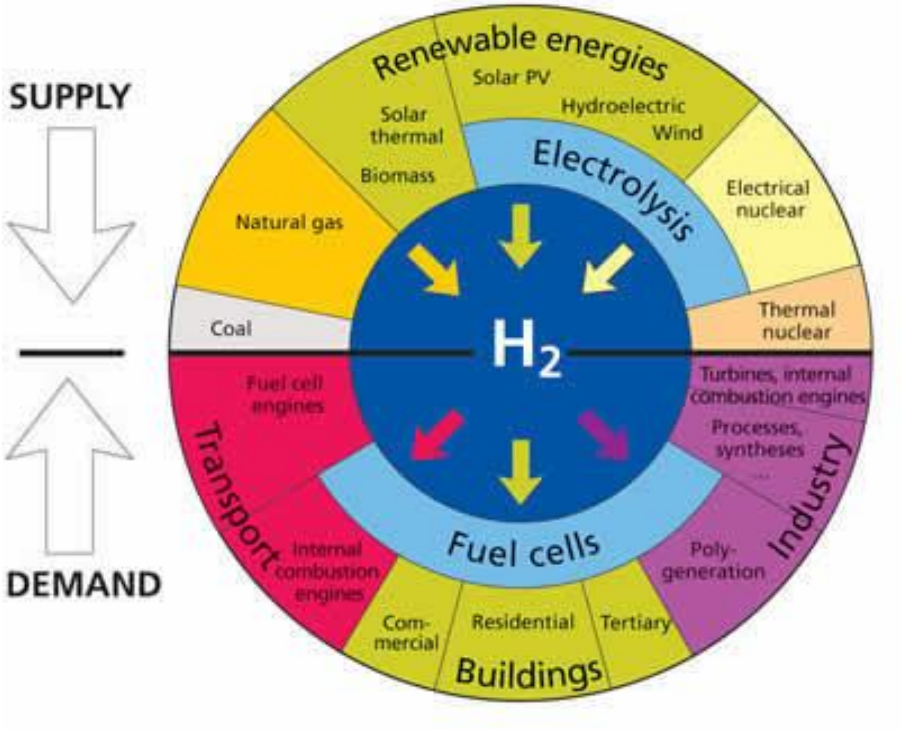

Figure 1. The hydrogen economy.

The electrochemistry of oxygen (including its reduction to water and the electrolytic splitting of the latter into molecular hydrogen and oxygen), in short parlance the oxygen electrode, has proved to be of perennial interest both from a fundamental and an applied perspective, especially in the important areas of energy conversion and storage. In recent times there has been a considerable renewal in interest in the optimization of oxygen evolution reaction (OER) and oxygen reduction reaction (ORR) electrode materials, since the oxygen evolution overpotential is the principal factor in limiting the efficiency of hydrogen production via alkaline water electrolysis [2] and the oxygen reduction the rate limiting bottleneck in the operation of polymer electrolyte membrane (PEM) fuel cells [3] . As noted recently by Gattrell and MacDougall [4] oxygen reduction is the key to achieving

the overall fuel oxidation reaction in fuel cells, is a vital reaction in metal-air batteries and comprises the complementary reaction in many low temperature corrosion processes. Oxygen evolution occurs at the anode in water electrolysis cells, as a counter electrode reaction in electrowinning and as a parallel competing process in many oxidative synthetic reactions such as chlorine evolution. It is also of importance in the recharging of metal air batteries and regenerative fuel cells. Fundamentally ORR or OER provide a realistic prototype of a complex multistep, multielectron transfer electrocatalytic reaction involving adsorbed intermediates. Understanding and optimizing the operation of the oxygen electrode is one of the remaining grand challenges in Physical Electrochemistry and Energy Science .

Although both the ORR and OER have been subjected to considerable and intensive study for more than fifty years [5-9] there is still much new and useful information to be gained from a study of oxygen electrochemistry which will aid in the development and optimization of devices for use in energy conversion and storage technology. In the present review (part 2 in an ongoing series, for part 1 see [10]) we will attempt to present a survey of progress gained to date in this important, challenging and fascinating area, paying special attention to work performed in our laboratories. We will especially focus attention on the mechanism and kinetics of the anodic oxygen evolution reaction at oxidized transition metal and metal oxide electrodes. However it should be noted that the pronounced irreversibility of the cathodic ORR and anodic OER in aqueous solution has imposed severe limitations on the information which can be obtained outlining detailed reaction pathways from electrochemical rate studies. In most instances, at current densities suitable for kinetic analysis, the current-potential data are not sensitive to the reverse reaction, and consequently yield information only up to the rate determining step, which usually occurs early in the multiple step reaction sequence. Furthermore, due to the irreversibility of the electrode reaction, the reduction and oxidation processes are studied at widely separated potentials, and consequently the electrode surface conditions differ appreciably and it is likely that the reduction and oxidation pathways are not complementary. The situation is also complicated by the large number of possible reaction pathways for oxygen electrode reactions. The relation between the overall electrode kinetics and substrate surface electronic properties is also unclear although this situation has improved during the last few years. It is also well established that metal electrodes immersed in aqueous solution are covered with anodic films at potentials at which the oxygen reduction and oxygen evolution processes occur. The surface state of such anodic (i.e. electrochemically grown) films is generally strongly potential dependent, and in most instances, also time dependent, with the result that quite complex kinetic behaviour has been observed as a function of potential.

Adopting a more positive viewpoint however, it should be noted that opportunities for the detailed study of complex electro-catalytic reactions have been enhanced considerably in recent years due to the introduction of surface science and scanning probe methodologies to interrogate the electrode/solution interface in real time [11,12] and to the development of advanced computational methods such as Density Functional Theory (DFT) which can be applied to complex reactions such as the ORR and OER with profit [13-16].

Over the past thirty years considerable research effort has been related to the design, synthesis and characterization of anode materials, with the aim of achieving useful rates of the OER at the lowest possible overpotential in order to optimize the water electrolysis process. At

practical current densities anodes of RuO_2 or IrO_2 exhibit the lowest OER overpotentials [17]. However these oxides suffer from poor chemical stability in alkaline media [18]. The oxides of the first row transition metals, in particular Nickel and Cobalt, offer a compromise solution – although they possess inferior catalytic activity for the OER, they display excellent long term corrosion resistance in aqueous alkaline solution and have the added advantage of being relatively inexpensive [19]. In view of this, nickel hydroxides [20], spinels (ABO_3) including Co_3O_4 [21], $NiCo_2O_4$ [22], and various ferrites [23], perovskites [24] (ABO_3 where A denotes a lanthanide and B is a first row transition metal, e.g. $LaNiO_3$), and transition metal based amorphous alloys [25], have all been proposed for OER anode applications. These oxides have been prepared from inorganic precursor materials using a wide variety of approaches, including thermal decomposition, spray pyrolysis, sol-gel routes and freeze drying, precipitation or electrodeposition from solution. Despite all this intense activity the mechanism of the OER at first row transition metal oxide surfaces remains controversial. The experimental confirmation that a common OER mechanism pertains for these materials would be a significant aid in the eventual development of a general predictive theory of OER electrocatalysis for such materials.

2. TRANSITION METAL OXIDES: ANHYDROUS AND HYDROUS VARIANTS

For the purpose of this paper it is convenient to classify oxides into two groups: (i) compact, anhydrous oxides such as rutile, perovskite, and spinel, in which oxygen is present only as a bridging species between two metal cations and ideal crystals constitute tightly packed giant molecules; and, (ii) dispersed, hydrous oxides where oxygen is present not just as a bridging species between metal ions, but also as O^-, OH and OH_2 species in coordinated terminal group form. Furthermore, in many cases the latter materials when in contact with aqueous media contain considerable quantities of loosely bound and trapped water, plus, occasionally, electrolyte species. A comprehensive overview of the electrochemistry of hydrated transition metal oxide films has been provided by Burke and Lyons [26], whereas the electrochemical and catalytic behavior of compact anhydrous oxides has been produced by Trasatti [27]. Indeed Burke and Lyons [26] noted that with highly dispersed materials (dispersion in the present context referring to the molecular level, i.e. microdispersion), the boundary between the solid and aqueous phases may be somewhat nebulous as the two phases virtually intermingle. Furthermore while compact oxides are usually prepared by thermal techniques such as , for example, by the direct combination of the elements, decomposition of an unstable salt or by dehydration of a hydrous oxide, the dispersed oxides in contrast are almost invariably prepared in an aqueous environment, using, for example, base precipitation or electrochemical techniques. In the latter methodology, the potential applied to the electrode of the parent metal is cycled in a repetitive manner between suitable limits in an aqueous solution of appropriate pH. It is very important to stress here that very often the materials obtained in such reactions are deposited in the kinetically most accessible, rather than the thermodynamically most stable form. Hence they are often amorphous or only poorly crystalline and will indeed be prone to rearrangement in a manner that is directly influenced by factors such as temperature, pH and ionic strength. Microdispersion is usually due to the presence of strand,

layer, tunnel or cage structures which allow not just small ions, but also in many cases solvent molecules to permeate the oxide or hydroxide phase.

Hydrous oxide preparation is a routine procedure in gravimetric analysis, the transition metal ions usually being precipitated in hydrous form by addition of base. While oxide suspensions prepared in this manner may be used to examine double layer phenomena such as measurement of the potential of zero charge and ion adsorption phenomena [28], the investigation of the redox and electrocatalytic properties of these materials requires that the hydrous oxide, ideally present in a uniform, homogeneous thin film form, be attached to some type of inert electronic conductor (the supporting electrode). There are various ways of preparing such coated chemically modified electrodes. One of the most simple involves the direct anodization of the metal in an electrolyte using simple potentiostatic or galvanostatic techniques. This is frequently regarded as involving layer growth via a dissolution/precipitation hydrolysis type mechanism. The technique is also effective for some of the noble metals such as Pt [29] and Au [30] , but seems to be ineffective for Ir [31,32] as the hydrous oxide dissolves under the highly anodic dc conditions that are successful in the case of Pt.

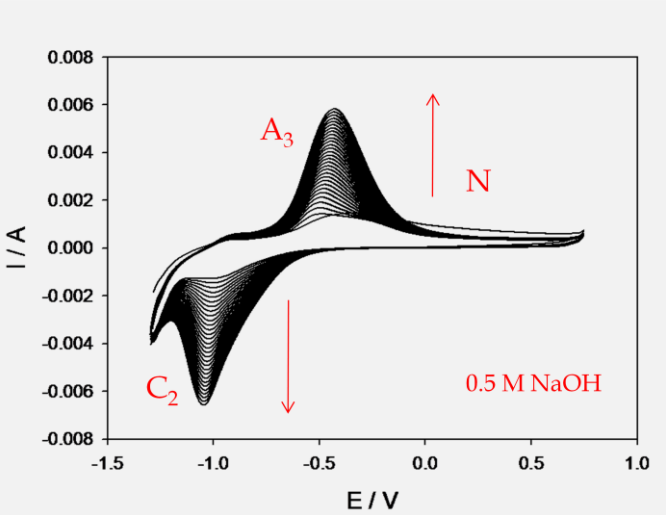

Figure 2. Growth of hydrous iron oxide thin film on Fe support electrode monitored via analysis of the evolution of the real time voltammogram in 0.5 M NaOH.

Cathodic electro-precipitation is a technique used commercially [33] to prepare nickel hydroxide deposits for use in battery applications. Here a nickel salt is present in solution at low pH (ca.3.0) and hydrogen gas evolution around the cathode causes a local increase in pH thereby resulting in the precipitation of an adherent layer of nickel hydroxide at the electrode surface. Similarly anodic electro-precipitation is used commercially [34] to produce layers of the highly active battery material γ- MnO_2. This type of preparation method has been developed extensively over the last few years due to the increasing interest in the development of nanostructured oxide materials for super-capacitor applications [35].

One of the most versatile and convenient techniques used to generate hydrous oxides in a form suitable for the real time determination of their redox switching and electrocatalytic behavior

is that of potential cycling [36]. In this method the potential of an electrode of the parent metal (which may be noble or non-noble) is cycled repetitively between suitable lower and upper limits in an aqueous solution of appropriate pH. The type of potential perturbation used for oxide growth – sinusoidal, square or triangular wave- apparently makes little difference . Indeed the triangular wave is most convenient as changes in the current vs potential response (the voltammogram) can be employed during the oxide growth reaction to monitor changes in redox behavior associated with the latter as illustrated in fig.2 for the growth of hydrous oxide thin films on Fe electrodes in aqueous alkaline solution (0.5 M NaOH). The growth of the hydrous oxide film on the Fe electrode can be readily monitored by following the development of the set of redox peaks A_3 and C_2 as a function of either the time or the number of cycles N. The variation of the integrated voltammetric charge Q (which is directly related to the oxide layer thickness L) as a function of number of potential cycles N is outlined in fig.3. It is possible to fit the Q vs N data quantitatively. We have shown that a useful expression is

$$Q = a\left(1 - \exp\left[-bN\right]\right) \qquad (1)$$

This expression implies that as N → ∞ then Q → a, a constant limiting value. This is often observed experimentally.

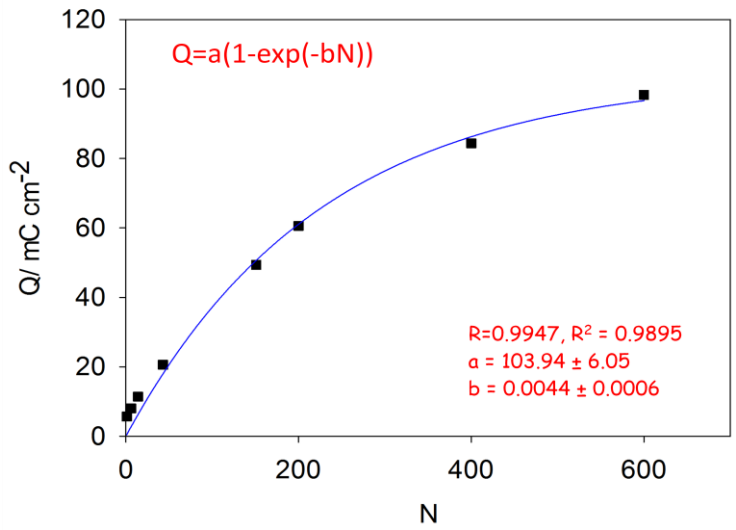

Figure 3. Variation of integrated voltammetric charge Q recorded for the anodic peak A_3 outlined in fig.2 as a function of growth cycle number N. The full line is the least squares fit to eqn.1.

The mechanism of hydrous oxide growth on repetitive potential cycling is now reasonably well understood, at least at a qualitative level and has been discussed by Lyons and Burke [36(a)] and by Pickup and Birss [37]. It may be assumed that the initial oxidation process involves the formation of OH and O radicals which adsorb, initially in a reversible manner on the metal surface.

With increasing degree of surface coverage adsorption assumes a more irreversible character accompanied by the formation, via a place exchange mechanism, of a thin, largely anhydrous, compact passivating phase oxide layer . Under conventional steady state anodization conditions such layers are usually of limited thickness as the activation energy for atom or ion migration in the compact film is generally quite large. However there are some exceptions, e.g. molybdenum has been shown to oxidize at a steady rate at quite low potentials – evidently in this case the oxide produced rearranges readily to a crystalline form, rather than remaining as a compact amorphous layer.

Even though it is directly produced in the initial electrochemical oxidation process, the anhydrous film is probably not the most stable metal oxidation product in the aqueous medium but it may be regarded as an intermediate or metastable product in the formation of a hydrous oxide layer. In the anhydrous film ions are held in a rigid manner in an extended network of polar covalent bonds which drastically reduce ion transport through (and consequently extension of) the surface layer. The next stage of the film thickening process, the hydration reaction, is generally very slow, because as in phase transformation reactions, it involves rupture of primary coordination metal-oxygen bonds. It has been shown that the extent of hydrous oxide growth depends strongly on the value chosen for the upper and lower limit of the potential sweep as well as on the cycling frequency adopted, the solution temperature and the solution pH.

The marked dependence of oxide growth rate on the lower limit of the potential sweep is indicative of the essential role that partial reduction of the anhydrous oxide plays in the production of a thick deposit. Partial reduction of the compact oxide layer apparently facilitates rearrangement of oxycation species at the metal surface, leaving it in a somewhat disrupted state. It is established that in the case of both platinum [38] and gold [30, 39] the anhydrous film is reduced much more readily than the hydrated film. The greater stability of the latter is possibly due to a variety of reasons such as lower repulsion between cations owing to greater separation and decreased charge (the latter effect being due to hydroxyl ion coordination by cations present) and polymer formation. Indeed it has been established that in the case of metal-gas interactions [40] the adsorption-desorption process effects displacement of atoms in the outer layer of the metallic phase, and that potential cycling causes roughening of the surface of noble metals such as platinum under certain conditions [41].

On subsequent re-oxidation of the partially reduced metal surface the compact layer is restored but the outer region of the compact film is present in a more dispersed form. On further reduction the latter material becomes incorporated into the hydrated outer layer. It is not clear whether this rearrangement process involves detachment of oxycations, i.e. a dissolution-reprecipitation mechanism, or a certain weakening, with only a partial detachment of oxycation binding in the compact oxide layer. In the latter case the partially reduced cations are assumed to be displaced from normal lattice sites, and, as such, are more susceptible to oxidation in the subsequent anodic sweep during which they complete their oxygen coordination shell of six oxygen atoms to form a rather open polymeric inorganic bronze or zeolite type structure. Hence under conditions of thick film growth the interfacial region may be represented by : $M/MO_x/MO_a(OH)_b(OH_2)_c$/aqueous phase as is outlined in figure 4. This is the duplex layer model

of the oxide/solution interphase region. Here MO_x represents the inner compact layer and $MO_a(OH)_b(OH_2)_c$ denotes the outer hydrous layer. This model was first suggested by Burke and O'Sullivan [42].

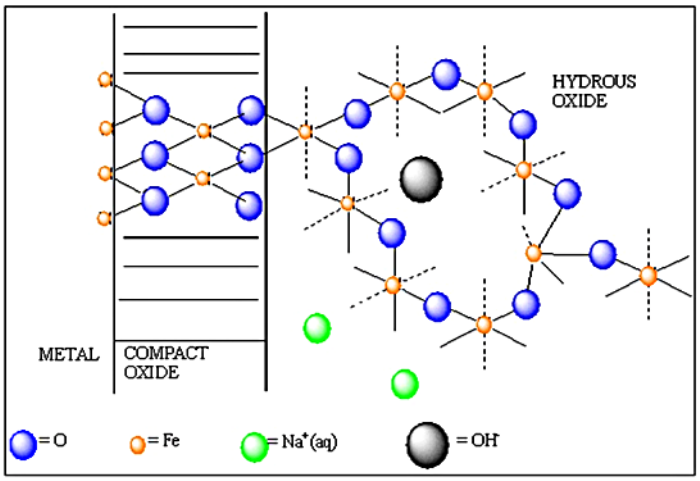

Figure 4. Schematic representation of the Burke-O'Sullivan Duplex Layer Model of the oxide-solution interface.

The upper limit of the potential sweep has also an important effect on the rate of oxide growth. The importance of this parameter probably lies in the fact that it extends oxygen penetration into the outer regions of the metal lattice. It may also help to generate a slight expansion and stress associated disruption at the metal-oxide interface. The upper limit may also facilitate uptake of a slight excess of oxyhen by the oxide phase. It has often been observed that there is an optimal value of upper limit : hydrous oxide growth (as manifested by oxide charge capacity Q) is less at values more cathodic and indeed more anodic than this optimal value. The fall off in oxide growth efficiency at more anodic values of upper potential limit may be possibly associated with the increasing difficulty of reduction of the surface – which is likely to be considerably passivated at more extreme anodic potentials -- at lower potentials. Indeed it has been established that the oxide reduction reaction involves a nucleation process which occurs less rapidly as the film formation potential is raised [43]. Hence the optimum upper limit probably corresponds to a potential which represents the best compromise between two opposing effects, e.g. the compact layer must attain a reasonable thickness (hence the need for a relatively high anodic potential), but too high an upper limit results in a very unreactive layer which does not reduce readily at the lower potential limit.

In summary, for most metals, but especially gold, platinum, iridium and rhodium, extension of oxide growth beyond the monolayer level under conventional galvanostatic or potentiostatic conditions is usually quite slow. This is obvoiously due to the presence of the initial compact oxide product layer which acts as a diffusive barrier to further growth (such compact oxides often exhibit parabolic growth kinetics). Under potential cycling conditions the upper limit plays a

significant role. There is probably a combination of thermodynamic and kinetic factors involved, but evidently the upper limit must be sufficiently anodic that compact oxide formation exceeds significantly the single monolayer level so that on subsequent reduction, a disturbed, highly disordered layer of metal atoms is prepared on the electrode surface (fig.4). Thus with platinum [44] and gold [45], two metals where oxide monolayer behaviour is well defined, the optimum lower limit lies at a potential value at, or below,, the value of the monolayer oxide reduction peak.. On subsequent reoxidation the disturbed layer of metal atoms is evidently converted to hydrated, or partially hydrated oxide – complete hydration under these circumstances may involve several redox cycles – with a fresh inner compact layer being regenerated at the metal surface on each anodic sweep. On repetitive cycling the porous outer layer increases in thickness at the expense of the underlying metal. Lack of stirring dependence in such oxide growth reactions suggests that solution species, i.e. a dissolution/hydrolysis mechanism, are not involved.

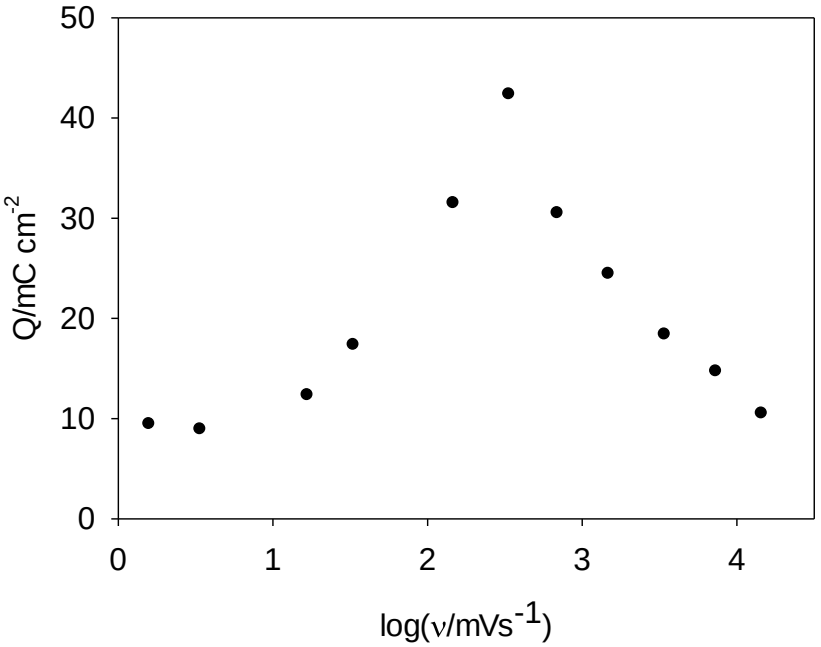

Figure 5. Effect of oxide growth sweep rate ν on the development of the hydrous oxide charge storage capacity Q (evaluated voltammetrically) developed after 30 cycles for an iron electrode in 1.0 M NaOH.

In general when considering the efficiency of thick hydrous oxide growth, it is important to recognize the rather critical balance that exists between the extent of oxide reduction needed to allow some type of breakdown or rearrangement of the metal/compact oxide interface, and the loss of growth efficiency that follows if reduction is too vigorous and extends to the thicker hydrated charge storage layer. Furthermore, it is not just the magnitude of the potential applied to the electrode – the time spent in the critical regions of the upper and lower limit of the sweep also appears to be important as demonstrated by the sharp maximum on the charge capacity Q versus

growth sweep rate curve found for many transition metals such as iron (fig.5) . The decrease in the efficiency of multilayer oxide growth with increasing sweep rate for values greater than the optimum (340 mV/s for iron in 1.0 M NaOH as illustrated in fig.5), may possibly be due to a hysteresis effect. Lyons has shown that the voltammetric peak potentials for the outer hydrous and compact oxide oxidation and reduction peaks shift with increasing sweep rate. The oxidation peak potential shifts to more anodic values and the reduction peaks shift to more cathodic values. Hence a certain amount of hysteresis exists between formation and reduction of the compact and hydrous films. It is quite probable that the reduction region of the film shifts gradually to more cathodic potentials as the sweep rate increases, which results in insufficient reduction or rupture of the anhydrous layer. Conversely, the decrease in oxide growth rate below 350 mV/s may be due to excessive reduction of the compact layer. Hence the important role of sweep rate in the development of charge storage capacity of the surface film clearly demonstrates the importance of kinetic factors in the potential cycling route to hydrous oxide film formation.

An interesting series of results for oxide growth on iron electrodes in aqueous alkaline solution are outlined in Figs. 6 and 7. The variation, is outlined in Fig. 6, of the film redox charge capacity Q for the outer hydrous and inner anhydrous oxide layers as a function of the number of growth cycles N at two different hydroxide ion concentrations ($[OH^-]$ = 0.1 and 1.0 M). A number of important features are to be noted. Firstly the rate of hydrous oxide growth, dQ/dN, is dependent on the electrolyte concentration. During the initial stages of layer growth (small N), the growth rate is more rapid in the more concentrated as opposed to the more dilute hydroxide solution. However the growth rate decreases quite rapidly with increasing N in the more concentrated medium, whereas the growth rate is little affected with increasing N in the more dilute solution. Indeed, significantly larger redox capacities may be observed at a given N value in the dilute solution, once a certain threshold cycle number (ca. 70) is exceeded. In contrast the inner compact oxide charge capacity does not vary with increasing number of cycles, but does depend on the hydroxide ion concentration, slightly greater Q values being observed for the more dilute alkaline solution.

The variation of the extent of hydrous oxide growth (expresed again in terms of redox charge capacity recorded after a given number of potential cycles) with hydroxide ion concentration is illustrated in Fig. 7. Two sets of experiments are outlined. In the first, the layer was grown at a constant sweep rate of 350 mVs^{-1} for 30 cycles (this corresponds to 5 minutes activation) in differing concentrations of hydroxide, whereas in the second series of experiments, the number of growth cycles was increased to 120 (corresponding to 20 minutes activation at 350 mVs^{-1}). Markedly differing behaviour is observed in the two sets of experiments. In the case of layers grown for a shorter activation time, a maximum charge capacity is observed when $[OH^-]$ = 1.0M. In contrast, with layers grown for the longer activation time, a sharp decrease in charge capacity with increasing hydroxide ion concentration is observed. Hence in this latter situation the layer exhibits greatest electroactivity in the most dilute hydroxide solution. Note that Q values were always determined at a slow analytical sweep rate (40 mVs^{-1}) to ensure that one had maximum titration of all redox centres in the layer, and so the integrated voltammetric response accurately reflected the amount of redox active sites in the hydrous layer.

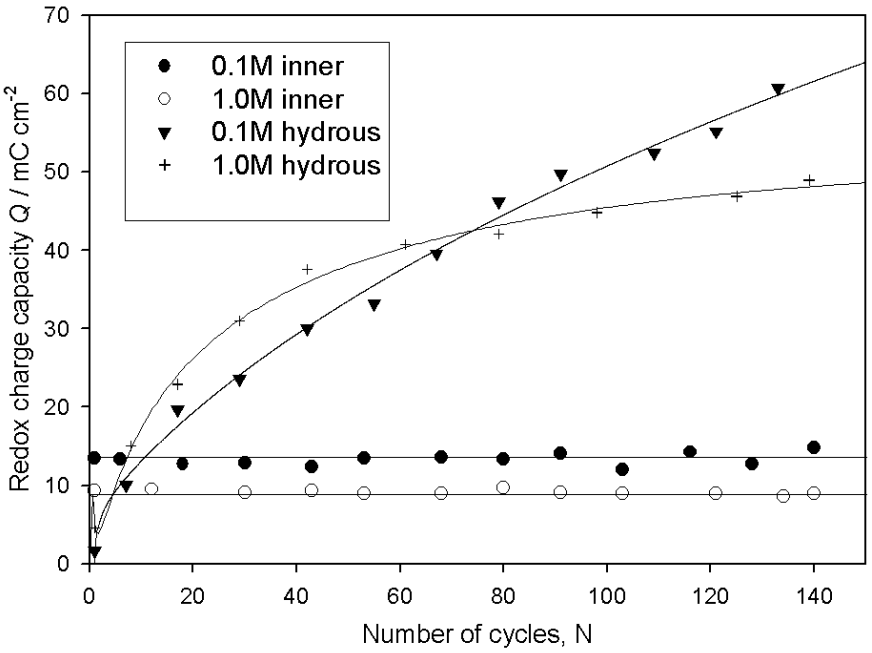

Figure 6. Variation of the charge capacity *Q* associated with the outer hydrated oxide film (evaluated by integration of the A3 peak) and the inner compact oxide film (based on integration of the C1 peak) with increasing number of cycles, *N*, as a function of OH^- ion concentration at 25°C. The oxide films were grown by repetitive potential cycling between –1.425 and 0.325 V at a sweep rate of 0.35 Vs^{-1}.

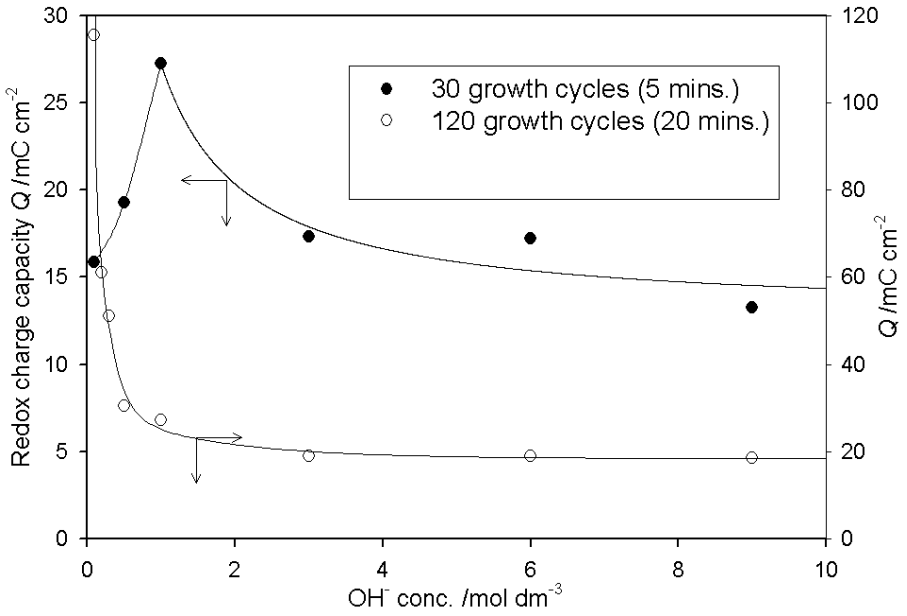

Figure 7. Variation of multi-layer oxide growth with OH^- concentration for multi-cycled iron electrodes (–1.425 to 0.325 V, 0.35 Vs^{-1} at 25°C) with different growth times. *Q* was evaluated by integration of the A3 voltammetric peak.

The decrease in oxide growth rate with time (or equivalently with increasing film thickness) can be attributed to the increasing inhibition of water and hydroxide ion transfer to the inner region of the oxide layer, with increasing hydrous oxide thickness. The data outlined in Figs. 6 and 7 indicate that the effect is more marked with increasing base concentration. Evidently, increased hydroxide ion activity suppresses hydroxide dissociation and /or favours adsorption of this species. This will result in the inhibition of crystallization of the hydrous oxide layer, and the resulting more amorphous film will be more effective in excluding water from the inner region of the oxide film, thereby inhibiting the growth of the microdisperse hydrous layer.

3. TRANSITION NON NOBLE METAL HYDROUS OXIDES: GENERAL REDOX BEHAVIOUR IN AQUEOUS ALKALINE SOLUTION

The redox behavior exhibited by both noble and non-noble metals in contact with aqueous acidic and alkaline solution is in general time and potential dependent and complex, and can be readily monitored in real time using potential sweep voltammetry. The behavior of iron, nickel and cobalt electrodes in aqueous alkaline solution may be quoted as typical examples of the complexity found when probing the interfacial redox chemistry of non noble metal electro-oxidation in aqueous media. The reader is referred to the reviews by Burke and Lyons [26] and Brandon [46] for a more comprehensive review of metal oxidation and electrochemical hydrous oxide formation.

3.1. Interfacial redox chemistry of iron electrodes in aqueous alkaline solution

A series of voltammetric curves, are presented in figure 8 recorded (-1.42 V to 0.68 V, 40 mVs^{-1}) during the initial stages of the electrodeposition of a multilayer microdisperse hydrous iron oxyhydroxide film in 1M NaOH solution. In figure 7 the profiles arising from the application of an extended number of potential cycles are presented. The experimental conditions used during the multicycling procedure has previously been optimized [36a]. The voltammetric profiles exhibit quite an amount of fine structure, especially during the earlier sweeps (resolved most clearly in figure 6). For a polycrystalline Fe electrode polished to a “mirror bright” finish, we usually observed four well defined anodic peaks (A1 – A4) and two cathodic peaks (C1, C2) during the initial stages of oxidation, reflecting surface redox processes involving bound oxy iron species. This fine structure has been observed by other workers [47,48], and the general features of the voltammetric response remain unchanged, even if the concentration of base is increased. The various features have been previously assigned, both by us [36a,49] , and other workers [47,48]. Our viewpoint on the voltammetric peak assignment is summarized as follows. Peak A1 is most probably due to the formation of a layer of adsorbed hydroxy species,

$$Fe + OH^- \rightarrow FeOH_{(ads.)} + e^- \qquad (3.1)$$

combined with the electrochemical displacement of adsorbed hydrogen:

$$FeH_{(ads.)} \rightarrow Fe + H^+ + e^- \quad (3.2)$$

Peak A2 may then represent the conversion of both Fe and FeOH(ads.) to a thin film of Fe(II) hydroxide or oxide according to:

$$FeOH_{(ads.)} + OH^- \rightarrow Fe(OH)_2 + e^- \quad (3.3)$$

$$FeOH_{(ads.)} + OH^- \rightarrow FeO_{(ads)} + H_2O + e^- \quad (3.4)$$

The overall interfacial reaction resulting in Fe(II) film formation may be more complex than that outlined above due to a variety of other possible reactions. For instance hydroxylation reactions such as:

$$FeO + H_2O \rightarrow Fe(OH)_2 \quad (3.5)$$

Will result in the conversion of oxy to hydroxy species in the outer region of the surface layer. Place exchange processes [50,51] can result in an increase in the thickness of the surface layer. The latter type of growth process has been proposed to involve a rapid place exchange step followed by a rate determining Temkin discharge of OH^- ions onto sites in which a surface iron atom is already attached to a hydroxyl group displaced into the first layer beneath the surface, viz:

$$FeOH_{(ads)} \rightarrow HOFe \quad \text{(fast)} \quad (3.6)$$

$$HOFe + OH^- \rightarrow HOFeOH_{(ads)} \quad \text{(slow rds)} \quad (3.7)$$

$$HOFeOH_{(ads)} \rightarrow Fe(OH)_2 \rightarrow FeO + H_2O \quad (3.8)$$

One should note that with a non noble metal such as iron, the aforementioned surface processes are likely to be accompanied by film thickening (i.e. place exchange reactions [50,51]), even at quite low potentials. It should also be noted that active dissolution to form soluble oxy iron species such as $HFeO_2^-$ and FeO_2^{2-} according to:

$$FeO + OH^- \rightarrow HFeO_2^- \quad (3.9)$$

$$HFeO_2^- + OH^- \rightarrow FeO_2^{2-} + H_2O \quad (3.10)$$

Note that a deposit of gelatinous ferrous oxide $Fe(OH)_2$ that is weakly bound to the metal can subsequently be formed by hydrolysis of the $HFeO_2^-$ ion:

$$HFeO_2^- + H_2O \rightarrow Fe(OH)_2 + OH^- \quad (3.11)$$

Armstrong and Baurhoo [52] did not detect any soluble reaction products in cycling experiments using the rotating ring disk electrode (RRDE) in the collection mode, for the case of iron in 1M KOH at 25°C. However they did detect the presence of $HFeO_2^-$ species in solution at potentials near that of the A2 peak in strongly alkaline solution at more elevated temperature. In further experiments, Lyons [53] has confirmed that such dissolution processes are significant at more elevated base concentrations. It should be noted that a reaction scheme similar to that presented here was envisaged many years ago by Frumkin and co-workers [54].

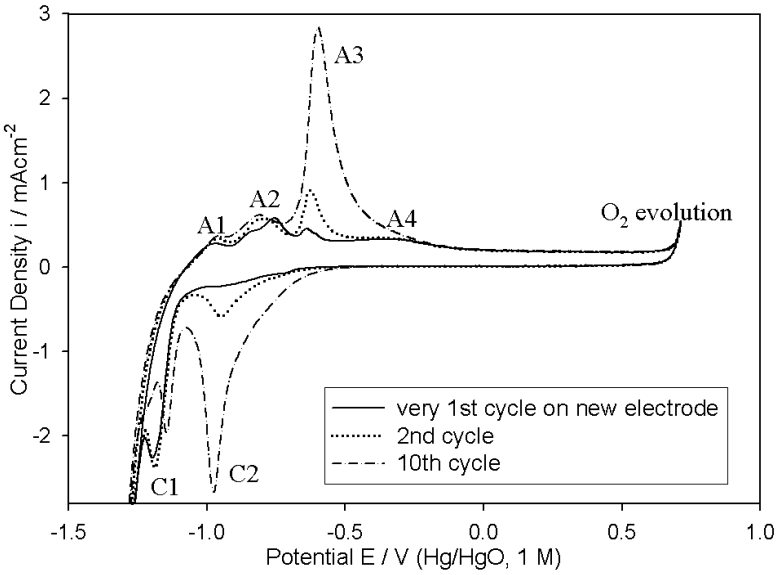

Figure 8. 1st, 2nd and 10th voltammetric cycles (-1.42 V to 0.68 V, 40 mVs^{-1}) of a freshly prepared bright polycrystalline iron electrode in 1M NaOH at 25°C.

Peak A3 shows some of the characteristics of a hydrated layer. Since traces of this peak appears even during the first sweep of a bright electrode, it is possible that at the outer regions of the oxide film the process $FeO + H_2O \rightarrow Fe(OH)_2$ is succeeded by a further stage which involves coordination of additional H_2O and OH^- species. Peaks A3 and C2 are the only peaks that display a significant enhancement on repetitive cycling (figure 8). In simple terms peaks A3/C2 are attributed to the following Fe(II)/Fe(III) redox transformation which involves an electrochromic colour change from transparent to yellow green as the oxidation state changes from Fe(II) to Fe(III):

$$Fe(OH)_2 + OH^- \rightarrow FeOOH + H_2O + e^- \qquad (3.12)$$

We have previously shown [36(a)] that the A3/C2 peaks exhibit the usual characteristic of a hydrous or hyper-extended oxide, i.e. *a super-nernstian potential-pH shift*, which has the value of $dE/dpH = -2.303(3RT/2F) = -0.088$V/pH unit at T = 298 K (see next section for further details). Hence the latter peak combination is attributed to an Fe(II)/Fe(III) redox transition in a polymeric

microdispersed hydrous oxide layer, formed initially (even during the first anodic voltammetric sweep) by hydration of the outer regions of the $Fe(OH)_2$ or FeO film. By analogy with a scheme produced by Burke and Whelan [55] for redox switching of iridium oxide films, one may propose that the main redox switching reaction may be written as:

$$[Fe_2(OH)_6(OH_2)_3]^{2-} + 3OH^- \rightarrow [Fe_2O_3(OH)_3(OH_2)_3]^{3-} + 3H_2O + 2e^- \quad (3.13)$$

The ratio of hydroxide ions to electrons will, by a simple Nernstian analysis, yield the experimentally observed pH dependence. Hence, one has a rapid topotactic reaction involving hydroxide ion ingress and solvent egress at the oxide/solution interface, and electron injection at the metal/oxide interface.

The Fe(II)→Fe(III) redox switching reaction proposed above, is quite similar to that exhibited by conductive polymer materials such as poly(aniline), and other hydrous polymeric oxides such as iridium oxide, in that it involves the transport of both counterions and electrons and is therefore a mixed electronic/ionic conductor. The physical transport processes within the material may be described in terms of a dual rail electrical transmission line model (figure 9) of the type recently proposed for electronically conducting polymers and transition metal oxide materials (especially DSA type IrO_2 based thermal oxides) by Bisquert and co-workers [56] and others [57]. The TL circuit consists of distributed impedances corresponding to charge transport along the polymer strand (Z), ion transport within the pore electrolyte (X) and an impedance representing the interface between the strand and the pore (Y). At the simplest level Z corresponds to the electronic resistance R_E, X to the ionic resistance R_I, and Y to a distributed capacitance C_Σ .

The redox switching and interfacial behaviour of hydrous metal oxide modified electrodes has been probed in recent years using the powerful techniques of Probe Beam Deflection (PBD) and the Electrochemical Quartz Crystal Microbalance (EQCM). These techniques are proved very useful in the real time examination of coupled electron/ion transport processes in this films and have been described by Lyons [58] and by Oyama and Ohsaka [59]. The EQCM is a piezoelectric device capable of monolayer mass sensitivity. The method involves sandwiching a quartz crystal between two electrodes, one of which is used as the working electrode of an electrochemical cell. These electrodes are used to produce a radio frequency (RF) electric field across the crystal at a resonant frequency determined by the crystals dimensions and total mass loading. A change in the mass of the working electrode causes a change in the resonant frequency of the device which can then be used to determine the quantity of the added mass. This effect is quantified by the Sauerbrey equation which relates the change in resonant frequency Δf from its value f at the start of the experiment and the mass change ΔM per unit area of the electrode as follows: $\Delta f = -\left(2f^2/\rho\upsilon\right)\Delta M$ where ρ denotes the density of the crystal and υ is the velocity of the shear wave within the immobilized film. The negative sign indicates that Δf decreases as ΔM increases. It is important to note that the Sauerbrey equation is valid when the deposited film behaves like a rigid layer, i.e. when the film is perfectly elastic (exhibits zero viscosity) and thin enough so that the frequency change is small compared with the resonant frequency. If the layer is very thick,

then this linearity between frequency change and mass may not be observed due to viscous damping of the acoustic shear wave within the modifying film.

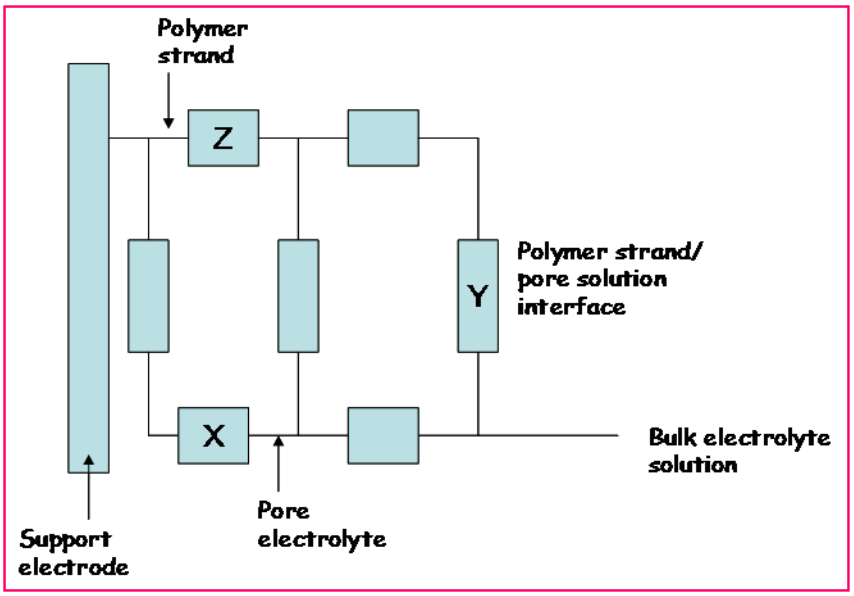

Figure 9. Schematic representation of dual rail transmission line model for electroactive polymer and nanostructured metal oxide thin film.

The great advantage of the EQCM method is that a simultaneous in situ determination of working electrrode mass and electrochemical parameters can be obtained. Thus one may electrochemically induce mass changes (such as those caused by solvent or ion transport during redox switching) in electroactive electroactive polymer thin films, oxidized metal surfaces and metal oxide thin films, and monitor these mass changes concurrently with such conventional electrochemical measuring techniques such as cyclic voltammetry or chronoamperometry. The EQCM technique has been used to study both overall thermodynamic changes in ion and solvent populations within electroactive polymer thin films, and the dynamics of ion and solvent motion within these films. For instance Calvo and co-workers [60] have examined the redox switching process involved in the $Ni(OH)_2$/NiOOH redox transition, whereas Hillman and co-workers [61] have examined the effect of timescale on redox driven ions and solvent transfers at nickel hydroxide thin film modified electrodes using EQCM and EPBD techniques in tandem. This work has lead to the development of a qualitative picture of the mechanism of mobile species transport and polymer relaxation during redox switching in electroactive polymer thin films which may be readily extended by analogy to microdispersed hydrous transition metal oxide coated electrodes.

The fundamental theory of Electrochemical Probe Beam Deflection (EPBD) is well described by Royce and co-workers [62], Pawlisyzn et al [63] , Russo and co-workers [64], Mandelis and Royce [65] and Barbero et al [66]. This technique provides information on concentration and thermal gradients adjacent to an electrode by examining the deflection of a laser beam aligned parallel and very close to a planar electrode surface. The beam undergoes deflection

(refraction) due to the existance of refractive index gradients in the interface region. The latter gradients are due to the generation or consumption of species in the electrolyte phase. The delection Ψ of a laser beam traveling along a concentration profile adjacent to a planar electrode surface is given by: $\Psi = (w/n)\frac{\partial n}{\partial c}\left(\frac{\partial c}{\partial x}\right)$ where c represents concentration, n is the refractive index of the electrolyte solution, and w is the path length over which the laser beam interacts with the concentration profile. Under most conditions, w, $\partial n/\partial c$, and n are constant, to that the deflection, Ψ, is mainly proportional to the concentration gradient $\partial c/\partial x$.

A detailed calculation of the path of a laser beam probing an interfacial concentration gradient is provided by Mandelis and Royce [65]. We note from figure 10 that a positive deflection of the probe beam results from a positive concentration gradient at the electrode/solution intrerface, whereas a negative deflection is obtained if the interfacial concentration gradient is negative. Consequently the sign of the beam deflection indicates whether an interfacial electrochemical reaction is accompanied by a net ion flux away from the electrode surface or toward the electrode surface. Combined with the sign of the simultaneously measured current obtained from a cyclic voltammetry experiment, it is possible to determine whether anions or cations are exchanged at the interface. Hence the EPBD method can be applied to oxide and polymer film modified electrodes when ion transport plays a major role in redox switching. We note however that although EPBD probes concentration gradients, it is not possible to distinguish between a concentration gradient produced by an ion transfer or solvent transfer in the opposite direction. In practise additional experiments such as the EQCM or radio tracer measurements are necessary to evaluate solvent transfer contributions to the total beam deflection.

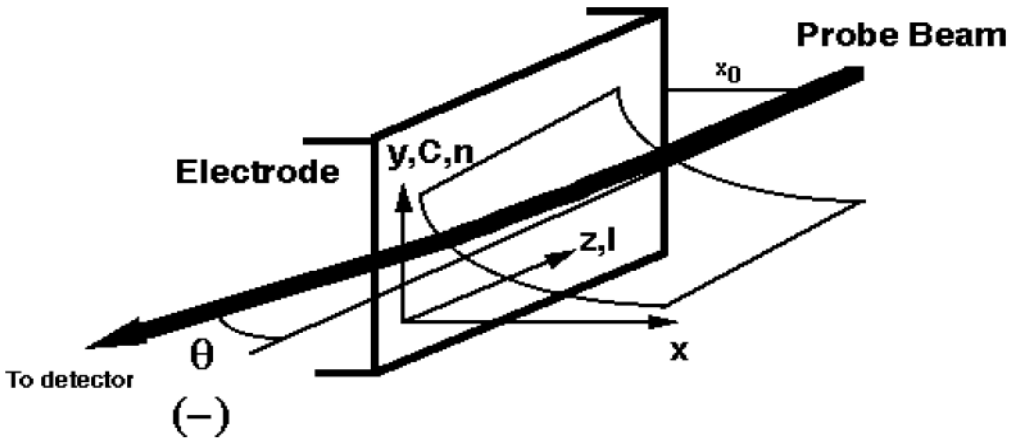

Figure 10. Probe beam deflection at electrode/solution interface.

EQCM and EPBD methods have been used extensively in recent years to examine oxide growth processes and the interfacial redox properties of metal oxide and oxidized metal electrodes

[67,68]. Using the Probe Beam Deflection (PBD) technique, Kotz and co-workers [69] determined that for iridium oxyhydroxide films, protons are ejected from the film during the course of oxidation in acid solution, whereas hydroxide ions are consumed for the same process in base. The redox switching in these solutions may be represented as [55],

$$[Ir_2(OH)_9]^{3-}.3H^+_f + 3H_2O \rightarrow 2\{[Ir_2(OH)_6]^{2-}.2H^+_f\} + 3H^+_s + 2e^- \quad (3.14)$$

$$[Ir_2(OH)_9]^{3-}.3Na^+_f + Na^+_s + 3OH^- \rightarrow 2\{[Ir_2(OH)_6]^{2-}.2Na^+_f\} + 2e^- \quad (3.15)$$

where mobile charge compensating counterions in the oxide matrix are denoted by the subscript f, whilst ions which transfer between the film and the solution during redox switching are identified by the subscript s. Hence for anodically generated iridium oxide, the oxidised form of the latter (Ir(IV)) is assumed to consist of an aggregate of octahedral species $Ir(OH)_6^{2-}$ or possibly $[IrO_2(OH)_2(OH_2)_2]^{2-}$, whereas the reduced form (Ir(III)) is given by the aggregate $Ir_2(OH)_9^{3-}$ or possibly $[Ir_2O_3(OH)_3(OH_2)_3]^{3-}$. Hence by analogy with this work reported for iridium oxide, it is reasonable to suppose that both Na^+ and OH^- species are also involved in the redox switching reaction of iron oxyhydroxide layers and we propose that the following scheme be adopted:

$$[Fe_2(OH)_6(OH_2)_3]^{2-}.2Na^+_f + Na^+_s + 3OH^- \rightarrow [Fe_2O_3(OH)_3(OH_2)_3]^{3-}.3Na^+_f + 3H_2O + 2e^- \quad (3.16)$$

The redox switching reaction represented directly above, involving the Fe(II)/Fe(III) redox process is accompanied by a reversible colour change: the reduced material being transparent, whereas the oxidised material is greenish-yellow. Hence the hydrated oxide polymer exhibits electrochromic activity.

The formulae presented above should only be considered as a general guide. Other forms of Fe(II) and Fe(III) hydrated oxides are possible and in fact mixtures such as Fe_3O_4(hyd) are quite likely. Indeed the slightly irreversible nature of the main charge storage peaks (as evidenced by the difference in potential between A3 and C2) is more akin to the behavior exhibited by manganese, rather than that of iridium and rhodium, where mixed oxide or hydroxide intermediate formation (Mn_3O_4, $Mn(OH)_3$) may also be involved [70]. As has been found for a large variety of other transition metal oxides, the growth of the charge storage peaks A3 and C2 is accompanied by the onset of electrochromic behavior at the electrode surface. In this type of process it is assumed that a redox reaction (resulting in a change in oxide stoichiometry) allied with a proton or hydroxide ion transfer in the hydrated surface layer is involved. The electrochromic effect is found to diminish with decreasing experimental timescale (sweep rate) and or larger film thickness. This observation can be explained in terms of change in the film's microstructure or stoichiometry which progressively reduces the proportion of the film participating in the redox reaction represented by the A3/C2 peaks.

The anodic peak A4 is probably due to a Fe(II)/Fe(III) redox transition in the compact layer of FeO or $Fe(OH)_2$ at the metal surface, leading to the formation of such species as γ-Fe_2O_3, Fe_3O_4 or FeOOH.

The cathodic peak C1 corresponds to the reduction of the compact, anhydrous inner layer

(see schematic of Fig. 3) according to the following reaction:

$$FeO.FeOOH + H_2O + 3e^- \rightarrow Fe + FeO_2^{2-} + H_2O + OH^- \quad (3.17)$$

A useful aspect of this reaction is that the charge capacity of peak C1 (which can be calculated by integration of the peak between appropriate limits) can be used to estimate the extent of the compact layer growth. We note from fig. 6 that this compact layer does not continue to grow to any great extent with increasing number of potential cycles N regardless of the base concentration used.

3.2. Interfacial redox behaviour of nickel electrodes in aqueous alkaline solution

It is probably fair to say that the redox switching behaviour of nickel hydroxides and oxyhydroxides is one of the most studied systems in all of electrochemistry. This arises for several reasons relating to the practical utilization of nickel and nickel oxide electrodes in several technologically important areas. Nickel hydroxides have long been used as the active material in the positive electrodes of several alkaline batteries – e.g. the commercially important nickel-cadmium battery. In addition to this, their high corrosion resistance and relative inexpensiveness (as compared to materials such as RuO_2 and IrO_2) has lead to Ni and some of its alloys becoming the materials of choice for use in commercial alkaline electrolysis [71]. Despite the widespread practical application of nickel and nickel hydroxide electrodes, progress in understanding the nature of the redox reactions of these materials in aqueous solution has been slow, owing to the complexity of these reactions and their variability with respect to factors such as the electrode preparation and electrode history. As commented by McBreen [72] in his review on the electrochemistry of nickel hydroxides; "Items which are normally trivial exercises for most battery electrodes, such as the determination of the open circuit potential, the overall reaction, and the oxidation state of the charged material, have required much effort and ingenuity". A point which must be kept in mind is that, although the present discussion has as its focus nickel oxide and hydroxide films grown electrochemically by anodic polarisation, much of the potentially useful data that has been obtained over the years, relates to nickel hydroxides that have been electrodeposited on various substrates, or indeed (in the case of XRD measurements) to crystalline precipitates of nickel hydroxide. The physical and chemical properties of these materials have been found to depend on the details of their preparation, and therefore one must attach a degree of caution in generalizing the applicability of data obtained on nickel hydroxide prepared by a particular technique.

The voltammetric behavior exhibited by a polycrystalline Ni electrode in aqueous 1.0 M NaOH when subjected to a repetitive potential cycling regime is outlined in fig.11. Similar voltammetric response profiles are presented in many works in the literature – random examples include publications due to Seghiouer and co-workers [73], Burke et al. [74], Visscher and Barendrecht [75], de Souza et al. [76] and Simpraga and Conway [77] to name but a few.

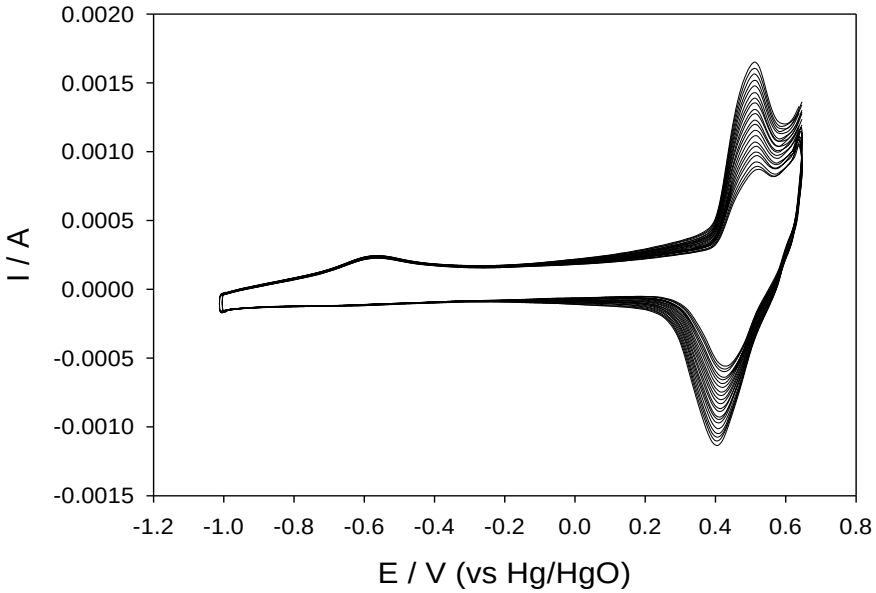

Figure 11. Typical CV profiles recorded for a polycrystalline Ni electrode in 1 M NaOH at 25°C when subjected to a repetitive potential cycling regime at 150 mV/s.

It is almost universally agreed that the lower anodic peak observed at –0.8 to -0.6 V in figure 11 is principally associated with the oxidation of metallic Ni(0) to Ni(II) species. There has been historically, some disagreement about the nature of the Ni(II) oxide species formed at this potential with, for example, Makrides [78] proposing the production of NiO and $Ni(OH)_2$, while Okuyama [79] proposed that the oxide film in this potential region was non-stiochiometric, consisting of NiO and Ni_3O_4. More recently the complex nature of the film even at these low potentials has been emphasised. Based on the variation of the peak potential with pH in alkaline solution, Burke and Twomey [74] proposed that both oxidation and hydrolysis processes were operative in this potential region, leading to the formation of a somewhat anodic species, tentatively assigned the formula (for the purpose of rationalization) of $Ni(OH)_{2.4}^{0.4-}$.

When the anodic limit of the potential sweep was maintained well below the upper redox peaks Burke and Twomey [74] observed a pH invariant cathodic peak at potentials of the order of 0.3V lower than the anodic peak. In view of this they concluded that with the change in sweep direction the initially produced anodic hydrous species alters to a more anhydrous form, e.g. NiO, so that the reduction peak would be due to the process $NiO + H_2O + 2e^- \rightarrow Ni + 2OH^-$. In essence their proposal is that, due to post electrochemical place exchange reactions, the anionic oxide becomes neutral before being reduced back to Ni metal. They also point out that the lower oxidation peak appears to be superimposed on a background current that is probably due to a combination of adsorbed hydrogen oxidation, and formation of a layer of OH_{ads} species. In an ellipsometric study, de Souza et al. [76] found that the first layer of oxide formed in the vicinity of the lower anodic peak consists of NiO, however this becomes covered with a thick film of $Ni(OH)_2$ upon further increase of potential. A further significant observation of Burke and Twomey [74] was that the magnitude and position of the

lower anodic peak didn't alter much upon repetitive cycling. This lead them to the important conclusion that it is the inner oxide layer that is reduced at significant cathodic potentials and thus even on cycling, the lower anodic peak is associated with oxidation of Ni metal to Ni(II) at the metal/porous hydrous oxide interface. Seghiouer et al. [73] observed that a bright polycrystalline Ni electrode, displayed an open-circuit potential of ca. –0.4 V (vs. Hg/HgO 1M KOH), and thus concluded, in agreement with several earlier works [80,81], that the formation of Ni(II) oxide species occurs immediately upon the immersion of Ni in aqueous alkaline solution.

The upper anodic peak observed at approximately 0.45 → 0.55 V in Figure 11 is associated with the oxidation of Ni(II) ($Ni(OH)_2$) to Ni(III) (NiOOH) species. The rising part of the profile, anodic to this peak is due to the onset of the o.e.r. Therefore the state of the electrode surface, at potential values, just below that at which the o.e.r. becomes the dominant process, is largely dictated by the redox process occurring at the upper anodic peak. The magnitude of the area under the anodic peak and under its cathodic counterpart increase on repetitive cycling [74,75] , and so it is the Ni(II) → Ni(III) transition that is associated with the development of a charge storage film on nickel hydroxide electrodes in alkaline solution. Hence it is the $Ni(OH)_2$/ NiOOH redox system that is of interest in the battery applications of nickel and nickel hydroxide electrodes. It is often observed that upon, ageing or repetitive cycling of a Ni electrode in alkaline solution, the upper cathodic response will split into a doublet [75], or will display a shoulder adjacent to the main peak at lower potentials [74,82] as illustrated in fig.12. These observations hint towards the great complexity inherent in the redox switching behaviour of $Ni(OH)_2$ films in alkaline solution, referred to in the introduction to this section. The ill defined shoulder at potentials close to 0.6 V immediately prior to the onset of active oxygen evolution may lend credence to the suggestion that a Ni(III) /Ni(IV) redox transformation may occur at these high anodic potentials.

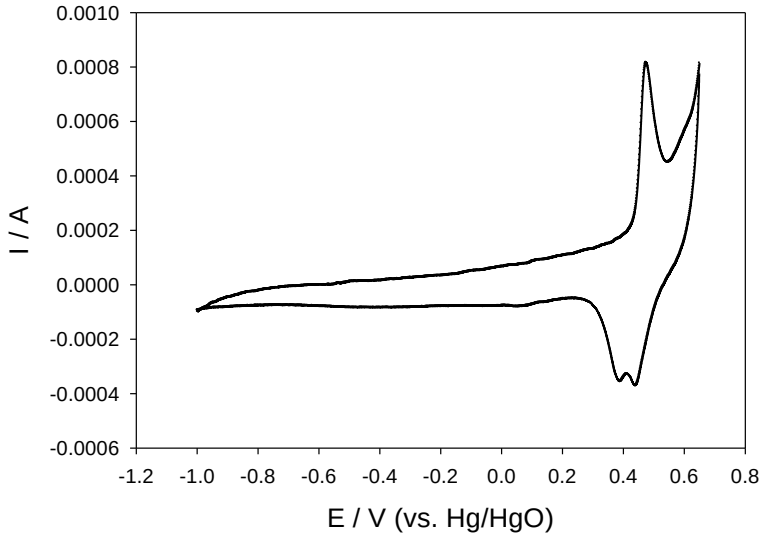

Figure 12. Typical cyclic voltammetric response recorded ay 40 mV/s in 1.0 M NaOH for a multi-cycled hydrous oxide coated nickel electrode. Note the fine structure at elevated anodic potentials prior to the onset of active oxygen evolution.

A major advance in the understanding of the Ni(II) → Ni(III) transition was made by Bode et al. [81] in 1966. These workers rationalised the redox switching behaviour of nickel hydroxide films in terms of four phases. Thus the discharged $Ni(OH)_2$ material could exist as a hydrous phase denoted as α-$Ni(OH)_2$ or as a largely anhydrous phase denoted as β-$Ni(OH)_2$. Oxidation of β-$Ni(OH)_2$ is envisaged to yield a phase referred to as β-NiOOH, whereas oxidation of α-$Ni(OH)_2$ yields γ-NiOOH. The Bode scheme is presented in Figure 13 in its traditional cyclical formation, and also in a useful graphical format reproduced from a recent review paper [82]. From these diagrams it can be seen that upon ageing (especially in more concentrated alkali solution) the α-$Ni(OH)_2$ can dehydrate and recrystallise as β-$Ni(OH)_2$. Furthermore, upon overcharge, β-NiOOH can convert to γ-NiOOH. The non-stiochiometric nature of both the discharged and charged material is indicated by the average oxidation states of Ni in each phase as indicated in Figure 1.4.3. Bode et al. [81] envisaged that the oxidation of α-$Ni(OH)_2$ to γ-NiOOH, would occur at a lower potential than the redox transition between the two β phases, a point that has been experimentally verified [83]. Indeed in his review of nickel hydroxides, Mc Breen [72] states that "all subsequent work has in general validated" the broad conclusions of the Bode model.

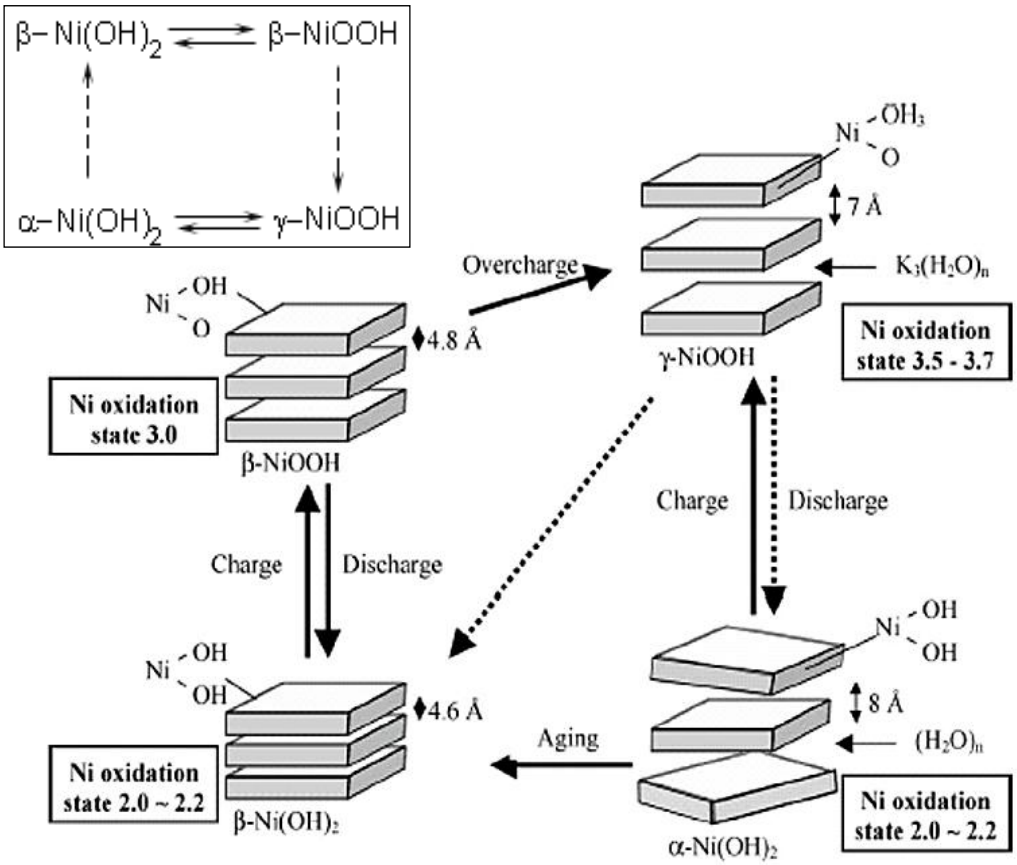

Figure 13. Graphical representation of the Bode scheme for the $Ni(OH)_2$ →NiOOH redox transformation in alkaline solution. Inset – More traditional representation of the Bode scheme.

While there is general acceptance for the principles of the Bode model, it is important to understand that it is inappropriate to think about the formation of a compound or phase with a definite stoichiometry, during the complex $Ni(OH)_2$ to NiOOH transformation. Instead, the four phases of the Bode scheme should be considered as the limiting divalent and trivalent materials, - the actual composition of the oxide at a given potential depending on a range of factors including, its history, method of preparation, degree of hydration, concentration of defects etc. Nonetheless it is instructive to briefly review what is known of the nature and structures of the four limiting model phases.

The definitive crystallographic work on β-$Ni(OH)_2$ was performed by Greaves and Thomas [84] . These workers conducted powder neutron and X-ray diffraction studies on both a well crystallised deuterated $Ni(OD)_2$ sample pretreated by a hydrothermal method, and also a high surface area $Ni(OH)_2$ sample that was precipitated from a $NiSO_4$ solution upon the addition of KOH. They found that well crystallised β-$Ni(OD)_2$ adopts a brucite-type structure with layers of $Ni(OD)_2$ (the basal planes) perfectly stacked along the c-axis – see Figure 14. The $Ni(OD)_2$ layers consist of a hexagonal planar arrangement of Ni^{2+}-oxygen octahedra. As commented by McBreen [72] the nickel ions are all in the (0001) plane and are surrounded by six hydroxyl groups, each of which is alternatively above and below this plane. The brucite structure of β-$Ni(OH)_2$ is isomorphous with the divalent hydroxides of Ca, Mg, Cd, and significantly in the context of the present work, Fe and Co [74(a)] . For the well crystallized $Ni(OD)_2$, the unit cell parameter in the basal plane, a_0, was found to be 3.126 Å, the interlamellar distance, c_0, was determined as 4.593 Å, while 0.973 Å was reported for the O-H bond length. The less well crystallized material precipitated from the sulphate solution, yielded the following values for these parameters; a_0 = 3.119 Å, c_0 = 4.686 Å and O-H bond length = 1.08 Å. On the basis of this data Greaves and Thomas [84] concluded that the structure of the high surface area as-precipitated β-$Ni(OH)_2$ is similar to the well crystallized material, but has a much greater amount of defects related to a high concentration of surface OH^- groups. Significantly, it was noted that the well crystallised material displayed much lower electrochemical activity than the defective as-precipitated species.

Greaves and Thomas [89] also applied infrared spectroscopy to the study of the two aforementioned materials. They observed a broad absorption band in the region of 1630 cm^{-1} in the spectrum for the high surface area material, which was absent from the spectrum of the well crystallised hydroxide. They attributed this to the presence of a small amount of absorbed water in the more defective material. This hypothesis is consistent with the increase in the O-H bond length and c_0 parameter for the defective material, in comparison with the more crystallised material, as was detailed above. In his review on nickel hydroxides, McBreen [72] reports that other workers using XRD, IR, Raman spectroscopy, and Thermogravimetric analysis (TGA) have arrived at conclusions similar to those of Greaves and Thomas [84] . In summary the discharge product on the β cycle in nickel hydroxide battery materials is similar, but not identical to well crystallized β-$Ni(OH)_2$. Its defect structure permits water adsorption and facilitates enhanced electrochemical activity. Following this analysis it is probably reasonable to assume that anodically generated β-$Ni(OH)_2$ will also be defective and contain some absorbed water, despite being formally described as the anhydrous form of the hydroxide.

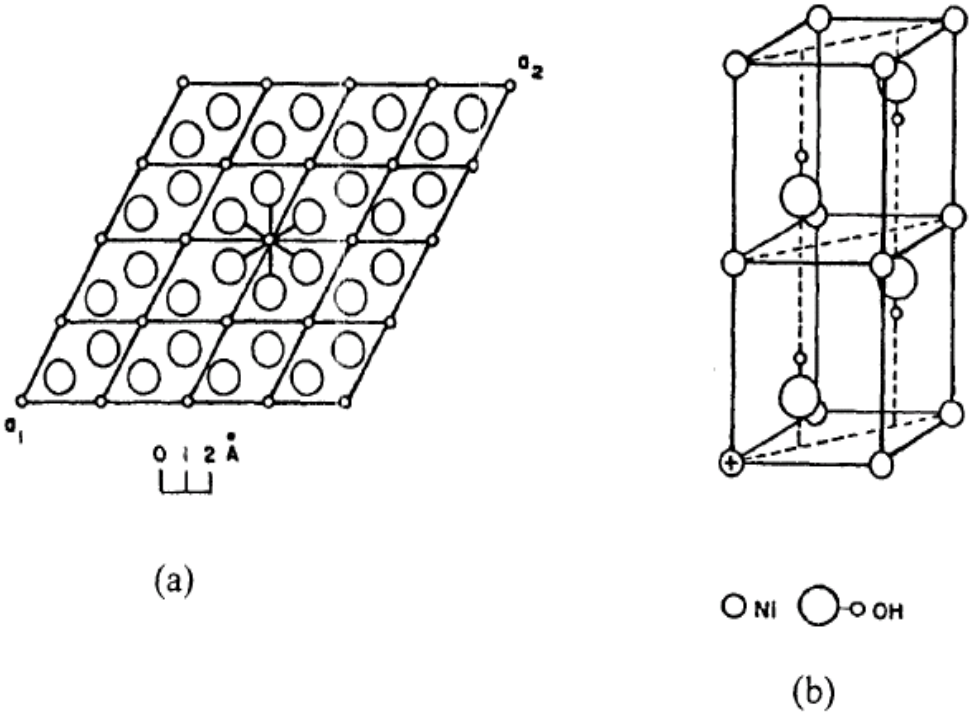

Figure 14. The brucite structure of β-$Ni(OH)_2$. (a) The hexagonal brucite layer – alternate O atoms are above and below the plane of the Ni atoms. (b) The stacking of the planes showing the orientation of the O-H bonds. Modified from Ref. [72].

Typical XRD spectra [85] for both α-$Ni(OH)_2$ and β-$Ni(OH)_2$ are reproduced in Figure 1.4.5. The α-$Ni(OH)_2$ was prepared [86] by the cathodic electrodeposition of a film of the oxide onto a Pt plate in a solution of 0.1 M $Ni(NO_3)_2$. The film was removed from the plate, washed, dried in desiccator, and ground into powder form for the XRD measurement. The β-$Ni(OH)_2$ material was prepared according to the Bode scheme by ageing a sample of the α powder in a 6 M KOH solution at 70°C for 45 minutes.

Comparison of the diffraction patterns in Figure 15 indicates that the α phase is significantly more amorphous than the β phase, which displays crystallographic peaks with superior resolution and intensity. This data corroborates older XRD work by Le Bihan and Figlarz [84]. These workers demonstrated that the principal difference between the α-$Ni(OH)_2$ and β-$Ni(OH)_2$ phases arises in the stacking of the planes along the c axis. They reported an interlamellar distance of ca. 8 Å and envisaged that the brucite like layers are misoriented with respect to each other. Furthermore they proposed that the expansion of the c-axis spacing, relative to that characteristic of the β phase, is due to the presence of water molecules and anionic species in the van der Waals gap, leading to the formation of a turbostratic phase. They further contended that the water molecules separating the brucite planes are hydrogen bonded to the Ni-OH groups in these planes. These hydrogen bonded interlamellar H_2O molecules are often referred to as *intercalated* water [74(a)] as distinct from adsorbed surface water. TGA measurements performed by Mani and deNeufville [85] found that the surface adsorbed water is removed at temperatures between 50° and 90°C, while the intercalated water is removed at higher temperatures up to 180°C.

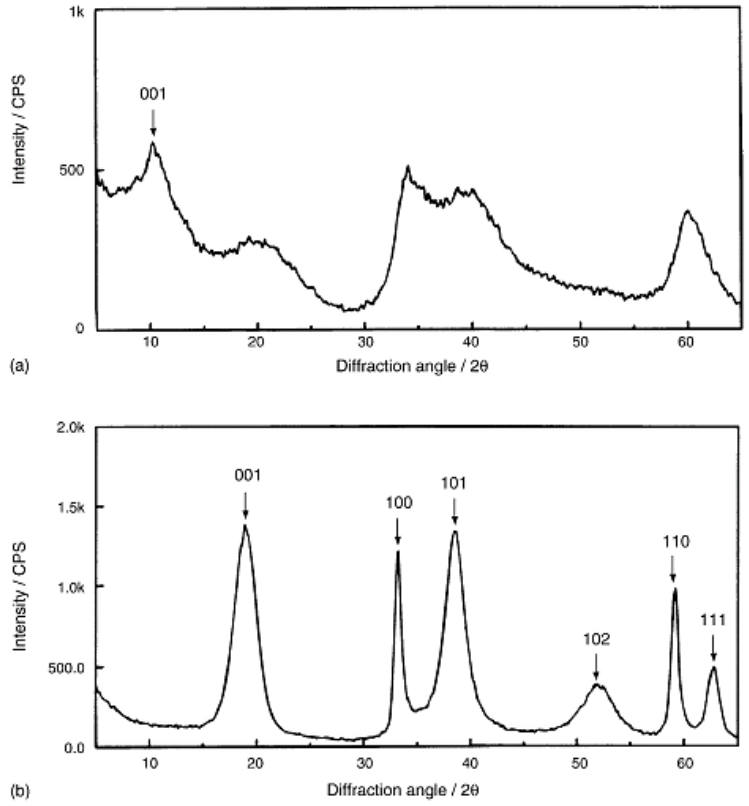

Figure 15. XRD patterns of (a) α-$Ni(OH)_2$ and (b) β-$Ni(OH)_2$. See text for more details. Modified from Ref. [85]

In his nickel hydroxide review [72] McBreen, has compared Raman spectroscopy results, obtained by various workers, on α-$Ni(OH)_2$ prepared by different means, including chemical precipitation, cathodic deposition and electrochemical reduction of γ-NiOOH. He concluded that there were differences in these spectra, both in the lattice modes and the O-H stretching modes, depending on the preparation method. Interestingly, in terms of the present work, he proposes that the shifts in the lattice modes for the reduced γ-NiOOH, may be due to the material having an oxidation state greater than Ni(II) (c.f. the graphical scheme in Figure 13). From the point of view of electronic conductivity, it has been found using photoelectrochemical measurements, that $Ni(OH)_2$ is a rather poor electronic conductor [87,88]. It displays p-type conductivity with an estimated band-gap of ca. 3.7 eV [88].

It is difficult to make accurate determinations of the structures of the β-NiOOH and γ-NiOOH since they are amorphous materials [74(a)], however it is generally accepted that they do display greater structural organization than α-$Ni(OH)_2$ [89] . In the case of β-NiOOH it is thought that the brucite structure is more or less maintained upon oxidation of β-$Ni(OH)_2$. The unit cell parameters change from a_0 = 3.126 Å and c_0 = 4.605 Å for β-$Ni(OH)_2$ to a_0 = 2.82 Å and c_0 = 4.85 Å for β-NiOOH [74(a)] . Clearly this indicates an expansion along the c-axis, but a contraction in the in-plane Ni distance [90] on the oxidation of β-$Ni(OH)_2$ to β-NiOOH. It has long been appreciated [91,92] that β-NiOOH obtained from the electrochemical oxidation of β-$Ni(OH)_2$ displays a Ni oxidation state of

2.7-2.8 rather than the expected value of 3.0, again pointing to the non-stoichiometric nature of the various phases envisaged by the Bode scheme. Despite this it is often pointed out (e.g. [91, 93]) that anodically prepared NiOOH will rarely be free from some amount of Ni in the +IV oxidation state. Kober [90,92] reported the replacement of a sharp infrared band at 3644 cm^{-1}, attributed to hydroxyl groups in the brucite structure (see Figure 14), by a more diffuse band at 3450cm^{-1} upon oxidation of β-$Ni(OH)_2$. The later band indicates, that upon the removal of half the protons from the unit cell, hydrogen bonding occurs between the remaining protons and the O atoms in the brucite structure, thus rationalizing the observed changes in a_0 and c_0. Having reviewed much literature in this area McBreen [72] comments that "β-NiOOH probably has some adsorbed and absorbed water" but there is a lack of relevant data (e.g. TGA data) available on this question.

From the point of view of electronic conductivity, the photoelectrochemical work of Carpenter et al. [93] and Madou et al. [86] indicates that β-NiOOH is a much better conductor than its reduced form – it displays n-type conductivity with an estimated band-gap of ca. 1.75 eV [93]. This enhanced conductivity relative to $Ni(OH)_2$ and also the γ form of NiOOH (which contains more Ni^{4+} - this forms an oxide of lower conductivity [94,95]) is probably one of the reasons that that β-NiOOH is sometimes referred to as "the right type of oxide" [95] for the catalysis of the o.e.r.

As indicated by the Bode scheme (Figure 13) γ-NiOOH is obtained by the oxidation of the turbostratic α-$Ni(OH)_2$ phase, or by the overcharge of β-NiOOH in concentrated alkaline solution. In comparison to the disorganized α-$Ni(OH)_2$ precursor with its misoriented layers, γ-NiOOH has a much more organized layer structure with a c_0 value of 7.2 Å [72]. Having compared XRD data for the various phases in the Bode scheme, McBreen [72] comments that the diffraction patterns for γ-NiOOH have more and much sharper lines than those for either α-$Ni(OH)_2$ or β-NiOOH. The increase in the inter-lamellar distance upon overcharge of β-NiOOH is attributed [72,90] to the incorporation of water solvated alkali ions in the van der Waals gap. Sac-Epee et al [96] used high resolution electron microscopy (HREM) to view, along the c-axis, both well crystallised β-$Ni(OH)_2$, and γ-NiOOH obtained from the overcharge of the former. They found that the β phase demonstrated well stacked parallel planes with a regular inter-lamellar distance of 4.6 Å. In contrast the γ-NiOOH layers were found to be strongly exfoliated, rendering interlayer distance measurement difficult (they report an average value of 7 Å). These authors summed up their findings with the following elegant description – "the solid-state process associated with the β(II) → γ(III) oxidation reaction involves strains along the c axis which are relieved by the exfoliation of the NiO_2 sheets along the c axis".

From the results of a series of charging and discharging experiments on various forms of $Ni(OH)_2$, Barnard et. al. [83] concluded that the γ-NiOOH phase has a higher Ni oxidation state of 3.3 – 3.67, compared to the oxidation state of β-NiOOH (2.7 – 3.0), owing to the presence of a relatively greater amount of Ni^{4+} charge centres. Indeed, Aleshkevich et al.[94] estimated that less energy would be required to remove a proton from a hydroxyl group bonded to a Ni^{3+} ion, than from one bonded to a Ni^{2+} ion. On the basis of this they predicted that kinetic factors would favour the oxidation of Ni(II) to Ni(IV). This is an important point, since as commented by Briggs [97] , it means that anodically prepared NiOOH will rarely be free from Ni(IV). Barnard et al. [83] took this concept a step further when they proposed that the required Ni oxidation state of 3.67 in their γ phase material could best be rationalized in terms of an empirical formula achieved by using a mixture of Ni^{2+} and Ni^{4+} cations

rather than Ni^{3+} and Ni^{4+} cations. Noting that the oxidation of α-$Ni(OH)_2$ to the γ phase occurs at a lower potential than the oxidation of β-NiOOH to this phase, these authors commented that it "is easier to rationalize the development of the co-existing phases in the α-$Ni(OH)_2$/ γ-phase system in terms of only one high valent species".

Experimental determination of the equilibrium potential for the $Ni(OH)_2 \rightarrow$ NiOOH redox process is not a trivial matter [74, 91] and thus some consideration will presently be devoted to this problem. In general it can be difficult to reconcile theoretical thermodynamic reversible potentials for the various corrosion processes involved in the formation of anodic oxide films on metal electrodes, with experimentally observed potentials (e.g. as measured by cyclic voltammetry, potential decay or galvanostatic charging curves) for these processes. As was recently commented by Liu et al. [95] there is often disagreement between measured potentials and the thermodynamic potentials predicted in the Pourbaix atlas [98]. Liu et al.[95] comment that these discrepancies are not surprising since the behaviour of electrochemically formed thin films is rarely identical to that of well defined phases of bulk oxides, and that furthermore, these films are generally hydrous in nature, containing structural water, which has a significant bearing on the thermodynamic potentials exhibited. Many of the issues regarding the experimental determination of the equilibrium potential for the $Ni(OH)_2 \rightarrow$ NiOOH are therefore applicable to the electrolytically formed oxide films on Fe and Co.

McBreen [72] asserts, that, owing to the complexity of the redox reactions of the nickel hydroxide anode, a revised pH-potential phase diagram, devised by Silverman [99] is more appropriate than Pourbaix's original effort [98]. According to Silvermans' work [99], the calculated $Ni(OH)_2$/NiOOH reversible potential is 0.41V vs. Hg/HgO. An immediate problem, that is obvious when one thinks about attempting to experimentally measure this value, is that the α-$Ni(OH)_2$/γ and β-$Ni(OH)_2$/β –NiOOH transitions will have different reversible potentials. Early attempts to measure the $Ni(OH)_2$/NiOOH reversible potential yielded inconsistent and conflicting results. These measurements were performed before the "breakthrough" of the Bode scheme in 1966 and so were hindered by a lack of understanding regarding the different phases of the charged and discharged forms of nickel hydroxide. Another important realization, regarding the use of simple open circuit potential decay measurements to determine the reversible potential, was made by Conway and Bourgault [100]. These workers realized that the $Ni(OH)_2$/NiOOH reversible potential lay above the reversible oxygen potential, and thus that potential decay measurements yielded a mixed potential. In view of this, they developed an extrapolation technique [100-103] that enabled the removal of the influence of the o.e.r. from the analysis of experimental potential decay data. Significantly, Conway and Bourgault, found that the oxygen evolution partial reaction is rate-controlling in the self discharge of the nickel oxide electrode, and they utilized this fact to obtain fundamental data related to the o.e.r. from the potential decay curves [102, 103].

From the point of view of the Ni^{2+}/Ni^{3+} reversible potential, Conway et al. [103] obtained a value of 0.424 V (vs. Hg/HgO 1M KOH) – this work was published in 1962, several years before Bode's work [81] indicated that, two different reversible potentials are possible, depending on whether the nickel hydroxide electrode is operating on the α-γ or β-β cycle. Barnard et al. [83,104] and Bernard and co-workers [105] tackled this problem in the 1980s using a modification of the measurement and data treatment procedures of Conway et al. [100-103]. Barnard et al.[83,104] prepared what they

classified as "activated" and "deactivated" β-$Ni(OH)_2$ electrodes, and also "activated" and "deactivated" α-$Ni(OH)_2$ electrodes. The recorded open circuit potentials depended on which type of electrode was examined, however in general the recorded values were 0.44 – 0.47 V (vs.Hg/HgO) for the β-β transition, and 0.39 – 0.44 V (vs. Hg/HgO) for the α-γ transition [83] . In cyclic voltammetry experiments [83] on the β-β couple the oxidation peak potential was 0.5 V, while the reduction peak potential was 0.37 V (both vs. Hg/HgO). The corresponding values for the α-γ couple were 0.43 V for the oxidation peak and 0.34 V for the reduction peak.

Little variation of the reversible potential for the β-β transition was observed with changing KOH concentrations over a range of solution concentrations from 0.01 M to 7.1 M [83,104]. On the other hand the reversible potential for the "activated" α-γ couple was observed to fall from ~ 0.423 V to ~ 0.340 V with increasing concentration over the same concentration range, whereas the reversible potential dropped from ~ 0.443 V to ~ 0.356 V as the KOH concentration was varied from 1.0 M to 10.4 M [83,104]. Significantly, it was found [104] that the variation of reversible potential with OH^- activity was reduced upon ageing of the α-$Ni(OH)_2$ material, as the later was converted to β-$Ni(OH)_2$.

It is generally believed that the $Ni(OH)_2 \rightarrow NiOOH$ reaction is a solid-state topochemical type reaction that does not involve soluble intermediates [74] . Transmission electron microscope (TEM)[143] images of micro-scale particles of a pristine β-$Ni(OH)_2$ phase, showed that upon oxidation to the γ phase, the global size and shape of the particles are retained, strongly suggesting a solid state mechanism. As was discussed previously, the IR studies of Kober [90,92] suggest that protons are removed from the brucite lattice upon oxidation of $Ni(OH)_2$. In recent times EQCM has been applied by several groups of workers seeking to elucidate details of the $Ni(OH)_2 \rightarrow NiOOH$ redox transition, work that has been reviewed by Wehrens-Dijksma and Notten [82]. On the basis of their examination of the various EQCM work performed the latter authors state that during oxidation of $Ni(OH)_2$ more mass is transferred than can be accounted for by a simple H^+ extraction as suggested by the chemical equation, $Ni(OH)_2 + OH^- \rightarrow NiOOH + H_2O + e^-$. Because electro-neutrality has to be maintained, it is envisaged that this will be accompanied by the incorporation or release of either positive or negative ions from the solution, possibly accompanied by H_2O. A variety of redox models have been proposed to describe the mass changes that take place during the oxidation of $Ni(OH)_2$. Wehrens-Dijksma and Notten [82] have divided these models into two categories – H^+ transport models or OH^- transport models.

In the various H^+ transport models that have been proposed, it is generally agreed [82] that the oxidation of $Ni(OH)_2$ takes place in two steps – insertion of cations, and deprotonation. Bernard et al. [105] have proposed a model where, initially non-hydrated $Ni(OH)_2$ (i.e. the β phase) incorporates alkali cations and different amounts of water molecules upon oxidation, depending on the alkali cation present in solution (i.e. Li^+, Na^+, K^+, Rb^+, Cs^+). In the case of initially hydrated $Ni(OH)_2$, Cheek and O'Grady [106] have proposed a model, where as oxidation proceeds with cation incorporation, different amounts of water are expelled from the lattice, again depending on which alkali cation is present in solution.

The application of OH^- transport models, follow a proposal by Feuilade and Jacoud [107] on the basis of radio isotope measurements, that the transport of hydroxide rather than that of protons is predominant in $Ni(OH)_2$ films. Wehrens-Dijksma and Notten [82] summarize a number of these OH^-

transport models in their review. Again all the models seem to agree that as oxidation proceeds, alkali metal cations are incorporated into the oxide structure. There is disagreement between the various models on whether the mass change with oxidation should depend on the cation size, with some models proposing that it is cation independent, since relatively more H_2O will be incorporated into the oxide along with the lighter cations.

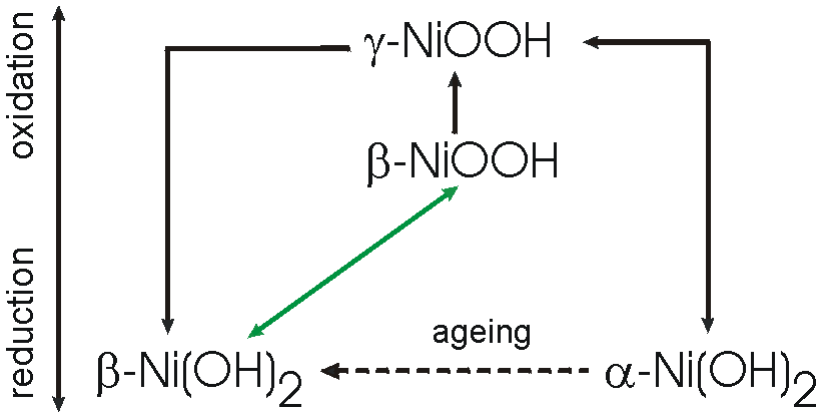

Figure 16. The Ni(II)→Ni(III) redox transition scheme envisaged by Sac-Epee et al. See text for more details.

A number of modifications to the Bode scheme (Figure 13) have been proposed. The scheme depicted in Figure 16 is due to Sac-Epee et al [96,108]. The leftmost transition in this scheme can be represented as γ-NiOOH↔ $\beta_{ex\gamma}$-Ni(OH)$_2$. The species $\beta_{ex\gamma}$-Ni(OH)$_2$ was first isolated by Sac-Epee et al.[96,108], with TEM measurements showing that this phase retained the textural features of its precursor γ(III) phase and therefore was different from the original β(II) phase. In addition these workers showed that the new $\beta_{ex\gamma}$- Ni(OH)$_2$ phase directly transformed to the γ(III) phase without having to go through the β-NiOOH phase as in the Bode sheme, i.e. the following reaction occurs directly - $\beta_{ex\gamma}$-Ni(OH)$_2$→ γ-NiOOH + H^+ +e^-. They point out that the γ-NiOOH↔ $\beta_{ex\gamma}$-Ni(OH)$_2$ cycle is a non-thermodynamically reversible process facilitated by defects, and it is possible that material locked in this cycle will remain in this reaction scheme for structural reasons, rather than following the thermodynamically predicted route (i.e. the Bode route).

Another approach has been detailed by Cornilsen and co workers [109], following their proposal, based upon Raman spectroscopy data [110], that the four electrochemically active materials (at least in their cathodically deposited forms) of the Bode scheme, actually share a common non close-packed structure with …ABBCCA…stacking. These workers assert [109] that this non close-packed structure should properly be called the γ structure and comment that it contrasts with close-packed β structure which is "electrochemically unstable under normal cycling conditions". They propose that the conventional β structure will be obtained on ageing of the "active mass" in concentrated alkaline solution. Their proposals can be summarized in the modified Bode scheme of Figure 17.

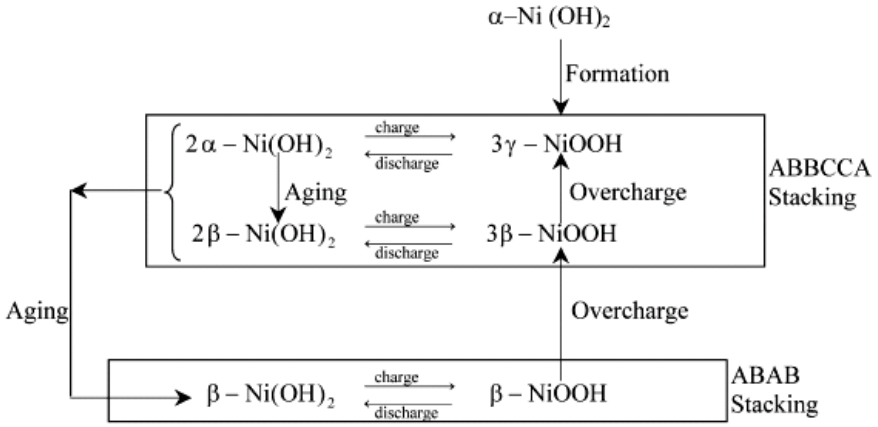

Figure 17. The Ni(II)→Ni(III) redox transition scheme envisaged by Cornilsen et al. See text for more details. Modified from [109].

Since the cycles denoted as 2α-3γ and 2β-3β involve non close-packed materials, Cornilsen et al. [109], point out that there is no phase transition involved in going from one cycle the other. They have developed a *point defect* model [110] to predict the properties of these non-stoichiometric materials, and point out that the difference between the 2α-3γ and 2β-3β cycles arises in the level of Ni vacancies, with materials in the 2α-3γ cycle having 25% Ni vacancies, while those in the 2β-3β cycle have 11% Ni vacancy defects. In their point defect model the Ni vacancies may be occupied by protons, alkali ions or may be left vacant. Varying the defect parameters can explain phenomena, such as the oxidation state of 3.67 observed by Barnard et al.[105], and can be used to quantitatively explain mass and charge capacity changes in coupled CV and EQCM experiments [109].

As was previously noted in the discussion of the lower anodic/cathodic peak couple in the CV of polycrystalline Ni in alkaline solution (Figure 11), it was postulated [74], on the basis of the variation of the anodic peak potential with pH, that the initially formed hydroxide species in this potential range is anionic in nature. In fact the peak potential decreased linearly from 0.35 V (vs. RHE) at pH 9 to ca. 0.3 V (vs. RHE) at pH 13.1, giving a mean potential/pH shift of around – 13mV/pH unit [74]. This negative potential/pH shift was rationalized in terms of the oxidised product having an overall negative charge of about 0.4 (i.e. $Ni(OH)_{2.4}^{0.4-}$) relative to the neutral reduced Ni metal, based on a two electron transfer. This is but one example of a so-called *super-Nernstian shift*, a phenomenon, that is often encountered in peak potential/pH studies on electrochemically generated hydrous oxide films, as reviewed by Burke and Lyons [26] .

Consider a metal oxide/hydroxide electrode system described by the general equation:

$$MO_n + nH_2O + 2ne^- \leftrightarrows M + 2nOH^- \quad (3.18)$$

The solubility constant, K_S, for the hydroxide is defined by reference to the equation,

$$M(OH)_n \leftrightarrows M^{n+} + nOH^- , \quad (3.19)$$

and is given by:

$$K_S = a_{M^{n+}} a_{OH-}^{n} \tag{3.20}$$

Rearranging for the metal ion activity achieves,

$$a_{M^{n+}} = \frac{K_S}{a_{OH-}^{n}} = \frac{K_S a_{H_3O+}^{n}}{K_w^{n}} \ , \tag{3.21}$$

where, K_w $(= a_{H_3O+}.a_{OH-})$ is the ionic product of water. The Nernst equation for the redox process, $M^{n+} + ne^- \leftrightarrows M$, can be written as:

$$E = E^0 - \frac{RT}{nF} \ln \frac{a_M}{a_{M^{n+}}} \tag{3.22}$$

Substituting for $a_{M^{n+}}$ from equation (4) and following the usual convention that $a_M = 1$ yields the following expression:

$$E = E^0 + \frac{RT}{nF} \ln \frac{K_S.a_{H_3O+}^{n}}{K_w^{n}} \tag{3.23}$$

Equation (3.23) can be re-written as:

$$E = E^0 + \frac{RT}{nF} \ln \frac{K_S}{K_w^{n}} - \frac{2.303RT}{F} pH \tag{3.24}$$

The potential variation with pH, for the redox transition $M^{n+} + ne^- \leftrightarrows M$, at 25ºC is then given by:

$$\frac{\partial E}{\partial pH} = -\frac{2.303RT}{F} = -0.059 \text{ V} \tag{3.25}$$

According to equation (8), the potential for an ideal oxide electrode system in aqueous solution at 25ºC, decreases with increasing pH by ca. 59 mV/pH unit, with respect to a pH independent reference electrode such as the NHE or the saturated calomel electrode (SCE). Such a shift in potential with pH, is referred to as a *Nernstian shift*, since it is predicted by the Nernst equation. It should be noted that if the reference electrode is pH dependent, such as the reversible hydrogen electrode (RHE) or the Hg/HgO electrode, no potential pH shift will be observed, since the potential of this type of electrode also alters by ca. 59 mV per unit change in pH at 25ºC.

As previously mentioned Burke and Lyons [26] have discussed super-Nernstain shifts that have been observed for various hydrous oxide systems – in these cases the potential/pH shift differs from the expected 0.059V/pH unit at 25^0C. The mathematical treatment of this situation is beyond the scope of the present review, but suffice to say, the phenomena have been qualitatively summarized [26, 36] as discussed presently. Thus, a zero potential shift (with respect to a pH dependent reference electrode) implies that both the reactants and the product possess the same net charge. A positive potential shift with pH, is indicative of an oxidised state that is more positive than the reduced state, whereas the converse is true in the case of an observed negative potential/pH shift.

Burke and Twomey [74] observed a decrease in peak potential of approximately ½(2.303 RT/F) V/pH unit for an upper cathodic peak in the CVs of a multicycled Ni anode. This was a peak that they attributed to the reduction of the γ phase to α-$Ni(OH)_2$. Another cathodic peak at slightly lower potential was assigned to the β-NiOOH → β-$Ni(OH)_2$ reduction [74] – this peak potential was found to be invariant with pH. The authors hypothesized that the pH invariant peak was indicative of an Ni(III)→ Ni(II) transition in an inner anhydrous region of the oxide film, consisting of β material. On the other hand the reduction process associated with the pH dependent peak was rationalized in terms of the following equation:

$$[Ni(OH)_{3.5} \bullet nH_2O]^{0.5-} \bullet (Na^+)_{0.5} + e^- \leftrightarrows Ni(OH)_2 \bullet n\, H_2O + 0.5Na^+ + 1.5OH^- \qquad (3.26)$$

Just like the assignment of the formula $Ni(OH)_{2.4}^{0.4-}$ to the species formed at the first anodic peak as discussed above, equation (1.4.9) represents an attempt to rationalize, in the simplest possible terms, a complex reaction, and the authors didn't necessarily claim that the reduction process follows the exact equation outlined. It was envisaged [74] that reaction outlined above occurs in an outer, dispersed hydrous region of the oxide layer, and thus super-Nernstian shifts might be regarded as being associated with the development of such hydrous films. In must be said that the model of an outer-dispersed oxide layer with a redox shift represented along the lines of the reaction presented above is consistent with the Raman based observations of Cornilsen et al. [109,110], that the nickel hydroxide film, upon cycling, consists of a non-close packed structure that doesn't conform to any of the model phases in the Bode scheme. The assignment by Burke and Twomey [74] of the structure on the left hand side of the equation outlined above to the charged form of the hydroxide, is consistent with the view of Barnard et al. [83,104] that the notion of a Ni(III) based γ phase (i.e. γ-NiOOH) is incompatible with the results of charge/discharge experiments.

Finally we should note that the ampotheric nature of metal oxides in aqueous solution can be discussed in terms of the formation of acidic -OH(a) and basic -OH(b) surface hydroxyl species. The interaction of such an acidic species with a hydrated potassium cation, in the case of immersion of the oxide in KOH solution was considered as follows; $-OH(a) + K_{aq}^+ \leftrightarrows -O^-(a)\cdot K^+ + H_{aq}^+$. Burke and co-workers [26,74] have proposed that the acidic character of hydrous oxides in involved in the formation of anionic oxidation products commenting that "anion formation may be regarded in various ways, e.g. loss of protons from coordinated water molecules, adsorption of hydroxide ions or hydroxyl complex formation".

3.3. Interfacial redox behavior of cobalt electrodes in aqueous alkaline solution

As with Ni and Fe, a brief review is presented on the electrochemistry of polycrystalline Co in aqueous alkaline solution, with the intention of gaining a conceptual understanding of the oxide surface that facilitates the o.e.r. at high anodic potentials. Cobalt hydroxides were also studied by Bode et al. [81] as part of the seminal work that lead to the development of the Bode scheme of Figure 13, that has already been discussed in relation to the nickel hydroxide electrode. In an analogous manner to the situation for divalent nickel hydroxides, there exists both hydrous α-$Co(OH)_2$ and the largely anhydrous β-$Co(OH)_2$ [81,97,111]. The structures of these materials are closely related to the corresponding phases in the nickel system. Again the β(II) phase has a brucite-like, lamellar structure, with the basal plane consisting of edge sharing CoO_6 octahedra [97,111]. This phase is pink in colour and displays a c_0 distance of 4.65 Å [111]. The α(II) phase contains excess H_2O and has an approximate composition range of $Co(OH)_2 \cdot 0.9\text{-}1.4\ H_2O$ [97]. It is blue in color, has a turbostratic structure, with a mean inter-lamellar distance of 8.4 Å [111].

Benson et al. [112], cathodically deposited blue α-$Co(OH)_2$ on Pt, and observed its oxidation behaviour in an alkaline medium. Chemical oxidation by air yielded, after some time, a brown CoOOH phase, which was found to be very resistant to oxidation beyond a formal Co charge of 2.14. This material has been studied by several workers, has been found to display a c_0 parameter of 4.40 Å, and is denoted as β-CoOOH [111]. On anodic polarization [112], the α-$Co(OH)_2$ was readily oxidized to a phase, that exhibited an average Co oxidation state of 3.3. The inter-lamellar distance of this phase is 6.80 Å [111] and it has been recognized [97] as the Co analogue of the γ-NiOOH phase discussed in the previous section.

Cyclic voltammograms of polycrystalline Co in 1 M KOH, typical of those observed in the literature, are depicted in Figure 18. Before discussing the assignment of the peaks in this voltammogram, some experimental results on the system, as obtained by both electrochemical and other means are reviewed.

In ring disk electrode studies, Behl and Toni [113] observed small but significant amounts of dissolved Co^{2+} species, the concentration of which reached a maximum at potentials just below those corresponding to peak II in Figure 18. The amount of dissolved Co^{2+} increased with increasing KOH concentration. No soluble Co^{3+} or Co^{4+} species were observed. This data was corroborated, and added to, by a combined rotating ring disk electrode (RRDE), scanning electrochemical microscopy (SECM) study carried out more recently by Erts et al. [114]. In their ring disk electrode experiments, they observed that ~ 3% soluble species were collected in 1M NaOH in the same potential region as Behl and Toni [113], made their soluble species observation. No soluble species were detected at the ring in 0.1 M NaOH[188]. According to Erts and co-workers [114], SECM offers a more accurate method of quantification of concentrations of soluble species since "the tip electrode can be located close to the surface and more short lived species can be detected". In 1.0 M NaOH in the potential region of peak II, they observed that a "much larger fraction of the reaction proceeds through the dissolution/ precipitation path than revealed from RRDE". The disparity between the SECM results and the RRDE data was explained in terms of a rapid precipitation of the soluble Co^{2+} species, with the result that much of the soluble species couldn't escape to the bulk solution and register a ring current. In 0.1 M

NaOH no soluble species were detected by SECM [114], indicating a solid-state oxidation mechanism, in the less concentrated solution.

Ellipsometry measurements have been carried out on electrochemically generated passive films on Co in alkaline solution [115,116]. The most general conclusion of these studies was that cobalt forms two types of passive layers in alkaline solution. The first is formed at lower potentials, has a pH dependent thickness, and consists of $Co(OH)_2$ and CoO. A second passive layer is formed outside the Co(II) layer at potentials above ca. 0 V (vs. Hg/HgO) and is envisaged to consist of Co(III) and possibly Co(IV) species. X-ray photoelectron spectroscopy (XPS) measurements by Foelske et al. [117] on polycrystalline Co in 0.1 M NaOH, also emphasizes the concept of a twin layer type passive film. Below the potential region corresponding to peak III in Figure 18, the passive layer is described as being a $Co(OH)_2$ film, which can grow to 40 nm thickness, depending on time and potential. Significantly, the authors claim that no CoO was detected, at least in the early stages of passivation. At potentials anodic to peak III the outer layers of the film are said to be dominated by Co(III) species, with the XPS measurements identifying Co_3O_4 and CoOOH. In an XPS investigation of a thick hydrous oxy-hydroxide layer formed by multi-cycling a polycrystalline Co electrode in 0.5 M NaOH over a potential range of 650 mV up to just below significant oxygen evolution, the dominant species identified was Co_3O_4 [118]. In agreement with the XPS data of Foelske et al. [117], an IR study [119] could identify only the presence $Co(OH)_2$ and not CoO in the lower potential region.

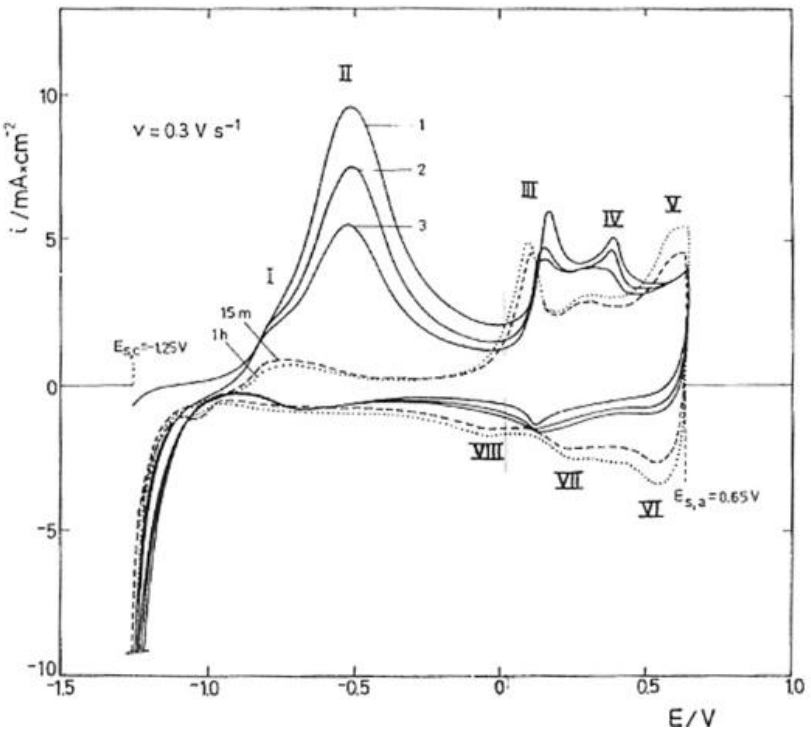

Figure 18. Cyclic Voltammograms of a polycrystalline Co electrode in 1M KOH at 25ºC vs. Hg/HgO 1M KOH. The sweep rate was 300mVs^{-1}. The first three sweeps and those recorded after both 15 min and 1 hr of cycling are shown.

Mössbauer spectroscopy studies performed in the 1970s [120] also indicated that α-$Co(OH)_2$ is the primary hydroxide species in the lower potential region. These studies involved analysis of emission spectra of the ^{57}Fe isotope derived from ^{57}Co isotopes that been plated on natural Co, which was then subjected to anodic polarization. Perhaps the most significant conclusion of this Mössbauer work was that, at high anodic potentials, the outer surface of a CoOOH film is oxidised to a Co(IV) state.

A very interesting series of papers were published by Šimpraga and Conway, in which voltammetry studies were conducted on polycrystalline Co [118] , Fe [121] and Ni [122] in alkaline media at temperatures down to 240 K. The aim of these experiments was to determine whether reversible formation of 2-D arrays of adsorbed OH or O species at sub-monolayer coverage, could be observed at low temperatures, at which re-construction of such 2-D layers into 3-D phase oxide by place exchange is thermally inhibited. It is known [123] in the cases of Pt, Rh, Ru, Ir, Pd, and Au that the initial stages of formation of anodic oxide films involves the quasi-reversible deposition of sub-monolayer extents of OH or O species. Further formation of the oxide film to monolayer coverage and beyond is highly irreversible due to the occurrence of place exchange processes. Although Šimpraga and Conway [118,121,122] noted that sub-monolayer coverage of $Co(OH)_2$, $Fe(OH)_2$ and α-$Ni(OH)_2$ could be achieved on the respective metals, in 0.5 M NaOH in a mixture of 80 mol% CH_3OH + 20 mol% H_2O at ca. 260 K, the formation and reduction processes remained completely irreversible, suggesting a nucleation and growth mechanism, rather than the 2-D surface process observed at the other metals mentioned above. Liu et al. [123], showed that the formation and reduction of the oxide film on Co in 0.5 M NaOH, progresses from the aforementioned irreversible behaviour during early potential cycles, to largely reversible behaviour upon the formation of a thick hydrous oxide with extensive cycling. Two "mirror image" reversible redox peaks, with peak potentials of ca. 525mV and 225mV (vs. Hg/HgO) were observed to become increasingly well resolved from about the 600^{th} voltammetric cycle (at 20 mV s^{-1}) through to the 2885^{th} cycle. It was found that the amount of anodic charge reversibly accessible in the 2885^{th} cycle, was only 3% of the total accumulated charge over the course of the film growth. This made the authors to conclude that, for this thick hydrous oxide film, it is only a surface region layer that displays accessible redox activity.

Regarding the interpretation of the various peaks in the CV of initially bright Co in alkaline solution (see Figure 18), there appears to be fairly good general agreement between the various authors who have tackled this problem [113,118, 123,124,125]. The approach adopted in most of the aforementioned works is based on that of Behl and Toni [113] who compared the observed peak potentials with thermodynamic data. Thus, peak I (Fig. 18) is attributed to the formation of adsorbed OH species on the electrode surface:

$$Co + OH^- \leftrightarrows CoOH_{ads} + e^- \quad (3.27)$$

The major peak II, is attributed to a combination of the formation of a passivating film of $Co(OH)_2$ and/or CoO,

$$Co + 2OH^- \leftrightarrows Co(OH)_2 + 2e^- \quad (3.28)$$

$$Co + 2OH^- \leftrightarrows CoO + H_2O + 2e^- \quad (3.29)$$

and on the basis of the ring disk electrode, and SECM measurements previously mentioned, a dissolution process forming the slightly soluble [125] Co(II) species $CoO \cdot OH^-$:

$$Co + 2OH^- \rightarrow CoO \cdot OH^-(aq) + H^+ + 2e^- \quad (3.30)$$

With repetitive potential cycling (Fig 18), it is obvious that the magnitude of peak II decreases, while the peak potential shifts to more negative values. While the charge associated with peak II is observed to decrease over the first three cycles, the magnitude of the corresponding broad cathodic peak at ca. –0.6 → -0.85 V (Hg/HgO) is observed to remain approximately invariant. Šimpraga [118] noted that the ratio of the charges associated with this set of corresponding anodic and cathodic peaks in 0.5M NaOH at 298 K, became unity after ca.15 cycles in the potential range of approximately –1.125 to -0.325 V (vs. Hg/HgO). Similar observations were made by other workers [123-125]. This behavior has been attributed to the stabilization of the developing anodic film with respect to the dissolution process of equation (1.2.26), so that after a number of cycles the anodic peak in the potential region of –0.6 to –0.8 V (Hg/HgO) should be almost entirely due to a solid state process. While the formation of a passivating CoO film is proposed by several authors [113,118, 123,124,125], it is noteworthy that, as mentioned above, more recent IR [119] and XPS [117] studies have discounted the formation of this particular Co(II) species, at least under certain conditions.

The rather poorly distinguished peaks III and IV are attributed to the oxidation of Co(II) species to Co(III) species. It is obvious that the voltammetric profile in this region changes significantly with cycling, tending eventually to the type of reversible behaviour observed by Liu et al. [123] and described above. On the first voltammetric sweep, thermodynamic data indicates that the oxidation of Co(II) species should begin in the region of –0.4 V (vs. Hg/HgO, 1M KOH), with Co_3O_4 being the initial oxidation product. Gomez Meier et al.[124] envisage this process in terms of the oxidation of an inner CoO layer to Co_3O_4 according to,

$$3CoO_{inner} + H_2O \leftrightarrows Co_3O_4 + 2H^+ + 2e^- \quad (3.31)$$

while Burke et al.[120] commented that an illustrative rationalization of the process could be provided by the reaction:

$$3Co(OH)_2 + 2OH^- \leftrightarrows Co_3O_4 + 4H_2O + 2e^- \quad (3.32)$$

As regards the actual peaks denoted III and IV in Figure 1.4.12, Burke and co-workers [125] commented that "in view of the large background currents in the anodic sweep, in the region above about 0.6 V (vs. RHE ≈ - 0.325 V vs. Hg/HgO IM), that a hydrous Co(II) film is gradually converted to such Co(III) containing species as Co_3O_4, Co_2O_3 and CoOOH". They point out that, the situation is further complicated by a number of other factors, such as the existence (according to Benson et al. [112]) of three forms of CoOOH, i.e. CoOOH(I), CoOOH(II) and $CoHO_2$. These authors add, that

hydration effects will tend to render inaccurate, the assignment, on the basis of thermodynamic data, of closely spaced peaks to specific Co(II)→Co(III) transitions. Gomez Meier et al. [124] also allude to the complex hydrous nature of the anodic oxide formed on Co in alkaline solution. These authors view the oxide growth process in terms of the formation of "sandwich-type" structures, with a $Co/CoO/Co(OH)_2$ "sandwich" formed at lower potentials. They then envisage the oxidation of a hydrous form of this "sandwich" to form a new hydrated "sandwich" structure at more positive potentials (peak III), according to the process,

$$[Co(CoO)(Co(OH)_2)\cdot xH_2O] \rightarrow [Co(CoO)(CoOOH\cdot x'H_2O)] + H^+ + x''H_2O + e^- \quad (3.33)$$

where, x"= x'+x. The nature of the "sandwich" will further change with increasing potential, with the CoO component being oxidised to Co_3O_4. According to this viewpoint, peak IV will then correspond to a process along the lines of:

$$[Co(Co_3O_4\cdot CoOOH)] + 2\ H_2O \rightarrow [Co\ (CoOOH)_4] + H^+ + e^- \quad (3.34)$$

On the basis of a perceived correlation between their voltammetric peak data and the predictions of thermodynamics, Gomez Meier et al. [124], conclude that, in the formation of the anodic film on Co, the electrochemical reactions involve fast proton transfers, and that the advance in the degree of oxidation of the metal is accompanied by a deprotonation and change in the water content at different parts of the complex electrochemical interface.

While Burke et al. [125] and Gomez Meier et al. [124] may disagree on the validity of using thermodynamic predictions to assign exact processes to given anodic peaks, there is agreement between these authors, and indeed others [118,123] that peak V is due to a surface Co(III) to Co(IV) oxidation. Burke et al. [125] attribute an electrochromic effect observed in this potential region to this Co(III) → Co(IV) transition, a process that they represent as:

$$CoOOH\ (orange) + OH^- \leftrightarrows CoO_2\ (dark\ brown) + H_2O + e^- \quad (3.35)$$

The charge associated with peak V increases on cycling, indeed cathodic peak VI corresponding to the reduction of Co(IV) species is virtually absent on the first cycle – peaks V and VI only become well defined at appreciable film thickness. This observation in tandem with the conclusions of Liu et al. [123], that the accessible reversible charge in a thick Co oxyhydroxide film resides adjacent to the surface, indicates very strongly that the oxidation of Co(III) to Co(IV) species is predominantly a surface process, occurring at the interface between a hydrous oxide layer and the solution phase. In the context of the present work, this formation of surface Co(IV) species is likely to be quite significant, occurring as it does at potentials immediately below those associated with a significant oxygen evolution current. Regarding the relatively small charge associated with the Co(III) ⇆ Co(IV) transition during the initial potential cycles, Burke et al. [125] comment that the initial film is possibly "of such a compact nature that the increase in oxygen coordination necessary to produce CoO_2 does not occur readily or, alternatively, the layer may not be of a porous hydrated structure".

The relatively small amounts of charge associated with the cathodic peaks in Figure 18 during the early potential cycles, indicates that the initially formed passivating film is not easily reduced. Peak VIII and the broad ill-defined cathodic peak at potentials between approximately –0.4 and –0.8 V (vs Hg/HgO 1M KCl) are generally attributed to the reduction of Co(III) species [123-126]. Although it is not particularly apparent in Figure 18, probably owing to the relatively fast scan rate at which these CVs were recorded, most workers [123-126] have observed a reasonably well-defined peak at ca. –1.0 V (vs. Hg/HgO, 1M). This peak is associated with the reduction of Co(II) species. As previously described, Liu et al. [123], have attributed the increasing reversibility achieved with increasing film thickness, to redox processes in the vicinity of the hydrous oxide surface. The contrast between this behaviour and the irreversibility noted during the earlier stages of film formation, reinforces the concept of the initially formed oxide (or inner regions of a thick film) being difficult to reduce.

4. TRANSITION NON NOBLE METAL HYDROUS OXIDES : MECHANISM OF ELECTROLYTIC OXYGEN EVOLUTION AND REDUCTION

4.1 . The Thermodynamics of the Oxygen Electrode

As noted in the introduction to this review, the electrochemical reduction of oxygen to water, and its anodic evolution from water, have received much research attention, owing to the importance of these reactions in practical applications and also due to their intrinsic complexity. Oxygen reduction is the normal cathodic reaction in electrochemical energy conversion and thus optimizing this reaction is the key to achieving maximum fuel oxidation in fuel cell systems. The oxygen reduction reaction (o.r.r.) is also of interest in metal-air batteries, and in corrosion studies since it serves as the counter electrode reaction in many corrosion systems. The oxygen evolution reaction (o.e.r.) is commercially important in alkaline water electrolysis, and as a counter electrode reaction for electrowinning. While one would seek to reduce the operational overpotential for the o.e.r. in an electrolyis cell, the optimisation of certain other processes calls for the inhibition of the o.e.r. For example, oxygen evolution is a competing anodic process for oxidative synthesis reactions such as chlorine production, while the o.e.r. can be detrimental to the operation of secondary alkaline batteries, owing to the so-called “self discharge” process. In this section of the review we will commence with a treatment of some of the thermodynamic aspects of the oxygen electrode, before moving on to a brief description of the o.r.r. Finally, a detailed literature review of the oxygen evolution reaction and associated issues, will be presented.

The thermodynamics of the oxygen electrode reaction has been discussed in detail by Hoare [5], Tarasevich et al. [7], and more recently in a succinct form by Lasia [127] . The following treatment is based upon the aforementioned works. Thus, the oxygen electrode reactions in both aqueous acidic (pH 0) and alkaline (pH 14) solutions at 25ºC are represented by reactions (4.1) and (4.2) respectively:

$$O_2 + 4H^+ + 4e^- \leftrightarrows 2H_2O \qquad E^0 = 1.229 \text{ V (vs. NHE)} \qquad (4.1)$$

$O_2 + 2H_2O + 4e^- \leftrightarrows 4OH^-$ $\quad E^0 = 0.401$ V (vs. NHE) (4.2)

The values of the standard potentials as quoted above have been calculated, from the best available literature values for the Gibbs free energy of formation of the various products and reactants in reactions (1.5.1) and (1.5.2) respectively. The Nernst equation for reactions (4.1) and (4.2) can be written, respectively as:

$$E = E^0 + \frac{RT}{4F}\ln p_{O_2} + \frac{RT}{F}\ln a_{H^+} - \frac{RT}{2F}\ln a_{H_2O} \quad (4.3)$$

$$E = E^0 + \frac{RT}{4F}\ln p_{O_2} + \frac{RT}{F}\ln a_{OH^-} - \frac{RT}{2F}\ln a_{H_2O} \quad (4.4)$$

where p_{O_2} denotes the partial pressure of gaseous oxygen. Examining equations (1.5.3) and (1.5.4), it is obvious that the oxygen electrode exhibits a shift in reversible potential E, with H_3O^+ or OH^- activity of RT/F per pH unit (≈ 59 mV/pH unit).

Experimental determination of the thermodynamic rest potential for the oxygen electrode has proved to be very difficult, owing to the irreversibility of the electrode reaction, even on noble metal electrodes, at which, i_0 is typically of the order of 10^{-10} A cm^{-2} at 298 K [128] .

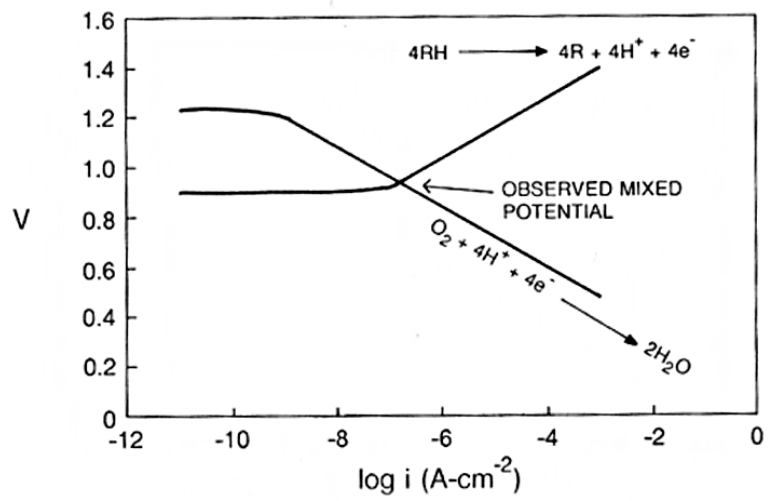

Figure 19. Schematic representation of the experimental observation of a mixed potential, for a Pt electrode in acidic solution in the presence of O_2 and an anodically oxidisable impurity RH.

This is in stark contrast to the situation for the hydrogen electrode reaction – $H^+ + e^- \leftrightarrows ½\ H_2$. The reversible potential for this reaction is easily achievable in acidic solution with a fixed H_2 gas pressure, leading to the choice of the NHE as the standard reference potential scale in aqueous electrochemistry. The essential difficulty in establishing the reversible potential arises from the low

exchange current value – thus even very low concentrations of depolarizing impurities will offset the oxygen reaction. Tarasevich et al. [7] have commented that even with very carefully prepared systems, the observed reversible potential at a Pt electrode in acidic solution with oxygen partial pressure of 1 atm at 298 K rarely exceeds 1.1 V vs. NHE. What is actually observed is a so-called *mixed potential* which is the net result of the simultaneous occurrence of two or more steady state electrode reactions. This situation is depicted schematically for the oxygen electrode in acidic solution in Figure 19.

Considering the model presented in Figure 19, the observed cathodic shift in open circuit potential from the thermodynamic reversible potential, would have to be caused by some anodic electrode reaction, providing a current of ~ 10^{-7} Acm^{-2}, to balance the oxygen reduction current at the open circuit potential.

Several theories have been advanced as to the nature of the possible depolarising reactions. Wroblowa et al. [129] considering the case of the oxygen reduction reaction at an oxide free Pt electrode in contact with an acidic solution containing O_2, proposed that the observed open circuit potential might arise from a mixed potential between the oxygen reduction reaction and an anodic reaction involving impurities. These authors listed a number of potential anodic reactions, including the following

$$Pt + 2H_2O \leftrightarrows Pt(OH)_2 + 2H^+ + 2e^- \qquad E^0 = 0.98 \text{ V (vs. NHE)} \qquad (4.5)$$

$$Pt + H_2O \leftrightarrows PtO + 2H^+ + 2e^- \qquad E^0 = 0.88 \text{ V (vs. NHE)} \qquad (4.6)$$

$$H_2O_2 \leftrightarrows O_2 + 2H^+ + 2e^- \qquad E^0 = 0.68 \text{ V (vs. NHE)} \qquad (4.7)$$

Bockris and Oldfield [130] emphasized the possible role of reaction (4.7) in determining the observed open circuit potential, while Giner [131] also suggested a mixed potential based on the O_2/H_2O_2 couple and the Pt/chemisorbed O_2 couple. In his book on the electrochemistry of oxygen, Hoare [5] is dismissive of the concept of peroxide species governing the mixed potential. His counter proposal is that the O_2/H_2O couple and a Pt/PtO couple (PtO refers to a layer of adsorbed oxygen atoms on the Pt surface) contribute to the observed open circuit potential.

The reversible oxygen potential was, first experimentally observed by Bockris and Huq [132] in 1956. These workers noted the Tafel plot for the o.e.r. deviated from the theoretical linear relation at progressively lower current densities as increasingly severe cathodic electrolysis was used to purify the electrolyte solution. To ultimately attain the reversible potential, they found that it was necessary to follow the cathodic electrolysis by an anodic purification electrolytic procedure. Strong experimental verification that the observed potential, was indeed the reversible oxygen potential, was provided by the fact that the measured potential conformed to the p_{O2} dependence predicted by equation (4.3).

The extreme irreversibility of the oxygen evolution and reduction processes, means that practical experimental kinetic studies on the respective reactions must be conducted at widely separated potentials. As a result of this, it is inevitable that the electrode surface differs considerably at the experimental potential windows of the reduction and evolution reactions, and hence the anodic and

cathodic processes are not complementary. It has, for example, been known since the 1960s [5] that while the o.r.r may proceed on both oxide-covered and bare electrode surfaces, the o.e.r. will always occur on a phase oxide surface. Therefore the principle of microscopic reversibility cannot be applied to mechanistic analysis based on current-potential data, and hence, such data can only provide information up to the rate-determining step. Earlier studies of the o.r.r. and o.e.r. used the experimentally determined value of the stoichiometric number ν given by:

$$\nu = 1 \Big/ \left[\frac{2.303RT}{n_{\Sigma}F} \left(\frac{1}{b_a} - \frac{1}{b_c} \right) \right] \tag{4.8}$$

calculated from the measured values of the cathodic and anodic Tafel slopes (b_c and b_a respectively), as a criterion in matching experimental data to a proposed reaction mechanism. This expression only applies if the activated complex in the rate determining reactions is the same for both the oxidation and reduction processes[1].

However, Parsons' analysis [133], which yielded the relation between ν and b_c and b_a, insisted

---

[1] Parsons [133] adopted a distinct yet useful approach to the problem of describing the kinetics of mutistep electrode reactions such as the o.e.r or the o.r.r. He utilized the hypothesis of *pseudo-equilibrium*, which holds that a step or number of steps preceding the rds can effectively be considered to be in equilibrium if their rate is much greater than that of the rate determining step (rds). The condition for a step j to be in pseudo-equilibrium is that $i_j \approx 0$. This in turn implies that the forward i_j and reverse i_{-j} rates are approximately equal - $i_j \approx i_{-j}$. Applying the pseudo-equilibrium approximation, Parsons obtained the following expression for the overall reaction current density,

$$i = i_0 \left\{ \exp\left[\left(\frac{n_s}{\nu_r} + n_r\beta \right) \frac{F\eta}{RT} \right] - \exp\left[-\left(\frac{n_{\Sigma} - n_s}{\nu_r} - n_r\beta \right) \frac{F\eta}{RT} \right] \right\} \tag{1}$$

where, n_r is the number of electrons transferred in the rds respectively, while n_{Σ} denotes the total number of electrons transferred in the overall reaction. The ν parameter is known as *the stoichiometric number* and is defined as the number of times the rds occurs for one act of the overall reaction. There seems to be some confusion over the meaning of the parameter n_s. For example, in Bockris and Khan's textbook [134][75], n_s is rather imprecisely defined as "the number of electrons passing before the rds". A more precise definition is provided by Damjanovic et al. [135][77], who define n_i as the number of electrons transferred in a single pre-rds step i, and ν_i as the stoichiometric number of step i. The n_s parameter is then defined as follows:

$$n_s = \sum_{i=1}^{r-1} \nu_i n_i \tag{2}$$

It is obvious that equation (1) is a version of the Butler-Volmer reaction, and may be written as:

$$i = i_0 \left\{ \exp\left[\vec{\alpha} \frac{F\eta}{RT} \right] - \exp\left[-\overleftarrow{\alpha} \frac{F\eta}{RT} \right] \right\} \tag{3}$$

where

$$\vec{\alpha} = \frac{n_s}{\nu} + n_r\beta \tag{4}$$

$$\overleftarrow{\alpha} = \frac{n_{\Sigma} - n_s}{\nu} - n_r\beta \tag{5}$$

The quantities $\vec{\alpha}$ and $\overleftarrow{\alpha}$ are the *transfer coefficients* for the forward and reverse directions of the overall reaction. While they might be considered as multistep reaction analogues of the symmetry factor β, an examination of equations (4) and (5) indicates that they are fundamentally different quantities. The symmetry factor arises from the activation of vibrational states and the energy required to break bonds. The physical basis of the transfer coefficient still incorporates these factors, since α is expressed in terms of β, however α is also associated with the stoichiometry of the reaction (through ν) and the succession of steps in the overall reaction (through n_{Σ}, n_r and n_s). It has been seen that β can generally be taken to be ½ - equations (4) and (5) imply that this isn't the case for α. In fact the value of the transfer coefficients determine the Tafel slope b ($=d\eta/d\log i$) of a multistep reaction and can be diagnostic of a particular reaction mechanism.

upon a common transition state for both anodic and cathodic reactions, a situation that is unlikely to prevail for the oxygen electrode reactions, owing to differences in the nature of the catalytic surfaces on which they occur. The dubiousness inherent in using the value of *v*, as determined from equation (4.8), as a criterion in mechanistic determinations for the o.r.r. and o.e.r., was well established by the time of Hoare's 1968 book [5].

4.2 . The Oxygen Reduction Reaction (ORR)

It perhaps is fair comment to propose that were one to choose a single electrode reaction having the greatest breadth of practical relevance, it would certainly have to be the oxygen reduction reaction (ORR). Owing to its range of practical applications the ORR has been extensively studied, and therefore there exists numerous reviews on the topic that have appeared over the years, including those due to Hoare [5], Tarasevich et al. [7], Damjanovic [136], Kinoshita [137], Bockris and Khan [128], and Gattrell and MacDougall [138], Appleby [139], Bagotskii and co-workers [140] to name but a few.

Although the kinetics and mechanism of the ORR are dependent on the electrocatalytic electrode material and the nature of the electrolyte solution, it is accepted that the overall process in aqueous solution proceeds via one of two overall pathways. The first of these is the *direct four electron pathway*, also referred to as the *parallel* pathway [138], and it can be represented by equations (4.9) and (4.10) for acidic and alkaline solutions respectively:

$$O_2 + 4H^+ + 4e^- \leftrightarrows 2H_2O \qquad E^0 = 1.229 \text{ V (vs. NHE)} \tag{4.9}$$

$$O_2 + 2H_2O + 4e^- \leftrightarrows 4OH^- \qquad E^0 = 0.401 \text{ V (vs. NHE)} \tag{4.10}$$

The E^0 values quoted, refer to the NHE, with electrolyte solutions of pH 0 for reaction (4.9) and pH 14 for reaction (4.10), and with all species in their standard states at 25ºC. The alternative pathway is the *peroxide* or *series* path [138]. This starts with a two electron reduction process, represented by equations (4.11) and (4.12) for acidic and alkaline electrolytes respectively:

$$O_2 + 2H^+ + 2e^- \leftrightarrows H_2O_2 \qquad E^0 = 0.67 \text{ V (vs. NHE)} \tag{4.11}$$

$$O_2 + H_2O + 2e^- \leftrightarrows HO_2^- + OH^- \qquad E^0 = -0.065 \text{ V (vs. NHE)} \tag{4.12}$$

These steps may be followed by the chemical decomposition of the peroxide species, according to equations (4.13) for acidic solutions and (4.14) for basic solutions:

$$2H_2O_2 \rightarrow 2H_2O + O_2 \tag{4.13}$$

$$2HO_2^- \rightarrow 2OH^- + O_2 \tag{4.14}$$

Alternatively, the peroxide species formed by reactions (4.11) and (4.12), may be electrochemically reduced, as represented by equations (4.15) and (4.16) respectively:

$$H_2O_2 + 2H^+ + 2e^- \leftrightarrows 2H_2O \qquad E^0 = 1.77 \text{ V (vs. NHE)} \qquad (4.15)$$

$$HO_2^- + H_2O + 2e^- \leftrightarrows 3OH^- \qquad E^0 = 0.867 \text{ V (vs. NHE)} \qquad (4.16)$$

As will be discussed below, the four electron pathway, consists of a number of intermediate steps, which may or may not involve an adsorbed peroxide intermediate species – however this direct pathway will not lead to solution phase peroxide. In contrast peroxide will exist as a solution phase species in the series path. This suggests that the rotating ring disk electrode studies, on the ORR at a given electrode in a particular electrolyte, should allow the determination of whether the reaction proceeds via the two electron or four electron reduction. If a ring current due to dissolved peroxide is observed then it can be concluded that the two electron path is operative, whereas no peroxide ring current would be expected for the four electron path. A problem arises with such an analysis, in the case of the series mechanism, where the electrochemical reduction of peroxide according to reactions (4.15) or (4.16) occurs at a much greater rate than the chemical decomposition of reactions (4.13) or (4.14). In this case the peroxide ring current would be very small and the analyst might be lead to the mistaken conclusion of a direct four electron pathway.

An approach towards circumventing this problem was initially proposed by Damjanovic Genshaw and Bockris [141] in the 1960s, Their idea is expressed in figure 20 in which the rotating ring disc electrode (RRDE) is used in collection mode.

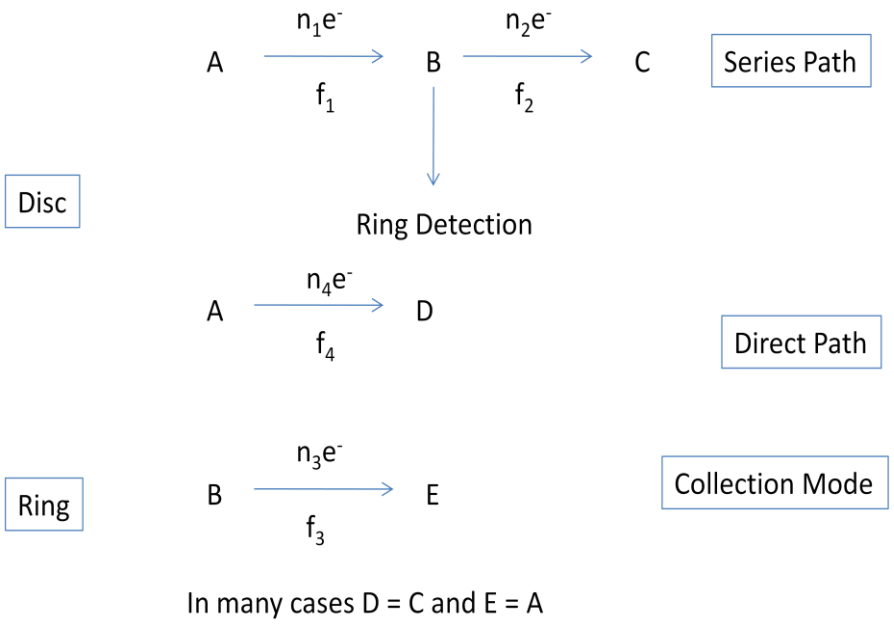

Figure 20. The DGB Model.

The DGB model [141] uses the RRDE to distinguish between an intermediate formed in an overall reaction path and a product formed in a parallel electrochemical reaction. It is useful to define a flux ratio $\chi = f_4 / f_1$, e.g. for the ORR process, $\chi = f_{O_2 \to H_2O} / f_{O_2 \to H_2O_2}$.

Now the disc current i_D is given by:

$$i_D = FAD\left\{\frac{n_1 + n_2 + \chi n_4}{1+\chi}\left(\frac{\partial a}{\partial z}\right)_0 + n_2\left(\frac{\partial b}{\partial z}\right)_0\right\} \tag{4.17}$$

Whereas the ring current i_R is given by:

$$i_R = -n_3 NFAD\left(\frac{\partial b}{\partial z}\right)_0 \tag{4.18}$$

where N denotes the collection efficiency of the RRDE assembly which is a function of electrode geometry and may be calculated using the Albery-Bruckenstein equation. At the ring we have:

$$\left(\frac{\partial b}{\partial z}\right)_0 = -\frac{b_0}{Z_D} \tag{4.19}$$

where Z_D denotes the diffusion layer thickness. Furthermore at the disc steady state conditions prevail and we require that:

$$\frac{1}{1+\chi}\left(\frac{\partial a}{\partial z}\right)_0 = -\left(\frac{\partial b}{\partial z}\right)_0 + k' b_0 \tag{4.20}$$

where k' denotes the rate constant for the reaction of the intermediate at the disc surface at z = 0. Elimination of $b_0, \left(\partial a/\partial z\right)_0, \left(\partial b/\partial z\right)_0$ yields the following characteristic expression for the disc to ring current ratio as a function of angular velocity ω:

$$\frac{i_D}{|i_R|} = \frac{n_1 + \chi n_4}{n_3 N} + \frac{\left(n_1 + n_2 + \chi n_4\right)}{n_3} k' \gamma \omega^{-1/2} \tag{4.21}$$

In the latter expression $\gamma = 1.61 D^{-2/3} \upsilon^{1/6}$ where D and ν represent the diffusion coefficient of the reactant and kinematic viscosity of the solution respectively. Hence the significant quantities k', χ may be evaluated. The DGB model predicts some limiting cases. Case I we have A → D only, so the direct process is solely operative. Here no intermediate is produced, no ring current flows and no diagnostic plot is possible. Case II pertains to A → B only, and the intermediate does not react further. Here $k' = 0$ and so $\chi = 0$. Hence the master equation reduces to:

$$\frac{i_D}{|i_R|} = \frac{n_1}{n_3} N^{-1} \tag{4.22}$$

Hence we see that $i_D/|i_R|$ is independent both of rotation speed ω and disc potential E_D (figure 21(a)). Case III pertains to the series mechanism only and so A → B → C. There is no parallel reaction so $\chi = 0$ and the master equation (4.21) reduces to:

$$\frac{i_D}{|i_R|} = \frac{n_1}{n_3} N^{-1} + \frac{(n_1 + n_2)}{n_3} N^{-1} k' \gamma \omega^{-1/2} \tag{4.23}$$

Hence plots of $i_D/|i_R|$ versus $\omega^{-1/2}$ measured at various disc potentials are linear, with slopes varying with disc potential (via the k' term) and with an intercept that is potential independent and given by the common value $n_1/n_3 N$ (figure 21(b)). Case IV considers the parallel mechanism A → B and A → D only. Here $k' = 0, \chi \neq 0$ and eqn.(4.21) reduces to:

$$\frac{i_D}{|i_R|} = \frac{n_1 + \chi n_4}{n_3 N} \tag{4.24}$$

Hence for case IV we predict that $i_D/|i_R|$ is independent of disc rotation speed ω and the intercept depends on the value of the applied disc potential E_D due to the χ term (figure 21(c)). Finally case V corresponds to the general case where both the parallel and series mechanisms conjointly operate and so A → B → C and A → D. Hence both k', χ are non-zero. This situation is illustrated in figure 21(d) where the master equation operates and both the slope and intercepts of the linear $i_D/|i_R|$ vs $\omega^{-1/2}$ plots depend on the magnitude of the disc potential E_D.

The DGB scheme depicted in figure 22 below specifically for ORR distinguishes between the peroxide mechanism via the steps characterized by rate constants k_2 and k_3, and the direct mechanism, with its earlier breaking of the O-O bond, characterized by rate constant k_1. Considering the steady state rate equations, these workers derived the following expression for the relation between the ratio of the disk current to the ring current I_D/I_R and the RRDE rotation rate ω,

$$\frac{I_D}{(I_R/N)} = \left(\frac{4k_1}{2k_2} + 1\right) + \left(\frac{4k_1}{2k_2} + 2\right) k_3 \gamma \omega^{-1/2} \tag{4.25}$$

In eqn.4.25 N is the ring collector efficiency and $\gamma = 1.61 D^{-2/3} v^{1/6}$ (D is the diffusion coefficient of peroxide and v is the kinematic viscosity).

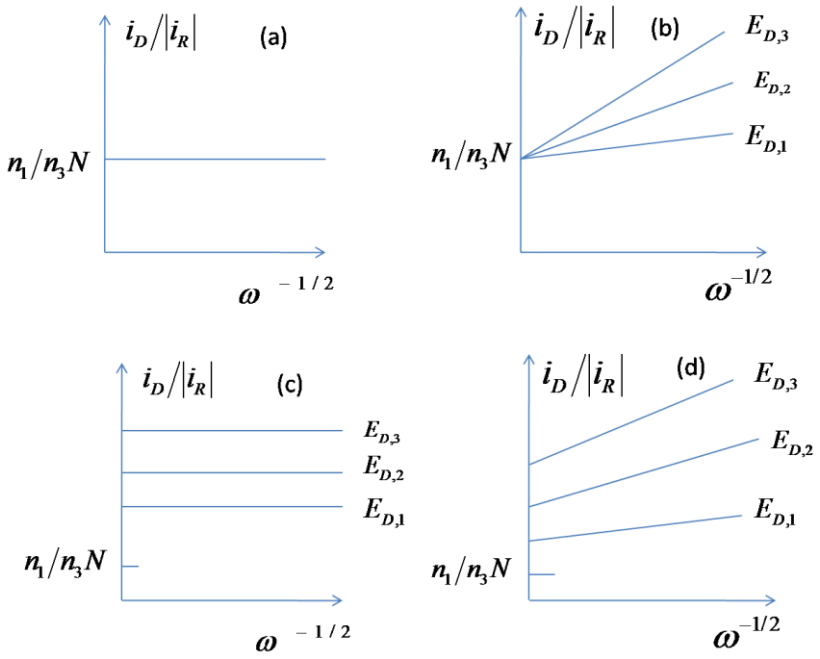

Figure 21. Diagnostic plots DGB Model.

By fitting the experimental I_D/I_R (ω) data to equation (4.25) it should be possible to determine the k_1/k_2 ratio, and thereby (recalling that for parallel reaction steps the faster one will predominate), ascertain whether the ORR proceeds via the four electron, or two electron route.

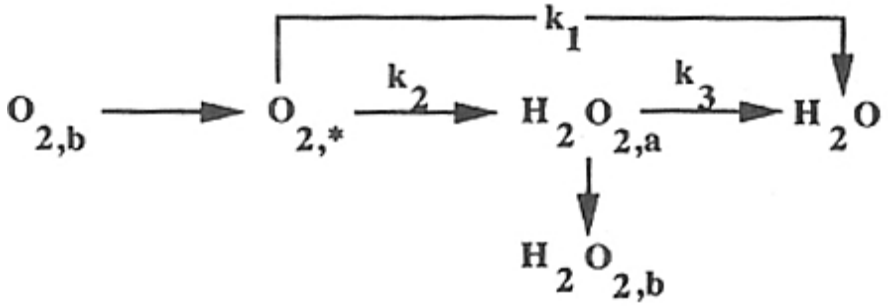

Figure 22. Model for oxygen reduction in aqueous electrolytes as proposed by Damjanovic et al.[208]. Key: a – adsorbed on electrode surface, * - in vicinity of electrode surface, b – in bulk solution. Reproduced from ref. 139.

Equation (4.25) is based on the assumption that the rate of release of the soluble peroxide species from the disk is governed by mass transport, which results in its dependence on rotation rate. This might not necessarily be the case, and in addition the simple model of Damjaniovic et al. [135(b), 141] is not sufficiently general [138] in that it doesn't include processes such as peroxide decomposition, and adsorption and desorption of reactants and products. This has limited its application to real systems, although it is reported [137] that the conclusions from Pt RRDE studies of

oxygen reduction in aqueous solutions of H_2SO_4, H_3PO_4, $HClO_4$ and KOH have been shown to be consistent with the model of Damjaniovic et al. [141]. More sophisticated modifications of the original model of Damjanovic et al. have been proposed by Wroblowa et al. [142], Appleby and Savy [143], Anastasijevic et al. [144], Bagotskii et al [145], van der Brink et al. [146] and Fischer and Heitbaum [147] amongst others. The model of Anastasijevic et al. [144] is depicted in Figure 21, and serves to show the potentially complex nature of the oxygen reduction reaction.

The operative pathway for the ORR depends strongly on the nature of the electrode surface. It would be reasonable to expect that materials that interact strongly with oxygen could bring about the dissociation of the O-O bond, thus readily facilitating the four electron mechanism. On the other hand, the two electron reduction to peroxide is more likely for electrode materials that have weak interaction with oxygen. It has been observed [139] that the direct four electron reduction is the most likely mechanism on the following substrates; the noble metals Pt, Pd, Ag, Pt alloys, perovskites, some transition metal macrocycles, metallic iron in neutral solution, and the gold (100) surface in alkaline solution. The peroxide mechanism is generally observed [138] for graphite and other carbon materials, gold (except the particular example mentioned above), mercury, most oxide covered metals including Ni and Co, mercury, most transition metal oxides e.g. NiO, and the passive film on iron in neutral solution. Platinum and its alloys generally display the greatest electrocatalytic activity towards the ORR., and are found in the vicinity of the 'apex' of volcano plots, correlating ORR activity against various physicochemical parameters.

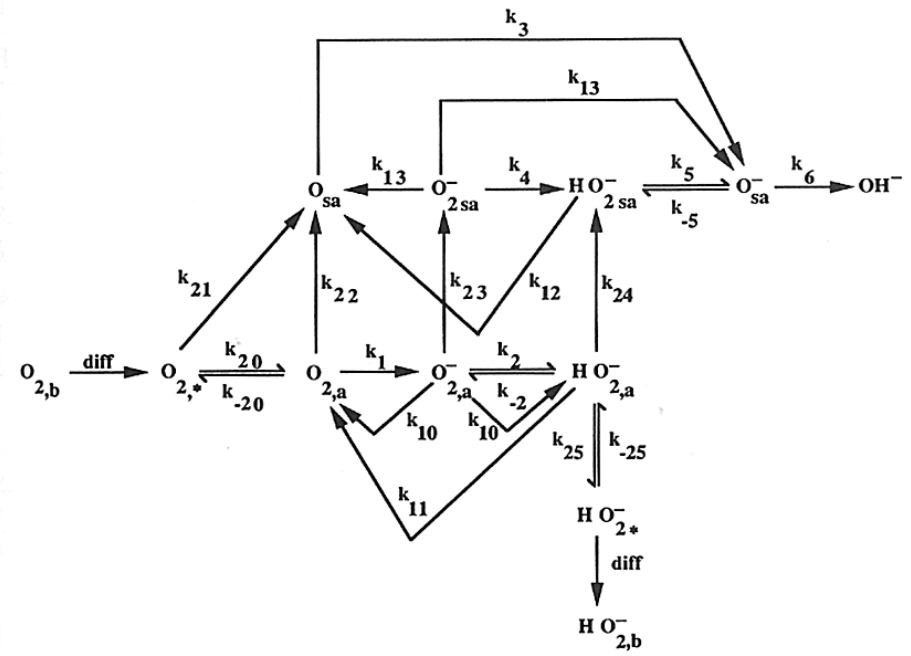

Figure 23. Model for oxygen reduction in aqueous alkaline solution proposed by Anastasijevic et al. [142]. Key: a – adsorbed on electrode surface, * - in vicinity of electrode surface, b – in bulk solution, sa – strongly adsorbed, wa – weakly adsorbed.

Table 1. ORR Mechanistic possibilities [149].

Rate-determining step	Langmuir						Temkin (0.2 < θ < 0.8)[a]		
	$\frac{\partial E}{\partial \ln i}$		$\left[\frac{\partial \ln i}{\partial \ln pO_2}\right]_{E,\ pH}$		$\left[\frac{\partial \ln i}{\partial \ln(2.3pH)}\right]_{E,\zeta^*}$		$\frac{\partial E}{\partial \ln i}$	$\left[\frac{\partial \ln i}{\partial \ln pO_2}\right]_{E,\ pH}$	$\left[\frac{\partial \ln i}{\partial \ln(2.3pH)}\right]_{E,\zeta^*}$
	θ→0	θ→1	θ→0	θ→1	θ→0	θ→1			
C-1. Bockris' electrochemical oxide path									
$O_2 \rightleftarrows 2\ O_{ads}$	∞	–	1.00	–	0	–	∞	1.00	0
$O_{ads} + H_2O + e^- \rightleftarrows OH_{ads} + OH^-$	2RT/F	2RT/F	0.50	0	0	0	2RT/F	0.00	0
$OH_{ads} + e^- \rightleftarrows OH^-$	2RT/3F	2RT/F	0.50	0	−1	0	2RT/F	0.25	0
C-2. Oxide path									
$O_2 \rightleftarrows 2\ O_{ads}$	∞	–	1.00	–	0	–	∞	1.00	0
$O_{ads} + H_2O \rightleftarrows 2\ OH_{ads}$	∞	∞	0.50	0	0	0	∞	−0.25	0
$OH_{ads} + e- \rightleftarrows OH^-$	2RT/F	2RT/F	0.25	0	0	0	2RT/F	0.50	0
C-3. Hydrogen peroxide path									
$O_2 + H_2O \rightleftarrows O_2H_{ads} + OH_{ads}$	∞	–	1.00	–	0	–	∞	1.00	0
$O_2H_{ads} + H_2O \rightleftarrows O_2H_{2ads} + OH_{ads}$	RT/F	∞	1.00	0	−1	0	∞	−0.25	0
$O_2H_{2ads} \rightleftarrows 2\ OH_{ads}$	RT/2F	∞	1.00	0	−2	0	∞	0.25	0
$OH_{ads} + e- \rightleftarrows OH^-$	2RT/F	2RT/F	0.25	0	0	0	2RT/F	0.25	0
C-4. Metal peroxide path									
$O_2 + H_2O \rightleftarrows O_2H_{ads} + OH_{ads}$	∞	–	1.00	–	0	–	∞	1.00	0
$O_2H_{ads} \rightleftarrows O_{ads} + OH_{ads}$	RT/F	∞	1.00	0	−1	0	∞	−0.25	0
$O_{ads} + H_2O \rightleftarrows 2\ OH_{ads}$	RT/2F	∞	1.00	0	−2	0	∞	0.25	0
$OH_{ads} + e- \rightleftarrows OH^-$	2RT/F	2RT/F	0.25	0	0	0	2RT/F	0.25	0
C-5. Electrochemical metal peroxide path									
$O_2 + H_2O \rightleftarrows O_2H_{ads} + OH_{ads}$	∞	–	1.00	–	0	–	∞	1.00	0
$O_2H_{ads} + e- \rightleftarrows O_{ads} + OH^-$	2RT/3F	2RT/F	1.00	0	−1	0	∞	0.00	0
$O_{ads} + H_2O \rightleftarrows 2\ OH_{ads}$	RT/2F	∞	1.00	0	−2	0	∞	0.25	0
$OH_{ads} + e- \rightleftarrows OH^-$	6RT/5F	2RT/F	0.33	0	−0.33	0	2RT/F	0.25	0
C-6. Hoar' path									
$O_2 + 2e- \rightleftarrows O^{2-}{}_{2ads}$	RT/F	–	1.00	–	0	–	RT/F	1.00	0
$O^{2-}{}_{2ads} + 2H_2O \rightleftarrows 2H_2O^-{}_{2ads}$	RT/F	∞	1.00	0	0	0	−RT/F	−0.50	0
$H_2O^-{}_{2ads} \rightleftarrows OH_{ads} + OH^-$	RT/F	∞	0.50	0	0	0	∞	0.00	0
$OH_{ads} + e- \rightleftarrows OH^-$	2RT/3F	2RT/F	0.50	0	−1	0	2RT/3F	0.50	0
C-7. Conway and Bourgaults' path									
$O_2 + H_2O \rightleftarrows O_2H_{ads} + OH_{ads}$									
$O_2H_{ads} \rightleftarrows O_{ads} + OH_{ads}$	∞	–	1.00	–	0	0	∞	1.00	0
$O_{ads} + H_2O + e^- \rightleftarrows OH_{ads} + OH^-$	RT/F	∞	1.00	0	−1	0	∞	−0.25	0
$OH_{ads} + e- \rightleftarrows OH^-$	2RT/5F	2RT/F	1.00	0	−2	0	2RT/F	0.00	0
	6RT/5F	2RT/F	0.33	0	−0.33	0	2RT/F	0.25	0
C-8. Electrochemical O_2H desorption path									
$O_2 + H_2O \rightleftarrows O_2H_{ads} + OH_{ads}$	∞	–	1.00	–	0	–	∞	1.00	0
$O_2H_{ads} + e- \rightleftarrows O_{ads} + OH^-$	2RT/3F	2RT/F	1.00	0	−1	0	2RT/F	0.00	0
$O_{ads} + H_2O + e^- \rightleftarrows OH_{ads} + OH^-$	2RT/5F	2RT/F	1.00	0	−2	0	2RT/F	0.00	0
$OH_{ads} + e- \rightleftarrows OH^-$	2RT/3F	2RT/F	0.50	0	−1	0	2RT/F	0.25	0
C-9. Riddiford's path									
$O_2 + H_2O + e^- \rightleftarrows O_2H_{ads} + OH^-$	2RT/F	–	1.00	–	0	–	2RT/F	1.00	0
$O_2H_{ads} + e- \rightleftarrows O_{ads} + OH^-$	2RT/3F	2RT/F	1.00	0	−1	0	2RT/F	0.00	0
$O_{ads} + H_2O \rightleftarrows 2\ OH_{ads}$	RT/2F	∞	1.00	0	−2	0	2RT/F	−0.50	0.5
$2\ OH_{ads} + e- \rightleftarrows OH^-$	2RT/3F	2RT/F	0.50	0	−1	0	RT/F	0.50	−0.5
C-10. Krasil'shchikov's path									
$O_2 \rightleftarrows 2\ O_{ads}$	∞	–	1.00	–	0	–	∞	1.00	0
$O_{ads} + e- \rightleftarrows O^-{}_{ads}$	2RT/F	2RT/F	0.50	0	0	0	2RT/F	0.00	0
$O^-{}_{ads} + H_2O \rightleftarrows OH_{ads} + OH^-$	RT/F	∞	0.50	0	0	0	∞	0.00	0
$OH_{ads} + e- \rightleftarrows OH^-$	2RT/3F	2RT/F	0.50	0	−1	0	2RT/F	0.25	0
C-11. Wade and Hackerman's path									
$O_2 + H_2O + 2e^- \rightleftarrows 2\ OH^-{}_{ads} + 2\ O_{ads}$									
$O_{ads} + H_2O + 2e^- \rightleftarrows 2\ OH^-{}_{ads}$	RT/F	–	1.00	0	0	–	RT/F	1.00	0
$2\ OH^-{}_{ads} \rightleftarrows 2\ OH^-$	RT/3F	2RT/F	1.00	0	−2	0	3RT/4F	0.17	0
	RT/4F	∞	1.00	0	−2	0	2RT/3F	0.33	0
C-12. Oxygen-water discharge path									
$O_2 + H_2O + e- \rightleftarrows O_2H_{ads} + OH^-$									
$O_2H_{ads} + e- \rightleftarrows O_{ads} + OH^-$	2RT/F	–	1.00	–	0	–	2RT/F	1.00	0
$O_{ads} + H_2O + e^- \rightleftarrows OH_{ads} + OH^-$	2RT/3F	2RT/F	1.00	0	−1	0	2RT/F	0.00	0
$OH_{ads} + e- \rightleftarrows OH^-$	2RT/5F	2RT/F	1.00	0	−2	0	2RT/F	0.00	0
	2RT/7F	2RT/F	1.00	0	−3	0	RT/F	0.50	−0.5

Table 1(Continued). ORR Mechanistic possibilities [149].

C-13. Damjanovic's path									
$O_2 \rightleftarrows 2\ O_{ads}$	**∞**	**—**	**1.00**	**—**	**0**	**—**	**∞**	**1.00**	**0**
$O_{ads} + H_2O \rightleftarrows (O\text{-}H\text{-}OH)_{ads}$	**∞**	**∞**	**0.50**	**0**	**0**	**0**	**∞**	**0.00**	**0**
$(O\text{-}H\text{-}OH)_{ads} + e^- \rightleftarrows (O\text{-}H\text{-}OH)^-_{ads}$	**2RT/F**	**2RT/F**	**0.50**	**0**	**0**	**0**	**2RT/F**	**0.00**	**0**
$(O\text{-}H\text{-}OH)^-_{ads} \rightleftarrows OH_{ads} + OH^-$	**RT/F**	**∞**	**0.50**	**0**	**0**	**0**	**∞**	**0.00**	**0**
$OH_{ads} + e^- \rightleftarrows OH^-$	**2RT/3F**	**2RT/F**	**0.50**	**0**	**−1**	**0**	**2RT/F**	**0.25**	**0**
C-14. Electrochemical hydrogen peroxide desorption path									
$O_2 + H_2O + e^- \rightleftarrows O_2H_{ads} + OH^-$	2RT/F	—	1.00	—	0	—	2RT/F	1.00	0
$O_2H_{ads} + e^- \rightleftarrows O_{ads} + OH^-$	2RT/3F	2RT/F	1.00	0	−1	0	2RT/F	0.00	0
$O_{ads} + H_2O \rightleftarrows (O\text{-}H\text{-}OH)_{ads}$	RT/2F	∞	1.00	0	−2	0	∞	0.00	0
$(O\text{-}H\text{-}OH)_{ads} + e^- \rightleftarrows (O\text{-}H\text{-}OH)^-_{ads}$	2RT/5F	2RT/F	1.00	0	−2	0	2RT/F	0.00	0
$(O\text{-}H\text{-}OH)^-_{ads} \rightleftarrows OH_{ads} + OH^-$	RT/3F	∞	1.00	0	−2	0	∞	0.00	0
$OH_{ads} + e^- \rightleftarrows OH^-$	2RT/7F	2RT/F	1.00	0	−3	0	RT/F	0.50	−0.5
C-15. O'Grady's path									
$O_2 + 2H_2O \rightleftarrows 2\ OH^+_{ads} + 2\ OH^-$	∞	—	1.00	—	0	—	∞	1.00	0
$OH^+_{ads} + e^- \rightleftarrows OH_{ads}$	2RT/F	2RT/F	0.50	0	−1	0	2RT/F	0.00	0
$OH_{ads} + e^- \rightleftarrows OH^-$	2RT/3F	2RT/F	0.50	0	−1	0	2RT/F	0.25	−0.5
C-16. Bagotskil's path									
$O_2 + e^- \rightleftarrows O^-_{2ads}$	2RT/F	—	1.00	—	0	—	2RT/F	1.00	0
$O^-_{2ads} + H_2O \rightleftarrows O_2H_{ads} + OH^-$	RT/F	∞	1.00	0	0	0	∞	0.00	0
$O_2H_{ads} + e^- \rightleftarrows O_2H^-_{ads}$	2RT/3F	2RT/F	1.00	0	−1	0	2RT/F	0.00	0
$2\ O_2H^-_{ads} \rightleftarrows O_2 + 2\ OH^-$	RT/4F	∞	2.00	0	−2	0	RT/F	1.00	0
C-17. O_2H^+ Electrochemical desorption path									
$O_2 + H_2O \rightleftarrows O_2H^+_{ads} + OH^-$	∞	—	1.00	—	0	—	∞	1.00	0
$O_2H^+_{ads} + e^- \rightleftarrows O_2H_{ads}$	2RT/F	2RT/F	1.00	0		0	2RT/F	0.00	0
$O_2H_{ads} + e^- \rightleftarrows O_2H^-_{ads}$	2RT/3F	2RT/F	1.00	0	$-1(-0.5)^b$	0	2RT/F	0.00	0
$2\ O_2H^-_{ads} \rightleftarrows O_2 + 2\ OH^-$	RT/4F	∞	2.00	0	−1 −2	0	∞	1.00	−1

***ζ is the p.d. between outer Helmholtz plane and the bulk of the solution.**
[a] Temkin interaction parameter for all intermediates is taken as equal.
[b] Value for the coefficient, when ζ is not constant. Thus, with the step

$$O_2H^+_{ads} + e^- \rightleftarrows O_2H_{ads}$$

as rds

$$[\partial \ln i / \partial (2.3pH)]_E = -1 + (\beta - 1)(F/2.303RT)\,[\partial \zeta / \partial pH]_E$$

The ζ potential may be related approximately to C_{OH^-} by an equilibrium equation

$$\zeta = \zeta_0 - (RT/F) \ln C_{OH^-}$$

Hence

$$[\partial \ln i / \partial (2.3pH)]_E = -0.5$$

There exists in the literature several comprehensive summaries of step-wise reaction mechanisms. The first of these was due to Damjanovic et al. [8,135] who listed 14 mechanistic schemes along with their theoretical Tafel slopes (calculated on the basis of Langmuir adsorption conditions) and stoichiometric numbers. Gnanamuthu and Petrocelli [148] listed 16 reaction schemes (the 14 listed in [8] plus 2 more) and indicated if a particular step was a candidate for RDS in either acid or alkaline solution, based upon the experimental data known for Pt and Au at the time. The most comprehensive and informative list of ORR mechanisms is that due to Pillai and Bockris [149].

This summary, illustrated in outline form in table 1 above, quotes 17 mechanisms, along with the predicted Tafel slopes, and reaction orders with respect to both oxygen partial pressure and H_3O^+ or OH^- concentration, in the case of any given step in any mechanism being the RDS. The theoretical mechanistic parameters are quoted for both Langmuir type ($\theta \rightarrow 0$ and $\theta \rightarrow 1$ cases) and Temkin type adsorption of the reaction intermediates. Obviously, the reverse of any listed ORR mechanism provides a potential OER mechanism, but it cannot in general be assumed, that if a particular oxygen

reduction mechanism applies to a given system, that the reverse of the same mechanism is operative for oxygen evolution from that system.

Recent developments and advances into developing non noble metal based electrodes for the ORR have been discussed by Viswanathan et al [150]. In recent years there has been a renewal of emphasis on examining the ORR at carbon based materials. Recent work has been reviewed by Compton and co-workers [151] and the work of Schiffrin et al [152] on ORR catalysis via surface redox catalysis at quinine modified carbon based and metallic alloy electrodes and that of the Compton group at Oxford [153] and Hu and Wang [154] on ORR catalysis at carbon nanotube modified electrodes is especially noteworthy. The seminal work reported by the McCreery group [155] is also of considerable significance. The high catalytic activity of nitrogen doped carbon nanofibre electrodes has been a topic of recent attention [156,157]. We finish this section by noting that with the exception of a recent paper by Chang and Wen [158] the ORR has not been examined in any great detail at hydrated metal oxide surfaces. This problem is currently being addressed in our laboratory and will be the report of separate communications in due course.

4.3. The oxygen evolution reaction (OER) at oxidized metal and metal oxide electrodes

Since, the principal focus of the present work is on the OER at polycrystalline Ni, Co and Fe electrodes in aqueous alkaline solution, a detailed review is now presented on the literature in this area. Although discussion of the nature of the reaction on the three aforementioned metals will receive priority in this presentation, many potentially relevant experimental observations have been made on other electrodes and in acidic solution, and some of these will also be included. Work on the OER. has been focused on gaining an understanding of the reaction mechanism, and on the development of anode materials that display stability and high catalytic activity towards the reaction. The driving forces behind this work include the need to improve the operational efficiency of alkaline water electrolysers, as well as the intrinsic scientific interest in the o.e.r. from the point of view of developing a better understanding of electrocatalysis in general. A consideration, that must be ever present in any study of oxygen evolution anodes, is that oxide growth is a parallel electrochemical process that always accompanies the OER, be it on initially oxide free metallic electrodes or on metal oxide electrodes. Thus, the possible impact of oxide growth and the influence of the oxide surface must always be born in mind when dealing with the OER. This matter will be discussed in tandem with kinetic and electrocatalytic considerations throughout this review. At the outset it is noted [137] that, in general, oxygen evolution on noble metal anodes (e.g. Pt, Ir, Rh, Ru) occurs at potentials where relatively thin oxide films are present. On base metals, such as those of interest in the present work, the oxide layers are likely to be significantly thicker. The work of Šimpraga and Conway [77,121,122] is worth recalling in this regard.

In general it has been found [137] that anodes composed of bulk metal oxides such as RuO_2, IrO_2, NiO and perovskites have superior electrocatalytic activity towards the OER relative to metallic electrodes. Briefly, addressing the question as to what general factors, dictate whether a material is a useful OER electrocatalyst or not, Ruetschi and Delahay [159] proposed that the electrocatalytic

activity of metallic electrodes decreased with an increase in metal-OH bond strength. Tseung and Jasem [160] performed a review of the properties of twenty metal oxides in order to provide guidelines for the choice of semiconducting oxides as oxygen evolving electrodes. The properties they considered were : the equilibrium potential of the metal/metal oxide or lower metal oxide/higher metal oxide couples, the conductivity, the corrosion resistance at pH 14, and the oxygen reduction performance. They found that it was difficult to get an oxide that fulfilled all of their criteria, but perhaps significantly they concluded that the most suitable candidate couples were Co_2O_3/CoO_2, Ni_2O_3/NiO_2, and 'lower' Co_2NiO_4/Co_2NiO_4. The later material, a spinel type oxide, was found to be preferable to the former two, owing to its superior electrical conductivity. While bulk RuO_2 had suitable electrical, and catalytic properties, its poor corrosion resistance in concentrated alkaline solution was highlighted by Tseung and Jasem [160], although they did note that when coated on Ti it would prove more stable with respect to corrosion. Miles et al. [161] observed the following trend in electrocatalytic activity of metal oxides towards the o.e.r. in alkaline solution Ru >Ir~Pt~Rh~Pd~Ni~Os>>Co>>Fe. Poor activities were observed on V, Cr, Mo, W, Mn, and Re oxide electrodes. The metal oxides were thermally prepared by electrodepositing from the appropriate metal chloride, and the electrocatalytic activity was measured in 30wt% KOH solutions at 80ºC.

Indeed it is accepted nowadays [17,162] that ruthenium oxide (RuO_x) is the best electrocatalyst towards the OER, especially in acidic solution where it is less prone to corrosion than in alkaline electrolyte. One of the factors contributing to its success as an o.e.r. electrocatalyst is its high electronic conductivity. Bulk samples of RuO_x display a metallic-like conductivity [137] (2×10^4 - 3×10^4 $\Omega^{-1}cm^{-1}$ at room temperature), in comparison to most other metal oxides, which are generally semiconductors or insulators. RuO_2 electrodes are generally prepared [17,162] by the thermal decomposition of $RuCl_3$, which is applied as a thin coating on a metallic substrate (generally Ti or Ni). Such electrodes are often called dimensionally stable anodes or DSAs. In contrast to the thermally prepared oxide, the anodic oxide film that forms on a metallic Ru electrode is a poor electrocatalyst towards the OER in alkaline solution [163]. Burke and Whelan [163] proposed that the poor electrocatalytic activity of the anodic oxide arose owing to a high rate of dissolution at positive potentials, with appreciable oxygen evolution currents only being observed at an over-potential of ca. 1.0 V. These workers envisaged that the anodically generated oxide layer was amorphous and hydrous in its outer region and contained a high defect concentration. The cations in the oxide film therefore exhibit a higher coordination number relative to those in the thermally prepared oxide, in which cation-cation bonding via oxygen bridging, is relatively stronger. The higher coordination number of the cations in the anodic film would allow them to pass easily into solution upon oxidation. IrO_2 also displays a low over-potential for oxygen evolution , however it is prone to corrosion in both acidic [137] and especially in alkaline [17] media.

The high corrosion resistance and relatively low cost of Ni and its alloys have lead to these metals becoming the most utilized anode materials for alkaline water electrolysis [137,164]. The choice of Ni as the anode material involves something of a balancing act, in that, while it offers advantages in cost and stability relative to other electrocatalytic materials, it also suffers from the disadvantage of having a higher oxygen evolution overpotential than, for example, RuO_2. The anodic overpotential is a major factor in limiting the operational efficiency of alkaline water electrolysers

[164], and thus efforts have been made to lower the value of this parameter as displayed by Ni. An approach [164] that has achieved some success in improving the efficiency of porous Ni anodes, involves impregnating the surface with $Ni(OH)_2$, which has the effect of lowering the overpotential by up to 60 mV in 30%wt KOH at 80ºC.

Table 2. Kinetic parameters derived for 5 most common OER mechanisms [169].

Rate-determining step	Langmuir					Temkin				
		$\frac{\partial E}{\partial \ln i}$		$\left[\frac{\partial \ln i}{\partial \ln C_{OH^-}}\right]_{E,\zeta^c}$		$\frac{\partial E}{\partial \ln i}$				
	ν^b	θ→0	θ→1	θ→0	θ→1	NA[d]	A[e]	NA[d]	A[e]	condition[f]
(I) Bockris's Oxide Path										
1. $M + OH^- \rightarrow MOH + e^-$	4	2RT/F		1						
2. $2MOH \rightarrow MO + M + H_2O$	2	RT/2F	∞	2	0	2RT/F		0.5		$r_{OH} \sim r_O$
						RT/F		1		$r_{OH} >> r_O$
3. $2MO \rightarrow 2M + O_2$	1	RT/4F	∞	4	0	RT/2F	RT/F	2	1	$K_2 \sim 1$
						RT/4F	RT/3F	2	1	$K_2 << 1$
(II) Bockris's Electrochemical Path										
1. $M + OH^- \rightarrow MOH + e^-$	2	2RT/F		1						
2. $MOH + OH^- \rightarrow MO + H_2O + e^-$	2	2RT/3F	2RT/F	2	1	2RT/F		1		$r_{OH} \sim r_O$
						RT/F		1.5		$r_{OH} >> r_O$
3. $2MO \rightarrow 2M + O_2$	1	RT/4F	∞	4	0	RT/2F	RT/F	2	1	$K_2 \sim 1$
						RT/4F	RT/3F	4	3	$K_2 << 1$
(III) Krasil'shchikov's Path										
1. $M + OH^- \rightarrow MOH + e^-$	2	2RT/F		1						
2. $MOH + OH^- \rightarrow MO^- + H_2O$	2	RT/F	∞	2	1	∞		1		$r_{OH} \sim r_{O-}$
						2RT/F		1.5		$r_{OH} >>$
3. $MO^- \rightarrow MO + e^-$	2	2RT/3F	2RT/F	2	0	2RT/F		0		r_{O-}
						2RT/F		1		$K_2 \sim 1$
4. $2MO \rightarrow 2M + O_2$	1	RT/4F	∞	4	0	RT/2F	RT/F	2	1	$K_2 << 1$
						RT/4F	RT/3F	2	1	$K_3 \sim 1$
										$K_3 << 1$
(IV) O'Grady's Path										
1. $M^z + OH^- \rightarrow M^zOH + e^-$	2	2RT/F		1						
2. $M^zOH \rightarrow M^{z+1}OH + e^-$	2	2RT/3F	2RT/F	1	0	2RT/F		0		$r_1 \sim r_2$[g]
						RT/F		0.5		$r_1 >> r_2$
3. $2M^{z+1}OH + 2OH^- \rightarrow M^z + H_2O + O_2$	1	RT/4F	∞	4	2	RT/2F	RT/F	4	3	$K_2 \sim 1$
						RT/4F	RT/3F	4	3	$K_2 << 1$
(V) Kobussen's Path										
1. $M + OH^- \rightarrow MOH + e^-$	1	2RT/F		1						
2. $MOH + OH^- \rightarrow MO + H_2O + e^-$	1	2RT/3F	2RT/3F	2	1	2RT/F		1		$r_{OH} \sim r_O$
						RT/F		1.5		$r_{OH} >> r_O$
3. $MO + OH^- \rightarrow MO_2H^-$	1	RT/2F	∞	3	1	∞		1		$K_2 \sim 1$
						RT/F		2		$K_2 << 1$
4. $MO_2H^- + OH^- \rightarrow MO_2^- + H_2O + e^-$	1	2RT/5F	2RT/F	4	1	2RT/F		1		$K_3 \sim 1$
						2RT/F		2		$K_3 << 1$
5. $MO_2^- \rightarrow M + O_2 + e^-$	1	2RT/7F	∞	4	0	RT/F	2RT/F	1		$K_4 \sim 1$
						RT/2F	2RT/3F	1	0.5	$K_4 << 1$
									1.5	

[a] **Symmetry factors, i.e. *β*, *γ*, and *δ*, in all steps, were taken as ½.** [b] **Stoichiometric number.** [c] **ζ is the potential difference between the outer Helmholtz plane and the bulk of the solution.** [d] **Nonactivated desorption of O_2.** [e] **Activated desorption of O_2.** [f] ***r* is a coefficient determining the variation of heat of adsorption of a particular species with coverage. Unless stated, *r* values for each species were taken as equal. K_i is the equilibrium constant of the *i*th step.** [g] **r_1 and r_2 refer to *r* for M^zOH and *r* for $M^{z+1}OH$, respectively.**

It is important to note [131] that akin to its cathodic counterpart the ORR, a large number of pathways for the OER can be envisaged, if all possible reaction intermediates are taken into account. Hoare [5] and Kinohita [137] both point out that if a number of assumptions are admitted, the number of possible pathways can be reduced to ten or eleven (see table 2 presented above). A further problem inherent in attempts at kinetic mechanistic analysis, lies in the fact, that even with this reduced number of candidate mechanisms, the values of kinetic parameters (such as Tafel slopes) predicted for a given path are not unique. Hence it is often very difficult to unambiguously identify the pathway operative for a particular system, however the compilation of further experimental evidence (beyond Tafel slopes) can point the analyst in a particular direction. An early kinetic mechanistic analysis of possible OER pathways was produced by Bockris [165] in 1956. In this work, the Christiansen method [166]

was applied to calculate the expected values of the Tafel slope under Langmuir intermediate adsorption conditions, in the case of any given step in a multistep mechanism being rate-determining. Five possible pathways were analysed. This analysis was advanced a step further by Conway and co-workers [103,167,168], who derived the predicted kinetic parameters for various pathways in the case of Temkin adsorption of intermediate species. Damjanovic et al. [135], listed 14 possible OER pathways giving the predicted Tafel slope value at both limitingly low and high adsorbed intermediate coverage, in the event of any given step in any one of the pathways being the RDS. Reproduced here as Table 2 is a more succinct summary of the diagnostic criteria of proposed paths for the OER that was originally provided by Bockris and Otagawa [169]. These authors describe the five particular mechanisms listed in Table 2 as being the paths most often considered in oxygen evolution studies.

The pathway of Krasil'shchikov [170] (mechanism III in Table 2), originally proposed for the OER on Ni, or modifications thereof, is almost certainly the most commonly proposed reaction mechanism for the OER on both anodic oxide films on metallic electrodes and on thermally prepared metal oxide electrodes. Authors who rationalize their data in terms of the Krasil'shchikov mechanism, have been able to attribute changes in the slopes of steady state polarisation curves with increasing overpotential, to changes in the rate determining step within the pathway. Steps 1, 2, or 3 are usually considered to be the RDS (depending on the observed Tafel slope), and thus it can be seen, that in general, the Krasil'shchikov pathway predicts that the O-O bond of the evolved oxygen molecule will be formed after the rate-determining step. The important early work of Damjanovic, Dey, and Bockris [135], regarding the OER on Pt electrodes in both acidic and alkaline solutions, led these authors to the general conclusion, that the following modified Krasil'shchikov scheme could explain the observed experimental kinetic parameters in the alkaline case:

$$M + OH^- \leftrightarrows MOH + e^- \quad (4.26)$$

$$MOH + OH^- \leftrightarrows MO\text{-}H\text{-}OH^- \quad (4.27)$$

$$MO\text{-}H\text{-}OH^- \leftrightarrows MO\text{-}H\text{-}OH + e^- \quad (4.28)$$

$$MO\text{-}H\text{-}OH \leftrightarrows MO + H_2O \quad (4.29)$$

$$2MO \leftrightarrows 2M + O_2 \quad (4.30)$$

In the scheme above (as indeed in all the pathways presented in Table 2), M represents a catalytically active site on the metal oxide surface. Experimentally, Damjanovic, Dey, and Bockris [135] had found that the anodic Tafel slope in 1 N KOH at 25ºC was approximately 2.303RT/F (~60 $mVdec^{-1}$) at lower values of overpotential η, changing to approximately 2.303×2RT/F (~120 $mVdec^{-1}$) at higher η. A cathodic slope of 2.303RT/F was measured, and hence a value of ~ 1.8 was determined for the stoichiometric number v, according to equation (1.2.83). At the time of this paper, the authors placed much value on v as a diagnostic criterion. There was perhaps some justification in this approach in the case of the pre-oxidised Pt electrodes that they utilized both in the determination of the OER and

ORR Tafel slopes. However as previously noted, the experimental value of v is rarely utilized as a diagnostic criterion in the more recent literature. In any case Damjanovic, Dey, and Bockris [135] proposed that the observed Tafel slope behaviour at low η could be rationalised by admitting step (4.27) as RDS, under low coverage Langmuir adsorption conditions, with step (4.26) becoming rate determining under Temkin adsorption conditions at higher overpotentials. Alternatively, they envisaged that step (4.27) could be rate determining over the entire Tafel region of potential, with the relevant adsorption isotherm for the reaction intermediates, being low coverage Langmuir at low η, changing to Temkin at higher η, in the case where the Temkin parameter $r_{MO} << r_{MOH}$. It can readily be seen that the value of v associated with either steps (4.26) or (4.27) is 2, corroborating the experimental value. The authors emphasized that this mechanistic rationalization of the experimental data for Pt in alkaline media was somewhat tentative – for example they didn't make a proposal for the physical conditions that might correspond to $r_{MO} << r_{MOH}$. It should be noted that in the case of adsorbed intermediates MOH and MO, the Temkin interaction parameters r values are expected to be very similar, since both species involve bonding by oxygen atoms to the substrate M.

Another important issue that was considered in detail by Damjanovic, Dey, and Bockris [135] was the origin of the change in Tafel slope observed in their experimental data from steady state polarisation measurements of Pt in 1N KOH, as outlined above. Such changes in Tafel slope with increasing overpotential are often observed in polarisation measurements that characterise the kinetics of the OER., and so the discussion of Damjanovic et al.[135] has wider applicability than the specific system that they investigated. The authors considered four possible explanations for the change in Tafel slope: (a) a change in reaction pathway, (b) a change in the electrode substrate, (c) a change in the RDS within a given pathway, and (d) the influence of changing potential on the adsorption of the reaction intermediate(s). They concluded that the latter two reasons were most likely, and that it might be possible to discriminate between behaviour due to (c) or (d) by carefully examining the steady state polarisation curves. For example, they provide a rough calculation which shows that, if the heat of adsorption of an intermediate species changes by a typical value of about 10 Kcal/mole as its fractional coverage increases from $\theta = 0.1$ to $\theta = 0.9$, then the range of potential over which Temkin conditions might be expected to prevail is limited to ~ 150 mV. Observation of the limitation of one of the straight line Tafel regions to such a potential range, would point towards (d) as opposed to (c) being the reason behind the dual slope behaviour in such a case.

Hoar [171] had also observed a Tafel slope of ca. 2.303RT/F at low overpotential for the OER. at Pt in alkaline solution, and furthermore had obtained an experimental stoichiometric number of approximately 2, data, which, as was mentioned above, was subsequently corroborated by Damjanovic, Dey, and Bockris [135]. Hoar's proposed path for the OER in alkaline media is presented below:

$$M + OH^- \leftrightarrows MOH + e^- \quad (4.31)$$

$$MOH + OH^- \leftrightarrows MH_2O_2^- \quad (4.32)$$

$$2\ MH_2O_2^- \leftrightarrows M + MO_2^{2-} + 2\ H_2O \quad (4.33)$$

$$MO_2^{2-} \leftrightarrows M + O_2 + 2e^- \quad (4.34)$$

The pathway of equation (4.31) predicts the values of *b* and *v*, found by Hoar, if step (4.32) is considered to be rate determining under Langmuir adsorption conditions. It is worth noting that Hoar's alkaline path is fundamentally different to the Krasil'shchikov mechanism, in that the O-O bond of the evolved O_2 molecule is formed as early as the second, and rate-determining step.

As is evident from Hoare's 1968 book [5] (which remained the standard text on oxygen electrochemistry for many years), with the exception of Ni, most of the early work on the OER was confined to precious metals. In view of the literature that he had reviewed, Hoare summarized the mechanisms that had been proposed up to that time (1968) for the OER in both alkaline and acidic solutions with the general scheme outlined below. He commented in the case of Pt that "most likely" the overall mechanism of oxygen evolution is the same in acid and alkaline solutions, as pointed out by Krasil'shchikov with the rate determining step as (written for acidic electrolyte)

$$(H_2O)_{ads} \rightarrow (OH)_{ads} + H^+ + e^- \text{ "} \quad (4.35)$$

He envisaged that this would be followed by a rapid reaction, either

$$(OH)_{ads} + (OH)_{ads} \rightarrow (O)_{ads} + H_2O \quad (4.36)$$

or

$$(OH)_{ads} \rightarrow (O)_{ads} + H^+ + e- \quad (4.37)$$

The final step would then be oxygen evolution,

$$(O)_{ads} + (O)_{ads} \rightarrow (O_2)_{ads} \quad (4.38)$$

and

$$(O_2)_{ads} \rightarrow O_2 \quad (4.39)$$

This scheme more or less covers , both Bockris's Electrochemical Path (which will be discussed later) and the Krasil'shchikov Path. The apparent coincidence of experimental data and theoretically predicted parameters for a scheme such as that outlined in the reaction scheme presented in eqn. (4.35) – (4.39) by Hoare, contributed to what Birss and Damjanovic [172] described in 1987 as a widely held view, that the mechanism of the OER at Pt electrodes in alkaline solution, was well understood. Experimental data in the intervening period seemed to support the view that the Krasil'shchikov pathway was the operative mechanism in the OER at Pt in alkaline media. Iwakura et al. [173], had, in agreement with the earlier work of Damjanovic, Dey, and Bockris [135], observed a

slope of ca. 60 $mVdec^{-1}$ at low current density and a second slope of ca. 120 $mVdec^{-1}$ at higher current density, during polarisation measurement on oxygen evolution at PtO_2 on a Ti substrate in alkaline solution. Furthermore they observed reaction orders with respect to OH^- concentration of approximately unity in both Tafel slope regions. This experimental data was rationalised in terms of the Krasil'shchikov mechanism (see Table 2) with the second step rate controlling at low current density, and the first step as RDS at higher current density.

Doubts however, were cast upon the conventional wisdom regarding the o.e.r. on Pt in alkaline solution, when the system was revisited by Damjanovic working with Birss [172]. These workers studied the OER. at a range of pH values between 12 and 14. They confirmed the older results of Damjanovic et al. [135] as regards the observation of a Tafel slope of ca. 60 $mVdec^{-1}$ at low current density and ca.120$mVdec^{-1}$ at higher values of current density. However, while they found a reaction order with respect to OH^- of ca. 2 at lower current densities, a value which can be accounted for by the Krasil'shchikov pathway, they observed a non-integral reaction order of 3/2 at higher values of current density. A Tafel slope of $2.303\times2RT/F$ and an associated reaction order of 3/2 cannot be reconciled with the Krasil'shchikov mechanism (or indeed according to the authors any other standard OER mechanism proposed in the literature) regardless of whether the Langmuir or Temkin isotherm is admitted. Birss and Damjanovic [172] also observed that, while the rate of reaction in the 60 $mVdec^{-1}$ Tafel region was independent of film thickness, it decreased with increasing film thickness in the upper Tafel region.

In a follow up publication [174] (oddly part II was published before part I!) they proposed a rather complex dual barrier mechanism to explain the observed behaviour. Dual barrier models will be discussed further in relation to the results obtained in our laboratory for oxide coated Fe, Ni and Co electrodes in base – for the moment it is noted that such theories envisage that only a fraction of the total potential difference across the metal/solution interface has a direct effect on the kinetics of the OER. Put simply, Birss and Damjanovic [174] proposed, that, while the potential drop between the IHP and the Pt metal varies with solution pH at a given applied potential, the potential drop across the OHP remains invariant with changing pH. They attributed the anomalous reaction order values to this effect, and showed that if the term for the potential drop across the entire interface in the kinetic equations, was replaced with a term representing the potential drop between the metal and the IHP (across the oxide film), then reaction orders of unity would be obtained for both Tafel slope regions. On the basis of this model, the authors proposed a reaction pathway, which effectively amounts to a Krasil'shchikov mechanism, altered to take account of the complex nature of the electrode/solution interface. Thus, they envisaged that the Tafel slope of ca. 120 $mVdec^{-1}$ arose from the initial discharge of an OH^- ion at the IHP, across the inner Helmholtz layer and the oxide film,

$$OH^-_{IHP} \rightarrow OH_{IHP} + e^- \quad , \qquad (4.40)$$

where a rapid equilibrium exists between the OH^- species at the IHP and those in the bulk solution. At lower current densities in the ca. 60 $mVdec^{-1}$ Tafel region, they proposed that a rate determining chemical step is operative – reactions such as,

$$OH_{IHP} + 2H_2O_{IHP} \rightarrow [H_2O_2^-{}_{IHP} + H_3O^+{}_{IHP}] \quad (4.41)$$

or,

$$OH_{IHP} + H_2O \rightarrow [O^-{}_{IHP} + H_3O^+] \quad (4.42)$$

satisfy the observed kinetic parameters. If nothing else, the example of these studies by Birss et al. [172,174], demonstrates the merits of re-examining the OER. at various substrates in the context of improving and developing the overall understanding of the reaction.

The Krasil'shchikov mechanism was originally devised for the o.e.r. on Ni [170] and several studies over the years [175] have concurred with its applicability to that system. Lu and Srinivasan [176] found that steady state polarisation measurements on the OER in 1M KOH at a Ni electrode, that had been pre-anodized at ca. 575 mV (vs. Hg/HgO 1M KOH) in the same solution (or rejuvenated by anodization under these conditions) yielded a single Tafel slope region with b = ~ 40 mV/dec^{-1}. On the other hand, Ni electrodes that had been pre-oxidised or rejuvenated at the higher potentials of ca. 0.875 V or ca. 1.075 V, yielded two Tafel slope regions – at lower current densities the slope was again ~ 40 mV/dec^{-1}, while at higher current densities a less well defined slope of ~ 170 mV/dec^{-1} was observed. The authors proposed that this kinetic data could be accounted for, by the following modified Krasil'shchikov mechanism, with step (4.45) rate determining in the low Tafel slope region of potential:

$$OH^-_{(ads)} \leftrightarrows OH_{(ads)} + e^-_{(latt)} \quad (4.43)$$

$$OH_{(ads)} + OH^- \leftrightarrows O^-_{(ads)} + H_2O \quad (4.44)$$

$$2\ \beta\text{-}NiOOH_{(surf)} + O^-_{(ads)} \leftrightarrows 2NiO_{2(surf)} + H_2O + e^-_{(latt)} \quad (4.45)$$

$$2NiO_{2(surf)} + H_2O \leftrightarrows 2\ \beta\text{-}NiOOH_{(surf)} + O_{(ads)} \quad (4.46)$$

$$O_{(ads)} + O_{(ads)} \leftrightarrows O_2 \quad (4.47)$$

Hence Lu and Srinivasan have suggested [176], based upon their experimental observations that β-NiOOH is the "right type of oxide" for the electrocatalysis of the OER. They have attributed the decrease in electrocatalytic activity, which they observed upon extended anodic polarisation, to the formation of NiO_2 on the surface of the oxide film, proposing that generation of each Ni^{4+} ion on the film surface creates an inert site for oxy evolution. The authors further proposed, based upon the optical constants derived from ellipsometric measurements on the oxide films, that the unusually high Tafel slopes of ~ 170 mV/dec^{-1} observed at high η in the case of the electrodes pre-anodized at higher potentials, arise from barrier layer effects associated with the poor conductivity of the oxide films generated at these potentials, owing to their relatively higher Ni^{4+} content.

Modified Krasil'shchikov mechanisms have also been proposed in the rationalisation of OER kinetic data obtained on Co electrodes in alkaline solution. Burke et al. [177] performed steady state polarisation measurements in 6 M KOH at 30ºC on a Co electrode, on which a hydrous oxyhydroxide layer had been grown by the potential cycling method, and also on an initially oxide free Co electrode. The potential cycling regime used in the oxide growth, involved cycling between limits of 0 and 1.2 V (vs. RHE) at 33 mVs^{-1} in 6 M KOH for 30 minutes. A Tafel slope of 60 $mVdec^{-1}$ was observed for the initially oxide free electrode, while a somewhat lower slope of 52 $mVdec^{-1}$ was recorded for the pre-cycled electrode. The polarisation curves for the two electrodes were coincident at the lowest current densities, however owing to its smaller Tafel slope, the current density achieved at the pre-cycled electrode was higher than the other electrode by a factor of 2-3 over a potential range between 1.6-1.7 V. The two polarization curves converged at higher over-potentials. These workers [177] proposed the following modification of the Krasil'shchikov pathway in order to explain their results:

$$OH^- \leftrightarrows OH_{ad} + e^- \quad (4.48)$$

$$OH_{ad} + OH^- \leftrightarrows O^-_{ad} + H_2O \quad (4.49)$$

$$Co{\cdot}O_2 + O^-_{ad} \leftrightarrows CoO_2{\cdot}O + e^- \quad (4.50)$$

$$CoO_2{\cdot}O \leftrightarrows CoO_2 + O_{ad} \quad (4.51)$$

$$2O_{ad} \leftrightarrows O_2 \quad (4.52)$$

It is noteworthy that reaction scheme presented by the set of expressions (4.48) – (4.52) is similar, in the first two steps, to that proposed by Lu and Srinivasan [176] (equations (4.43) – (4.47)), for the OER on Ni in alkaline solution as discussed above. A significant difference between these two schemes arises in the respective third steps. In step (4.45) of the scheme of Lu and Srinivasan [176], the electrocatalytically active surface species is a Ni(III) entity, with these authors placing particular emphasis on the importance of β-NiOOH in the course of the OER on an anodized Ni electrode. On the other hand, in the scheme of Burke et al. [177], the active surface species in the third step (eqn.(4.50)) is a Co(IV) entity. As was discussed earlier in this paper, there is reasonable evidence to support the existence of Co(IV) at the surface of the anodic film formed on Co in alkaline solution, at potentials immediately preceding the onset of significant oxygen evolution. Burke et al. [177] comment that the precise composition of the unstable cobalt species involved in the o.e.r. is uncertain, but do point out that cobalt peroxide can exist as a monohydrate ($CoO_2{\cdot}H_2O$), implying that the Co(IV) ion is capable of coordinating a further oxygen atom, as is envisaged in step (4.50).

In further contrast to the mechanism for the OER at Ni, as envisaged by Lu and Srinivasan [176], the experimental data of Burke et al. [177] is satisfied by admitting the second, chemical step (4.49) as the RDS, as opposed to the third electrochemical step that is rate-determining in the scheme of the former workers. Burke and co-workers [177] were unable to provide an exact explanation for the lower Tafel slope of 52 $mVdec^{-1}$ observed for the pre-cycled electrode – they made the tentative

suggestion that for this hydrous material the rate might be determined by a combination of steps (4.49) and (4.50).

Lyons and Burke [178] performed a study on both multi-cycled and initially oxide free Fe electrodes, similar to that outlined above for Co. In this case the steady state polarisation measurements were carried out in 1 M NaOH at 25ºC. The hydrous oxide film, was grown by sweeping the potential of the Fe electrode between –0.5 and 1.25 V (vs. RHE) at a rate of 350 mVs^{-1} in 1 M NaOH. It was observed that the rate of oxygen evolution was enhanced by a factor of approximately ten on the multi-cycled hydrous oxide film, relative to the rate on the initially oxide free electrode. Significantly from a mechanistic viewpoint, the same Tafel slope behaviour was observed on both types of electrode, indicating a common reaction pathway despite the differences in electrocatalytic activity. At lower overpotentials the Tafel slope adopted a value of ca. 60 $mVdec^{-1}$, changing to ca. 120 $mVdec^{-1}$ at higher potentials. As in the case of their study of oxygen evolution on Co, Lyons and Burke proposed a modified Krasil'shchikov pathway in the rationalization of their experimental data. This pathway does however exhibit some differences from reaction sequence defined in eqn.(4.48) to eqn. (4.52) as outlined below:

$$S + OH^- \leftrightarrows SOH + e^- \quad (4.53)$$

$$SOH + OH^- \leftrightarrows SO^- + H_2O \quad (4.54)$$

$$SO^- + OH^- \leftrightarrows SO_2H^- + e^- \quad (4.55)$$

$$SO_2H^- + OH^- \leftrightarrows S + O_2 + H_2O + 2e^- \quad (4.56)$$

An obvious difference between this pathway, and that proposed for Co in reactions outlined in eqn.(4.48) to eqn. (4.52) lies in the theoretical value of the stoichiometric number *v* for any given step being rate determining. For example, if any of the first three steps in the reaction sequence defined by eqn. (4.53) – eqn. (4.56) is the RDS, the associated value of *v* is 1. In contrast, if any of the first three steps in reactions defined by eqn. (4.48) – eqn.(4.52) is considered to be rate determining, then $v = 2$. Whatever about the validity of the experimental determination of *v* from anodic and cathodic polarization data in the case of the oxygen electrode reaction at Pt, it was commented by Lyons and Burke [178] that the mechanism of oxygen gas reduction on iron is most unlikely to involve the species SOH, i.e. the anodic and cathodic reactions are likely to follow considerably different pathways, thus rendering derivation of *v* from experimental data invalid in the case of Fe (and indeed Ni and Co). This is an illustration of the fact, alluded to earlier, that in the case of the oxygen electrode it simply isn't possible to obtain experimental data for steps following the RDS in oxygen evolution, by determining the Tafel slope for oxygen reduction (or indeed vice-versa). This was acknowledged by Lyons and Burke [178], who pointed out that their proposed mechanism (certainly in respect to the details of the step after the RDS) was only one of several possible sequences that could rationalize their data – a pathway analogous to reaction sequence defined by eqn.(4.53) – eqn.(4.56) might equally well be valid. In any case the real point is that traditional polarization measurements cannot yield information on an OER pathway beyond the RDS.

If the Lyons –Burke pathway is admitted, the observed 60 $mVdec^{-1}$slope corresponds to step (4.54) being rate limiting, whereas the 120 $mVdec^{-1}$slope indicates that rate control switches to the step outlined in (4.53) at high potentials. Also of interest is the identity of the catalytic species S at the oxide surface. Owing to the high potentials and high pH involved, Lyons and Burke [178] have proposed that it might well be a ferrate FeO_4^{2-} entity. This is a point worth bearing in mind, in the context of the voltammetry peaks observed by Joiret et al. [179] and attributed to Fe^{3+}/Fe^{6+} redox transition .

As previously mentioned the Krasil'shchikov pathway, is the mechanism most often invoked to explain experimental OER. data. Miles et al. [161] proposed that the polarization data that they collected for OER on oxides of various metals in 30wt% KOH solutions at 80ºC could be rationalised by the Krasil'shchikov mechanism for all the oxides. However the RDS differed depending on the exact material. Thus, it was proposed that the initial discharge step was rate limiting in the case of the oxides of Co and Fe. The chemical second step was envisaged to be the RDS for the oxides of Ru, Rh, Pd, Ni and Os. Finally, the authors attributed rate limitation in the cases of the oxides of Pt and Ir to the third step of the Krasil'shchikov path.

Gottesfeld and Srinivasan [180] observed a Tafel slope of ca. 50 $mVdec^{-1}$ for the o.e.r. on a thick hydrous layer of iridium oxide grown by potential multi-cycling on a metallic Ir electrode in 0.5 M H_2SO_4. They interpreted this data in terms of a rate determining second step of a Krasil'shchikov mechanism. Consultation of Table 2 indicates that the predicted slope in this case should be 2.303 RT/F (or ca. 60 $mVdec^{-1}$ at 25ºC). It could be suggested that the experimental slope of Gottesfeld and Srinivasan, might equally well be interpreted in terms of a rate determining third step (expected Tafel slope = ca. 40 $mVdec^{-1}$ at 25ºC), which would correspond to the prediction of Miles et al.[161] for iridium oxide as discussed above.

The OER has also been proposed to proceed via a Krasil'shchikov pathway in the case of certain perovskite materials in 1 M KOH at 25ºC. Matsumoto et al. [181] observed Tafel slopes of 65 $mVdec^{-1}$ for $La_{1-x}Sr_xCoO_3$ electrodes, both for the case of x = 0.2 and 0.4. In each case the reaction order with respect to OH^- activity was observed to be of the order of 1.8. Such data ties in very nicely with the proposal of an operative Krasil'shchikov pathway, with the chemical second step determining the overall reaction flux under limitingly low coverage of the reaction intermediate(s). A subsequent study [182] by the same authors on the OER at a wider range of perovskite materials was also indicative of oxygen evolution via the Krasil'shchikov mechanism, with the rate determining step dependent on oxide stoichiometry.

Some randomly selected more recent publications that have interpreted OER. polarisation data in terms of the Krasil'shchikov mechanism are those due to Wu et al. [183], Wang et al.[184] and Zhang et al.[185]. Wu et al.[183] studied the electrocatalytic activity of a Co and Ni mixed oxide electrode, towards the OER in alkaline media. They considered materials with five different Co^{2+}/Ni^{2+} mole ratios and found that polarization measurements on all the electrodes yielded two well defined Tafel regions. At low over-potentials the Tafel slopes ranged from 40 $mVdec^{-1}$ to 48 mV dec^{-1}, while at higher over-potentials the slopes lay between 110 and 120 $mVdec^{-1}$. The reaction orders with respect to OH^- concentration were ca. 2 in the lower Tafel region and ca. 1 in the upper Tafel region. On the basis of these observations, the authors proposed the classical Krasil'shchikov mechanism (as

presented in Table 2) to be operative for oxygen evolution on their anodes. Wang et al.[184] examined the OER at two nickel hydroxide electrodes, one of which was modified by electroless Co coating. A Tafel slope of 61 $mVdec^{-1}$, was noted for the modified electrode in an electrolyte consisting of 6 M KOH and 0.6 M LiOH, leading to the conclusion that the Krasil'shchikov mechanism with a rate determining second step was consistent with the experimental data.

The foregoing examples demonstrate that the kinetic predictions of the Krasil'shchikov mechanism have been found to be consistent with experimental data obtained for the OER on many different substrates in both alkaline and acidic media. There is a danger that this mechanism has become such an institution in this area of study, that researchers are inclined to interpret experimental kinetic data that falls anywhere close to its predicted kinetic parameters, as strong proof of the applicability of the Krasil'shchikov mechanism to the particular system under study. As an example of this Wu et al. [183] (although this phenomenon isn't limited to these workers, especially in the more recent literature) begin a communication regarding the effect of various amounts of Co on the catalytic activity of nickel hydroxide towards the OER by stating (citing Hoare's forty year old book [5]) that the Krasil'shchikov mechanism is the generally accepted pathway for the reaction on the nickel anode. They then proceed to interpret their data (a Tafel slope of 56.4 $mVdec^{-1}$ at low η, changing to 143 $mVdec^{-1}$ at higher η for the unmodified nickel hydroxide electrode) as being consistent with the Krasil'shchikov mechanism, which might be regarded as a somewhat dubious assertion.

Indeed much attention has been devoted to the Krasil'shchikov pathway in the present review – therefore the focus will now switch to some of the alternative mechanisms that have been proposed over the years. Damjanovic et al. [186] studied the kinetics of the OER at Rh, and Ir electrodes in both acidic and alkaline media. For Rh they observed a Tafel slope of 42 $mVdec^{-1}$ at low overpotentials and a slope of 115 $mVdec^{-1}$ at higher potentials in 1M NaOH. In the case of the Ir anode in the same solution a Tafel slope of 40 $mVdec^{-1}$ characterised the polarisation behaviour at low η, changing to 120 $mVdec^{-1}$ at higher values of η. This data was rationalized in terms of Bockris's Electrochemical Oxide Path (see Table 2). At low overpotential it was envisaged that the second step (an electron transfer but not the primary discharge of OH^- on the electrocatalytic site) was rate determining. At higher values of η, it was proposed that the initial discharge step becomes the RDS. This mechanism was also adopted by Sato and Okamoto [187] [237], who performed a study on the OER at the Ni anode in alkaline media. These workers observed a Tafel slope of 48 $mVdec^{-1}$ at low current densities. The steady state polarization curve adopted the properties of a limiting current (e.g. its position was highly dependent on the rate of solution stirring) at potentials anodic to the aforementioned Tafel region. At still higher current densities, a second straight line region was observed in the polarization curve with a slope of ca. 100 $mVdec^{-1}$. The authors proposed that a rate limiting adsorbed species-ion discharge step (step 2 in the Electrochemical oxide path) was compatible with the polarisation data at lower current densities. Sato and Okamoto [187] noted that the upper Tafel region appeared at the same overpotential in both alkaline and acidic media, and hence interpreted this behaviour as being indicative of a rate determining discharge of H_2O at these high current densities. Therefore the operative RDS in this region of the polarisation curve is the first step of the Electrochemical Oxide pathway, represented as $M + H_2O \leftrightarrows MOH + H^+ + e^-$.

Rasiyah and Tseung [188,189] conducted an interesting study into oxygen evolution at $NiCo_2O_4$ electrodes in alkaline media. These authors re-emphasized the earlier conclusions of Tseung and Jasem [160] [219] that for oxygen evolution on metal or metal oxide electrodes, the potential of the metal/metal oxide or the lower metal oxide/higher metal oxide couple must be achieved before gas evolution will occur. In the first part of the study [188] the nature of the oxide at the potential corresponding to the onset of significant oxygen evolution, and at potentials below this, was studied in 5M KOH at 25ºC. A cyclic voltammogram recorded at 110 $mVdec^{-1}$ showed the presence of two anodic peaks at potentials before the onset of a significant o.e.r. current, with a corresponding broad reduction peak (possibly with a shoulder) on the cathodic sweep. The authors commented that it was therefore unclear from voltammetry, whether the current passed was due to one or more oxides. They claim to have solved this problem using potential step chronocoulometry. By pulsing the potential from rest to various potentials in the potential region of interest, and then evaluating the charge passed with time as the system relaxed, the authors claim to have identified three distinct regions of current-potential behaviour. The first of these, extending from ca. 1.27 – 1.33 V (vs. NHE), they attributed to the oxidation of Co^{2+} species to Co^{3+}. The second region (1.33 – 1.43 V) was envisaged to be due to the oxidation of Ni^{2+} species to Ni^{3+}. Finally, they attributed the third region, which extended from ca. 1.43 V up to the potential of significant gas evolution, to either the oxidation of all Co^{3+} species to Co^{4+}, or alternatively to the oxidation of all trivalent, tetrahedrally coordinated ions M^{3+} to M^{4+}, stating that the latter suggestion may hold greater weight. These proposals arose from the author's earlier work, which showed that their $NiCo_2O_4$ material had the spinel structure $Co_{0.9}^{2+}Co_{0.1}^{3+}(Ni_{0.9}^{2+}Ni_{0.1}^{3+}Co^{3+})O_{3.2}^{2-}O_{0.8}^{-}$, where the ions in parentheses have tetrahedral coordination and those outside have octahedral coordination. They also observed that the total charge passed to form higher oxides was 9.7% of the maximum charge that would be passed if all cations in the $NiCo_2O_4$ material were oxidised to the +4 state, thus concluding that the formation of the higher oxides was limited to the surface of the $NiCo_2O_4$ particles. In conclusion they made the significant comment that the onset of oxygen evolution coincides with the formation of a higher valent oxide in a concerted reaction.

Rasiyah and Tseung concentrated on determining the mechanistic pathway for the OER on their $NiCo_2O_4$ electrodes in the second part [189] of the study. Galvanostatic steady state polarisation curves were recorded for the o.e.r. at various concentrations of KOH solution at 25ºC. At electrolyte concentrations $\geq$ 1.2 M, two Tafel slope regions were observed. At lower current densities the Tafel slope had a value of ~ 40 $mVdec^{-1}$, changing to a value of approximately ~ 120 $mVdec^{-1}$ at higher current densities. The Bockris Electrochemical Oxide path was proposed as the mechanism at higher current densities, where M in the scheme (see Table 2 (II)) is initially envisaged to be a divalent Ni or Co ion. This divalent species will be oxidised to a trivalent ion in the first step. In the subsequent step it is further oxidized to a tetravalent ion, as was observed in the first part of the study [188]. This second electron transfer step was proposed to be rate determining under a limitingly high fractional coverage of MOH ($\theta \rightarrow 1$).

Consulting the predicted Tafel parameters in Table 2, it would then appear that a logical explanation for the mechanism at lower current density, would be to assume the same pathway with the same RDS, except under the condition where $\theta_{MOH} \rightarrow 0$. The authors point out however that in this

potential region, according to the stoichiometric formula $Co_{0.9}^{2+}Co_{0.1}^{3+}(Ni_{0.9}^{2+}Ni_{0.1}^{3+}Co^{3+})O_{3.2}^{2-}O_{0.8}^{-}$, 2/5 of the cationic reaction sites are trivalent. If M in the Electrochemical Oxide path was assumed to be trivalent, step 2 of the mechanism would produce a pentavalent species, which runs contrary to the observations of the first part of the study [188]. Bearing this in mind the authors made the following novel prediction regarding the OER pathway at lower overpotentials:

$$T + OH^- \leftrightarrows TOH + e^- \quad (4.57)$$

$$TOH + OH^- \leftrightarrows TO^- + H_2O \quad (4.58)$$

$$TO^- + M \leftrightarrows T\text{-}O\text{-}M + e^- \quad (4.59)$$

$$2T\text{-}O\text{-}M + OH^- \leftrightarrows 2T + 2M + O_2 \quad (4.60)$$

In path defined by eqn. (4.57) – eqn. (4.60) T is a trivalent site, while M may be a divalent or trivalent site. The T-O-M site involves a bridge -bonded oxygen. Since the formal kinetic mechanistic analysis of this scheme is equivalent to that of the Krasil'shchikov pathway, the low η slope of ca. $2.303\times 2RT/3F$ can be rationalized by admitting step (4.59) as the RDS under low coverage Langmuir conditions.

Significantly, in the context of the present study a similar mechanism was proposed, for the oxygen evolution reaction on a Co anode in alkaline media, by Willems, Kobussen and co-workers [190]. The scheme (the WK pathway) envisaged by these workers takes the following form:

$$CoO + OH^- \leftrightarrows CoOOH + e^- \quad (4.61)$$

$$CoOOH + OH^- \leftrightarrows CoO_2^- + H_2O \quad (4.62)$$

$$CoO_2^- \leftrightarrows CoO_2 + e^- \quad (4.63)$$

$$CoO_2 \leftrightarrows CoO + O_{ad} \quad (4.64)$$

$$2O_{ad} \rightarrow O_2 \quad (4.65)$$

The analogy between pathway defined by eqn. (4.61) – eqn. (4.65) (which again is formally a Krasil'shchikov (type mechanism) and the pathway of Rasiyah and Tseung defined by eqn.(4.57) – eqn.(4.60) can be appreciated when one considers the charge state of the Co species in each step. In step (4.61) a Co(II) species is oxidised to Co(III). The second step in the mechanism consists of the formation of an unstable surface entity via a proton transfer step. The importance of proton transfer with solution phase species at the electrocatalytic oxide surface, in tandem with electron transfer has also been emphasized by Bockris and Otagawa [169] in their studies on the OER at perovskite

surfaces in alkaline media. The unstable Co(III) surface species is discharged in step (4.63) to form a more stable Co(IV) surface species – we recall from section 3, that significant evidence exists for the stabilisation of Co(IV) species at the surface of anodic Co oxides in concentrated alkaline solution at very positive potentials. Note that the WK pathway emphasizes that the oxygen evolution process on anodic oxide films cannot really be decoupled from the processes that occur in the formation and oxidation of the film. The oxygen evolution reaction cannot be understood without an appreciation of the surface chemistry of the substrate.

One of the few existing studies to consider together, the nature of the OER. on Ni, Co, and Fe anodes was performed by Scarr [191]. The author observed Tafel slopes of approximately 46 $mVdec^{-1}$ (~ 2.303×4RT/5F) for the OER on Ni, Co and Fe electrodes in 1M KOH at room temperature. He noted that a conventional kinetic analysis (assuming Langmuir adsorption conditions) of any of the standard proposed o.e.r. mechanisms, could not yield a prediction of a Tafel slope of 2.303×4RT/5F, regardless of which step was considered to be the RDS. A perusal of Table 2 will show that this is also the case if the Temkin adsorption isotherm is adopted. To explain his experimental data, Scarr [191] proposed the following reaction pathway:

$$M + OH^- \leftrightarrows MOH + e^- \quad (4.66)$$

$$MOH + OH^- \leftrightarrows MH_2O_2^- \quad (4.67)$$

$$MH_2O_2^- \leftrightarrows MH_2O_2 + e^- \quad (4.68)$$

$$MH_2O_2 + OH^- \leftrightarrows MHO_2^- + H_2O \quad (4.69)$$

$$MHO_2^- \leftrightarrows MHO_2 + e^- \quad (4.70)$$

$$MHO_2 + OH^- \rightarrow M + O_2 + H_2O + e^- \quad (4.71)$$

Of immediate note is the fact that the first two steps of this mechanism are common with the alkaline path of Hoar (defined by eqn.(4.31) – eqn. (4.34)) as discussed previously. An adsorbed peroxide species is formed in the second step, meaning that the O-O bond of the O_2 molecule to be evolved , is formed earlier in these pathways than in the Krasil'shchikov case.

The kinetic analysis of scheme defined by eqn.(4.66) – eqn.(4.71) is based on a dual barrier approach originally proposed by Gnanamuthu and Petrocelli [148] for the ORR, that considers the effect of the potential gradient on the reaction intermediates as a consequence of their position in the interfacial region. This means that adsorbed intermediates, which are involved in charge transfer with either the electrode or the bulk solution alone, are acted upon only by that portion of the potential associated with the particular interfacial region. The adsorbed intermediates reside at the inner Helmholtz plane, which was assumed by the author to mark the half way point in the potential gradient, therefore the fraction of the total potential applicable to either region is one half. Scarr [191] quotes the following expression for the Tafel slope *b* of a given mechanism step,

$$b = \frac{\nu}{\Sigma_i Z_i f_i + (1-\alpha) Z_r f_r} \cdot \rho \qquad (4.72)$$

where ν is the stoichiometric number, α is the transfer coefficient, Z_i is the number of charges transferred in a given step prior to the rate determining step, f_i is the fraction of the total potential difference which is effective in the i^{th} charge transfer, while Z_r and f_r have similar meanings for the RDS. Equation (4.72) arises from an expression derived by Gnanamuthu and Petrocelli [148] for this dual barrier theory, based upon Parsons' original analysis of the kinetics of multistep electrochemical mechanisms.

Applying equation (4.72) to scheme defined via eqn. (4.66) – eqn.(4.71) , if the first step is the RDS, ν = 1, α = ½ (as is conventional in this type of kinetic analysis), Z_r = 1 and f_r = 1 (since the charge is transferred between the electrode surface and the bulk solution). Inserting these values into eqn.(4.72) a Tafel slope b = 2RT/F is achieved, which means that if eqn. (4.66) were the r.d.s. a slope of ~ 120 $mVdec^{-1}$ would be expected at 25ºC. Working out b for step (4.67) we note that ν = 1, α = ½ and as before, Z_i = 1, f_i = 1 (one term in the sum since there is only one step prior to r.d.s.), Z_r = 1, and f_r = ½ since in this case the charge transfer occurs only between the bulk solution and the adsorbed intermediates. Inserting these values in equation (4.72), yields a predicted value for the Tafel slope b = 4RT/5F. It transpires that this is the only step in the latter pathway which yields this value of b upon analysis by equation (4.72). Thus Scarr [191] concluded that the OER polarisation data that he obtained on Ni, Co and Fe anodes in alkaline solution, could be satisfactorily explained by pathway defined by eqn.(4.66) – eqn.(4.71), with the chemical second step in which the O-O is formed as the RDS.

It should be commented at this stage that, if equation (4.72) is applied to either the Krasil'shchikov mechanism, as presented in Table 2, or Hoar's alkaline path, a value of 4RT/5F will also be predicted for the Tafel slope. Scarr [191] discriminated against these pathways on the basis that they involve the species MO^- or MO^{2-}. This arose from the fact that he had also observed a Tafel slope of ca. 46 $mVdec^{-1}$ at low overpotentials on a Pt electrode in 1 M KOH. On the basis of this, he proposed that the OER proceeded via a common mechanism on Ni, Co, Fe and Pt in alkaline solution. However, he believed that PtO, PtO^-, or PtO^{2-}, could not be an intermediate species in the OER at Pt, on the basis of his interpretation of results obtained some years previously by Rozental and Vesolovskii [192] [242]. Using O^{18} tracer techniques these workers had shown that O atoms that formed part of the anodic oxide layer on Pt, did not get evolved as gaseous oxygen under OER conditions. Scarr commented that oxygen adsorbed at these potentials is known to have the stoichiometry PtO, and if it is in fact not identical to the species MO, then the two should be equivalent through an exchange process. On this basis and in view of the conclusions of Rozental and Vesolovskii [192], Scarr [191] ruled out the involvement of MO^- or MO^{2-} species in the OER and thereby also ruled out the Krasil'shchikov mechanism and the Hoar alkaline mechanism. It must be said, that the question of whether oxygen atoms from an anodic oxide layer, can partake in the OER. remains contentious, and therefore Scarr's argument remains unproven.

A more recent proposal regarding the formation of the O-O bond as an adsorbed peroxide entity, in the second step of an OER pathway has come from Bockris and Otagawa [169] in an attempt to rationalize the OER behaviour observed on a range of thermally prepared perovskite materials $La_{1-x}A'_xMO_3$ (A' = Sr, K, Ca, Ce, Th, M = Cr, Mn, Fe, Co, Ni) in alkaline solution. The pathway that the authors proposed is as follows,

$$M^z + OH^- \leftrightarrows M^z\text{-}OH + e^- \quad (4.73)$$

$$M^z\text{-}OH + OH^- \leftrightarrows M^z\text{- -}H_2O_2 + e^- \quad (4.74)$$

$$(H_2O_2)_{phys} + OH^- \leftrightarrows (HO_2^-)_{phys} + H_2O \quad (4.75)$$

$$(H_2O_2)_{phys} + (HO_2^-)_{phys} \leftrightarrows O_2 + H_2O + OH^- \quad (4.76)$$

where, M^z is a transition metal ion with the valence state z+ at the surface of a perovskite. In the pathway defined by eqn.(4.73) – eqn.(4.76) the hydrogen peroxide species is envisaged to be physisorbed. Bockris and Otagawa [169] correlated the activity of the perovskite materials towards the OER with the M-OH bond strength , and concluded that the breaking of an M-OH bond is rate determining for the process. Thus, although the experimentally derived kinetic parameters could be accounted for, by either, the Bockris electrochemical oxide path, or O'Grady's path (see Table 2), these mechanisms were ruled out on the basis that the relevant rate determining steps contained M-OH or M-O species, both as reactants and products, thus making it difficult to reconcile such steps with the proposed inverse dependence of rate on M-OH bond strength. This problem is solved by admitting step (4.74) as the RDS, since, a chemical M-O bond is only involved on one side of this step. Thus the weaker the M^z-OH bond, the greater the rate of the overall reaction, in agreement with the authors hypothesis regarding the correlation of o.e.r. electrocatalytic activity with M-OH bond strength. Observed changes in Tafel slopes and reaction orders, both for different transition metals M, and at different over-potentials within the polarization curve of a given perovskite were successfully explained in terms of changes of M-OH coverage, rather than changes in the RDS [169]. A mechanism similar to the Bockris Otagawa path has been postulated by Singh and co-workers for Co_3O_4 and $NiCo_2O_4$ electrodes [193-195].

The final, possible OER pathway to be commented upon here, is that due to O'Grady et al. [196], presented in Table 2 as mechanism (IV). This mechanism was formulated to explain OER polarisation data obtained on RuO_2 electrodes in alkaline solution. O'Grady and co-workers observed a Tafel slope of ca. 40 $mVdec^{-1}$, with an associated reaction order with respect to OH^- concentration of ca. 1. In a similar manner to Rasiyah and Tseung[238, 239], these authors emphasize the importance of oxide redox transitions in the course of the OER. In the initial OH^- discharge step a surface oxide lattice ion of valance Z is oxidised to a higher valance state, with a partial transfer of electron charge from the OH^- to the metal, and the consequent formation of a $(MOH)^z$ surface complex. Oxidation of the M^z ion to $M^{z+1}OH$ is completed in the second step. Oxygen evolution occurs by the recombination of two of the higher valence $M^{z+1}OH$ species, with the regeneration of the original M^z sites. In the

original scheme of O'Grady et al. [196] it was envisaged that the M^z site corresponded to a Ru^{4+} ion. The authors rationalized their experimental data by proposing that the second step was rate determining, with low coverage Langmuir adsorption prevailing. A similar mechanism was proposed by O'Sullivan and Burke [197] for oxygen evolution on thick hydrous Rh oxides formed by repetitive potential cycling in 1 M NaOH.

In a series of recent papers [198-202] Lyons and Brandon have re-examined the OER mechanism at oxidized Fe, Ni and Co electrodes in aqueous alkaline solution using a combination of electrochemical techniques including steady state polarization, open circuit potential decay and electrochemical impedance spectroscopy. This effort had as a focus an attempt to obtain a general understanding of the OER mechanism at such oxidized electrodes. The key mechanistic indicators obtained were the Tafel slope and reaction order with respect to hydroxide ion activity. Recapping briefly on the experimental values of the OER kinetic parameters obtained by the latter workers, a lower Tafel slope of $b \approx 2.303\times 2RT/3F$ (= 39.4 mV dec^{-1} at 25°C) with $m_{OH^-} \approx 1$ was observed for electrochemically pre-treated Ni electrodes. By contrast, pre-reduced Co and Fe anodes exhibited $b \approx 2.303\times 4RT/5F$ with $m_{OH^-} \approx 1$. Upon ageing, following extensive experimental utilization, the Tafel slope for Co electrodes increased to $b \approx 2.303\times RT/F$ (= 59.2 mV dec^{-1} at 25°C) with a non-integral value of $m_{OH^-} \approx 3/2$. The latter values of Tafel slope and reaction order had previously been reported for aged Fe anodes [49]. For these aged Co and Fe electrodes, a second Tafel region was resolved at higher overpotentials with $b \approx 2.303\times 2RT/F$ (= 118.3 mV dec^{-1} at 25°C) and $m_{OH^-} \approx 1$. Values of b and m_{OH^-} have not been reported for higher overpotentials in the case of the "fresher" electrodes, owing to unsatisfactory reproducibility. Hence a common theme discerned by Lyons et al has been the observation that the nature of electrode pre-treatment and the degree of ageing can have a significant effect on the experimentally measured kinetic parameters. Pre-treatment routines (particularly cathodic pre-reduction followed by a single voltammetric cycle between the hydrogen and oxygen evolution regions of potential) have been found to be necessary in obtaining consistent data sets with meaningful values of the Tafel slope, b, and the OH^- ion reaction order, m_{OH^-}.

Lyons and Brandon [198-202] attempted to address the issue of whether any consistency can be derived from their combined results regarding the mechanism of the OER at passivated first row transition metals. Considering the OER at oxidized Ni electrodes in base they noted that in a conventional kinetic analysis, a Tafel slope of $2.303\times 2RT/3F$ is indicative of an RDS subsequent (although not necessarily directly subsequent) to the initial discharge, at each active site, of an OH^- ion from solution. Additionally, if the fractional coverage, θ, of the OER reaction intermediate(s) is assumed to follow the Langmuir isotherm at lower overpotentials (i.e. $\theta \rightarrow 0$), the reaction order of unity suggests that no further hydroxide ions are adsorbed from the bulk electrolyte, prior to, or during, the RDS. Lyons and Brandon could identify only two general pathways that satisfy these criteria. The first of these is due to Yeager [196], and takes the form,

$$S^z + OH^- \rightarrow (SOH)^z + e^- \quad (4.77)$$

$$(SOH)^z \rightarrow (SOH)^{z+1} + e^- \ldots \text{RDS} \quad (4.78)$$

$$2(SOH)^{z+1} + 2OH^- \rightarrow 2S^z + O_2 + 2H_2O \quad (4.79)$$

where, S is an active catalytic site. This scheme encompasses a concept often encountered in the literature, namely, the facilitation of the OER through the cyclic formation and decomposition of an unstable intermediate in a higher valence state (z+1) than the initial state (z) of the transition metal reaction centre. The other possibility, originally proposed for $LaNiO_3$ anodes, is due to Bockris [169]:

$$\{OH^-\}\text{-}S^z + OH^- \rightarrow \{OH^-\}\text{-}S^z\text{-}OH + e^- \quad (4.80)$$

$$\{OH^-\}\text{-}S^z\text{-}OH \rightarrow \{vac\}\text{-}S^z\text{- -}H_2O_2 + e^- \ldots RDS \quad (4.81)$$

$$(H_2O_2)_{phys} + OH^- \rightarrow (HO_2)^-_{phys} + H_2O \quad (4.82)$$

$$(H_2O_2)_{phys} + (HO_2)^-_{phys} \rightarrow OH^- + H_2O + O_2 \quad (4.83)$$

$$\{vac\}\text{-}S^z + OH^- \rightarrow \{OH^-\}\text{-}S^z \quad (4.84)$$

In the latter scheme {vac} is a vacant oxygen site in the oxide surface, while $\{OH^-\}$ denotes the occupation of such a site by an OH^- ion. This is a modification of the *physisorbed hydrogen peroxide pathway* (hence the "phys" subscript) proposed for other first row transition metal based perovskites [169] . The $\{OH^-\}\text{-}S^z$ site is formed initially upon the acceptance of a proton by a surface O^{2-} ion from the solvent water. This implies that lattice oxygen atoms participate directly in the gassing reaction, the possibility of which is a subject of literature controversy [203].

Lyons and Brandon [198] concluded that for their oxidised Ni anodes, a more satisfactory variation of the physisorbed peroxide mechanism could be envisaged, if attention was paid to the underlying surface chemistry. The group of Burke, has reported *negative super-nernstian E*-pH *shifts* for voltammetric peaks associated with hydrous oxide formation for a number of transition metals including Ni [74,], Fe[36], Au [204], Rh [205] and Ir [55]. Such shifts in peak potential with increasing pH, beyond the expected value of $dE/dpH = -2.303 \times RT/F$ vs. a pH independent reference electrode, imply that the oxidised state has acquired a negative charge relative to the reduced state. This anionic oxide formation arises [26] owing to the well known acidic properties of oxide surfaces in solutions of high pH [206], and can be equivalently regarded [74] in terms of, the adsorption of excess OH^- ions, proton loss from coordinated water molecules or the formation of hydroxyl surface complexes. Although *E*-pH data is not available for oxidised Co, aspects of the electrocatalytic behaviour of this metal in base are also suggestive of excess OH^- ion coordination at the hydrous oxide surface [207].

In view of the anionic nature of the anodic oxide formed on Rh in base, O'Sullivan and Burke [197] proposed that oxygen evolution on this substrate occurs at surface complexes that can be represented as $[Rh(IV)O_m(OH)_n]^{p-}$, where $p = 2m+n-4$. Similar considerations should be apply to any oxide phase known to acquire a net negative charge in alkaline solution, and therefore Lyons and Brandon [198] suggested the following as a feasible pathway for the OER at oxidised Ni in base:

$$[Ni(III)O_m(OH)_n]^{p-} + OH^- \rightarrow [Ni(III)O_m(OH)_{n+1}]^{p-} + e^- \quad (4.85)$$

$$[Ni(III)O_m(OH)_{n+1}]^{p-} \rightarrow [Ni(III)O_m(OH)_{n-1}]^{(p-1)-} \text{- -}H_2O_2 + e^- \ldots \text{RDS} \quad (4.86)$$

$$[Ni(III)O_m(OH)_{n-1}]^{(p-1)-} \text{- -}H_2O_2 + 2OH^- \rightarrow [Ni(III)O_m(OH)_n]^{p-} \text{- -}HO_2 + H_2O + e^- \quad (4.87)$$

$$[Ni(III)O_m(OH)_n]^{p-} \text{- -}HO_2 + OH^- \rightarrow [Ni(III)O_m(OH)_n]^{p-} + O_2 + H_2O + e^- \quad (4.88)$$

For a Ni(III) centred complex, p = 2m+n-3. Note also that if (as is most likely) m = 1, the $[Ni(III)O_m(OH)_n]^{p-}$ species is merely a NiOOH surface group that has coordinated extra hydroxide ions, owing to the acidic nature of the hydrous oxide. The rate limiting second step again involves the formation of a physisorbed peroxide entity (- $-H_2O_2$), however in contrast to the scheme outlined in eqn.(4.80) – eqn.(4.84), the electron passed to the external circuit is supplied by a coordinated OH^- ion, bringing a decrease of one in the overall negative charge on the surface complex. Of course the concepts of anionic surface complexes and of hydroxide ions occupying lattice vacancies are essentially just different model approaches to the observed anionic character of hydrous oxides in base. However, the fact that the scheme presented above in eqn. (4.85) – eqn.(4.88) dispenses with the need to admit the direct participation of lattice oxygen atoms in the OER, should make this representation more widely acceptable.

While the first two steps of the Lyons-Brandon scheme [198,200] are similar to those of the Bockris- Otagawa scheme [169], the details of the pathways diverge subsequent to the RDS. Lyons and Brandon elected to alter the latter steps of the Bockris pathway, because under low coverage Langmuir conditions it was assumed that it would be rather difficult to see how step (4.83) could proceed at a sufficient rate, such as not to render it rate limiting overall (even allowing for the surface mobility allowed in the classical model of physisorption). It may be noted that step (4.86) has an associated stoichiometric number of $v = 1$ compared to $v = 2$ for step (4.81) – however this helps little in elucidating the nature of the mechanism post RDS, since it has long been appreciated [5], that the principle of microscopic reversibility is unlikely to apply to the oxygen electrode.

Lyons and Brandon [200] also noted that an equivalent of the Yeager model could also be proposed to account for the OER mechanism at oxide covered Ni electrodes. The proposed pathway could be expressed as follows:

$$\left[Ni(III)O_m(OH)_n\right]^{p-} + OH^- \rightarrow \left[Ni(IV)O_m(OH)_{n+1}\right]^{p-} + e^- \quad (4.89)$$

$$\left[Ni(IV)O_m(OH)_{n+1}\right]^{p-} \rightarrow \left[Ni(IV)O_m(OH)_{n+1}\right]^{(p-1)-} + e^- \quad (4.90)$$

$$\left[Ni(IV)O_m(OH)_{n+1}\right]^{(p-1)-} + 2OH^- \rightarrow \left[Ni(III)O_m(OH)_{n-1}\right]^{(p-1)-} + O_2(g) + 2H_2O + e^- \quad (4.91)$$

$$\left[Ni(III)O_m\left(OH\right)_{n-1}\right]^{(p-1)-} + OH^- \rightarrow \left[Ni(III)O_m(OH)_n\right]^{p-} + e^- \quad (4.92)$$

Here molecular oxygen is generated via decomposition of the unstable anionic Ni(IV) species.

Lyons and Brandon [200] noted that their electrochemical measurements lead to the suggestion of two candidate mechanisms (effectively schemes expressed in eqn.(4.85) – eqn. (4.88) or eqn.(4.89) – eqn. (4.92)) to the exclusion of all other possible pathways, these measurements could not further discriminate between the two. It was suggested that the Ni(IV) intermediate mechanism would appeal to the school of thought that envisages the OER to be essentially a "side reaction" facilitating the decomposition of unstable higher oxide entities. In contrast it was noted that one of the major advantages of the Ni(III) intermediate mechanism is that it can account satisfactorily for the loss of oxygen evolution activity with time, that was observed and discussed by Lu and Srinivasan [176]. Quite reasonably, these authors attributed this behaviour to an increase in the relative proportion of Ni^{4+} compared to Ni^{3+} surface ions, envisaged to occur by the oxidation, upon extended polarisation, of the catalytically active β-NiOOH to NiO_2. However, their proposed reaction mechanism, a modified Krasil'shchikov scheme, also proposed that NiO_2 partakes in the OER as a transient reaction intermediate. Lyons and Brandon [200] found that it was rather difficult to rationalize how the Ni(IV) species can present an inert surface site for the OER, yet act as an intermediate for the same reaction. It was recognized that this difficulty was removed by their proposed Ni(III) pathway which did not require a Ni(IV) intermediate.

Lyons and Brandon [198, 201,202] noted that the Tafel slope of $b \approx 2.303 \times 4RT/5F$ observed for Co and Fe electrodes cannot be rationalized by kinetic analyses of any of the commonly cited OER pathways, regardless of which step is chosen as RDS, or the adsorption isotherm admitted (Langmuir or Temkin). They concluded that this does not however mean that mechanistic details cannot be derived – it merely implies that a more complicated model of the electrode/solution interface wais required. In the present context they introduced a *dual barrier model* developed by MacDonald and Conway [208] to rationalize OER kinetic data obtained for Au electrodes. This model owed much to earlier work by Meyer [209] on cathodic electrode processes. The model of MacDonald envisages that only a fraction, ΔV_{FS} of the total potential difference, $\Delta V_{MS} = \Delta V_{\Sigma}$, between the metallic electrode and the electrolyte is effective in lowering the potential barrier to interfacial electron transfer. In series with this, the remainder, ΔV_{MF}, appears across an electronically conducting "barrier" oxide, through which the charge passed in the OER must migrate under the influence of an electric field. Hence one visualizes an inner region labeled F and an outer solution region labeled S.

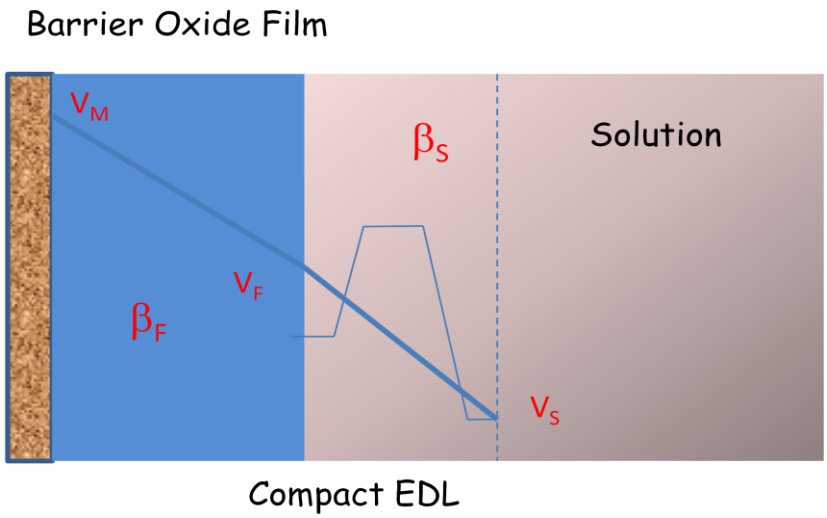

Figure 24. Schematic representation of the Dual Barrier model for charge transfer at the oxide/solution interface.

Hence the net reaction flux $f_\Sigma = i/nFA$ for a single interfacial charge transfer reaction across the dual barrier consisting of inner compact oxide and outer hydrous oxide is given by the following expression

$$f_\Sigma \cong k\prod_j (a_{j,s}^{m_{j,s}})^{\frac{\beta_F}{\beta_F+\beta_S}} \exp\left[\frac{\beta_\Sigma F\eta}{RT}\right] \tag{4.93}$$

In the latter expression η denotes the overpotential and $a_{j,S}$ and $m_{j,S}$ denote the activity and reaction order of species j in the outer solution region S. Note also that the composite symmetry factor is given by the following expression :

$$\beta_\Sigma \cong F(\beta)\beta_S = \left(\frac{\beta_F}{\beta_F+\beta_S}\right)\beta_S \tag{4.94}$$

Furthermore the effective Tafel slope b_{eff} is related to the Tafel slope expected in the absence of the oxide barrier b_S according to:

$$b_{eff} \cong F(\beta)^{-1} b_S \tag{4.95}$$

Or

$$b_{eff} = \left(\frac{\partial\eta}{\partial\log i}\right)_{a_S} = 2.303\left(\frac{RT}{\beta_\Sigma F}\right) = 2.303\frac{(\beta_F+\beta_S)}{\beta_F}\left(\frac{RT}{\beta_S F}\right) \tag{4.96}$$

Finally, the effective reaction order with respect to the activity of species j is :

$$m_{j,eff} \cong F(\beta) m_{j,S} = \left(\frac{\beta_F}{\beta_F + \beta_S} \right) m_{j,S} \tag{4.97}$$

In the latter expressions the correction factor $F(\beta)$ is given by:

$$F(\beta) = \frac{\beta_F}{\beta_F + \beta_S} \tag{4.98}$$

Neither Meyer [209] nor MacDonald [208] speculated as to the detailed nature of the barrier film charge migration process or indeed as to the exact identity of the charge carriers, since, as will become obvious, these factors are formally unimportant with regard to the identification of the mechanism of the OER at the oxide film/solution interface.

Lyons and Brandon noted that where a normal (symmetrical single barrier) kinetic analysis yields b = 2.303×2RT/3F for a particular step of an OER pathway considered to be rate limiting, the overall rate equation takes the general form :

$$i = i_0 \exp((1+\beta_s) F\eta / RT) \tag{4.99}$$

where i_0 is the exchange current density for the OER and β_S denotes the symmetry factor for the interfacial electron transfer process. On the other hand, if the OER is proceeding in the steady state under dual barrier conditions, its RDS must be in equilibrium with the barrier film charge migration process. Therefore it is possible to obtain an expression for the overall current density across the two barriers by equating eqn. 10 with the rate equation for the oxide charge migration. It can be shown [208,209] that the resulting expression has the form:

$$i = A\exp\left((1+\beta_\Sigma) F\eta / RT\right) \tag{4.100}$$

In the latter expression the composite symmetry factor is given by eqn.(4.94): $\beta_\Sigma = \frac{\beta_F \beta_S}{\beta_F + \beta_S}$. Here , β_F is the symmetry factor for field assisted charge transport through the oxide and β_S represents as before the symmetry factor for the rate determining interfacial electron transfer reaction. The pre-factor A in eqn. (4.100) depends on i_0 and also on the exchange current density for the charge migration process, which in turn depend respectively on a_{OH^-} and the activities of the barrier film charge carriers [209].

If we assume that $\beta_S = \beta_F = 1/2$ then we obtain that $\beta_\Sigma = 1/4$. Under these conditions, a logarithmic analysis of eqn.(4.100) yields b = 2.303×4RT/5F, implying that the OER mechanism we seek with the appropriate RDS is characterized by b = 2.303×2RT/3F under single barrier conditions.

Also, referring to eqn.(4.97) for the effective reaction order, $F(\beta) = \frac{\beta_F}{\beta_F + \beta_S} = 1/2$, which means that the reaction order of approximately unity, measured under dual barrier conditions, corresponds to an expected value of $m_{OH^-} = 2$ in a single barrier treatment of the appropriate pathway. Therefore a suitable OER mechanism for the Co and Fe electrodes must give rise to $b = 2.303 \times 2RT/3F$, $m_{OH^-} = 2$ in a conventional single barrier analysis.

Lyons and Brandon noted that several commonly cited mechanisms meet these criteria when a particular step is considered to be rate determining under conditions of low coverage ($\theta \rightarrow 0$) of intermediates. These include the often proposed Krasil'shchikov path [170], Bockris's electrochemical path [165] and the more general form of the physisorbed peroxide path [169]. However Lyons and Brandon [198] found it significant that only the latter path can rationalize the experimental values of b and m_{OH^-} observed for "aged" Co and Fe anodes. In view of this they proposed the following to be the most likely reaction mechanism for the OER at both fresh and aged Fe (and Co) electrodes:

$$[Fe(VI)O_m(OH)_n]^{p-} + OH^- \rightarrow [Fe(VI)O_m(OH)_{n+1}]^{p-} + e^- \quad (4.101)$$

$$[Fe(VI)O_m(OH)_{n+1}]^{p-} + OH^- \rightarrow [Fe(VI)O_m(OH)_n\text{-}\,\text{-}H_2O_2]^{p-} + e^- \ldots \text{RDS} \quad (4.102)$$

$$[Fe(VI)O_m(OH)_n\text{-}\,\text{-}H_2O_2]^{p-} + OH^- \rightarrow [Fe(VI)O_m(OH)_n\text{-}\,\text{-}HO_2]^{p-} + H_2O + e^- \quad (4.103)$$

$$[Fe(VI)O_m(OH)_n\text{-}\,\text{-}HO_2]^{p-} + OH^- \rightarrow [Fe(VI)O_m(OH)_n]^{p-} + O_2 + H_2O + e^- \quad (4.104)$$

The mechanism of the OER reaction is outlined schematically in figure 25 below.

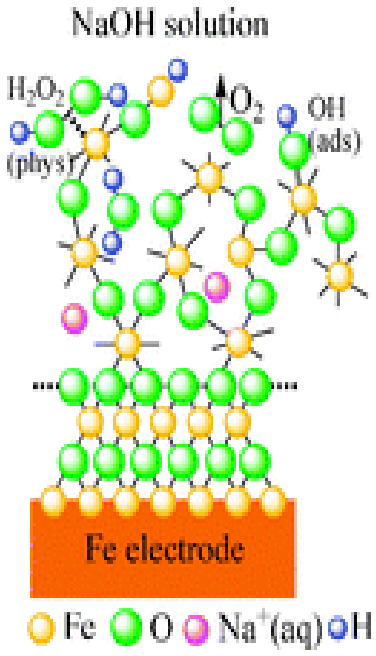

Figure 25. Schematic representation of Lyons-Brandon OER mechanism at the hydrous oxide/solution interface.

Note that the concept of the catalytically active site existing in the form of an hydroxylated anionic surface complex is maintained – for Fe(VI), p = 2m+n-6. Indeed, since Fe(VI) species (probably in the form of FeO_4^{2+}) are soluble in aqueous alkaline solution [74], their stabilization on the oxide surface by the coordination of excess OH^- ions provides a tentative explanation as to how they can act as OER active centres. Lyons and Brandon [198] noted that the OER pathway defined in eqn.(4.101) – eqn.(4.104) above is also suitable for Co anodes, except in this case the active site is represented as $[Co(IV)O_m(OH)_n]^{p-}$ (p = 2m+n-4), in agreement with the proposal of Gennero De Chialvo et al. [80] that the catalytic species is likely to exist as discrete CoO_2 entities.

In the limit of low intermediate species coverage ($\theta \rightarrow 0$), the kinetic analysis of the scheme defined in eqn.(4.101) – eqn.(4.104) is very similar to that of the scheme presented in eqn.(4.85) – eqn.(4.88), except that there is an additional factor of a_{OH} in the rate equation for the RDS relative to the corresponding expression for the RDS, eqn.(4.102).. This means that while the Tafel slope prediction remains $b = 2.303 \times 2RT/3F$, the anticipated reaction order doubles to $m_{OH^-} = 2$, as required (when correction is made for the dual barrier) to rationalize the data obtained by Lyons and Brandon (Figs. 6 and 9 ref [198]). In a further communication Lyons and Brandon We have described in detail elsewhere [49], how an analysis of steps (4.101) and (4.102) yields the values of $b = 2.303 \times RT/F$ and $m_{OH^-} = 3/2$ observed at lower η for aged Fe and Co anodes, if the fractional coverage of the intermediate formed in step (4.101) is governed by the Temkin adsorption isotherm ($0.2 \leq \theta \leq 0.8$). At higher η, the analysis predicts $b = 2.303 \times 2RT/F$ and $m_{OH^-} = 1$, where it is assumed that the intermediate coverage has passed beyond the Temkin potential window and can now be represented as $\theta \rightarrow 1$ [49]. It is of course possible that the different Tafel slopes observed for Co and Fe under different conditions of age and overpotential are indicative of different OER mechanisms, however as discussed for Pt electrodes by Damjanovic et al. [186], changes in intermediate coverage rather than pathway provide a more satisfactory solution for such observed behaviour. The kinetic behavior for the OER at oxide covered Ni, Fe and Co electrodes in base are summarized in Table 3 below.

It should be noted from Table 3 that that the nature of electrode pre-treatment and the degree of ageing can have a significant effect on the experimentally measured kinetic parameters. Pre-treatment routines (particularly cathodic pre-reduction followed by a single voltammetric cycle between the hydrogen and oxygen evolution regions of potential) have been found to be necessary in obtaining consistent data sets with meaningful values of the Tafel slope, b, and the OH^- ion reaction order, m_{OH^-}.

Oxygen evolution steady state polarisation curves, with the current density normalised to the active surface area through the indicated roughness factors, are plotted on the same graphs for fresh non-electrochemically pre-treated (Figure. 26) and pre-reduced (Figure. 27) Ni, Co and Fe electrodes in 1.0 M NaOH at 25°C. For the purpose of comparison, the same polarisation curves, where the values of $\log i(\eta)$ are referred to the geometric surface area are also depicted in the aforementioned figures. Some parameters, relevant to the comparison of the OER catalytic efficiencies of the various electrodes are listed in Tables 4 and 5, for the non-pre-treated and pre-reduced electrodes respectively.

Table 3. Summary of kinetic behavior for OER at oxidized Ni, Fe and Co electrodes in aqueous alkaline solution.

Electrode	Experimental b, m_{OH-}	Dual barrier	b, m_{OH-} for analysis	Isotherm L or T	Pathway
Ni no-pre-treat	2RT/3F, order not measureable	No	As listed left	L, θ→0	C
Ni pre-reduced	2RT/3F, 1	No	As listed left	L, θ→0	C
Ni pre-oxidised	2RT/3F, 1	No	As listed left	L, θ→0	C
Co no-pre-treat	2RT/3F(5M)→4RT/5F(1M)	low [OH^-]	-----	-----	-----
Co pre-reduced	4RT/5F, 1	Yes	2RT/3F, 2	L, θ→0	E
Co aged low η	RT/F, 3/2	No	As listed left	T, $r_I >> r_{II}$	E
Co aged high η	2RT/F, 1	No	As listed left	L, θ→1	E
Fe no-pre-treat	2RT/3F(1M)→4RT/5F(5M)	high [OH^-]	-----	-----	-----
Fe pre-reduced (fresh)	2RT/3F, order not measureable	No	-----	-----	-----
Fe pre-reduced (aged)	4RT/5F, 1	Yes	2RT/3F, 2	L, θ→0	E
Fe aged low η	RT/F, 3/2	No	As listed left	T, $r_I >> r_{II}$	E
Fe aged high η	2RT/F, 1	No	As listed left	L, θ→1	E

The electrocatalytic activities of different electrode materials for a given reaction are normally compared in terms of the experimentally observed values of the exchange current density i_0. However, as was pointed out by Conway et al.[210], the value of b is as important as i_0 in characterising electrocatalysis. Consider, for example, the parameters presented for the non pre-treated Ni and Co anodes in Table 4. From the quoted steady state current density values, it is obvious that, at an overpotential of η = 0.302 V (which lies within the lower straight line Tafel regions in the polarisation curves for both anodes), it is the Ni electrode that displays the superior catalytic activity – yet it is the Co electrode that has the higher i_0 value. This arises due to the larger value of b in the case of the Co anode. This leads to the general conclusion, that where different electrodes present significantly different Tafel slopes for a given reaction, a comparison of the exchange current densities is not a useful exercise [169,210], if one is interested in the relative catalytic abilities of the electrodes at practically useful rates of reaction.

An alternative approach, and that utilised by Lyons and Brandon [199-201], is to compare the values of active surface area normalised (or "real") steady state current densities at a given

overpotential. It was elected to conduct such comparisons at an overpotential of η = 0.302 V. This overpotential was selected because it facilitates ready comparison of the real current densities observed at Ni, Co and Fe electrodes in the present work, with those observed by Bockris and Otagawa [169] for nickelate, cobaltate and ferrite electrodes at η = 0.3 V. The latter authors have described this low overpotential section of the Tafel region as being the practically important region for comparison.

Table 4. Comparison, based on the data of Fig. 17, of various parameters related to the OER catalytic activity of fresh non-electrochemically pre-treated Ni, Co and Fe electrodes in 1.0 M NaOH at 25°C. The quoted current densities are based on the estimated active surface areas for the OER of each electrode.

Electrode	f_r	b (mV dec^{-1})	i_0 (A cm^{-2})	i(0.302 V) (A cm^{-2})
Ni	7.3 ± 0.1	37.5	2.75 (±.04) ×10^{-13}	3.34 (± 0.05) × 10^{-5}
Co	13.1 ± 0.5	46.0	3.2 (±0.1) ×10^{-12}	1.15 (± 0.04) × 10^{-5}
Fe	0.52 ± .02	37.0	6.1 (±0.2) ×10^{-15}	9.5 (±0.4) ×10^{-7} [a]

[a] Estimated by the extrapolation of the lower overpotential Tafel slope line.

Table 5. Comparison, based on the data of Fig. 18, of various parameters related to the OER catalytic activity of pre-reduced Ni, Co and Fe electrodes in 1.0 M NaOH at 25°C. The quoted current densities are based on the estimated active surface areas for the OER of each electrode.

Electrode	f_r	b (mV dec^{-1})	i_0 (A cm^{-2})	i(0.302 V) (A cm^{-2})
Ni	6.3 ± 0.2	38.5	1.78 (±.07) ×10^{-13}	1.21 (± 0.04) × 10^{-5}
Co	12.9 ± 0.7	47.5	3.3 (±0.2) ×10^{-12}	7.4 (± 0.4) × 10^{-6}
Fe	0.51 ± .02	39.5	2.9 (±0.2) ×10^{-14}	1.3 (± 0.1) × 10^{-6} [a]

[a] Estimated by the extrapolation of the lower overpotential Tafel slope line.

As mentioned previously, Scarr [191] conducted what was, until the work reported by Lyons and Brandon [198], the only comparative study on the catalytic performance of polycrystalline Ni, Co and Fe electrodes towards the OER in alkaline solution. This worker observed Tafel slopes of b = ~ 2.303×4RT/5F for each of the three metals in 1 M KOH, thereby rendering meaningful a comparison of catalytic activities based on the relative values of the exchange current densities. In agreement with the trend reported by Miles et al.[48], values of i_0 = 2 × 10^{-10} A cm^{-2}, i_0 = 8 × 10^{-11} A cm^{-2} and i_0 = 2 × 10^{-13} A cm^{-2} were observed by Scarr for the Ni, Co and Fe anodes respectively. Unfortunately, the reported i_0 values were again normalised to the geometric surface area.

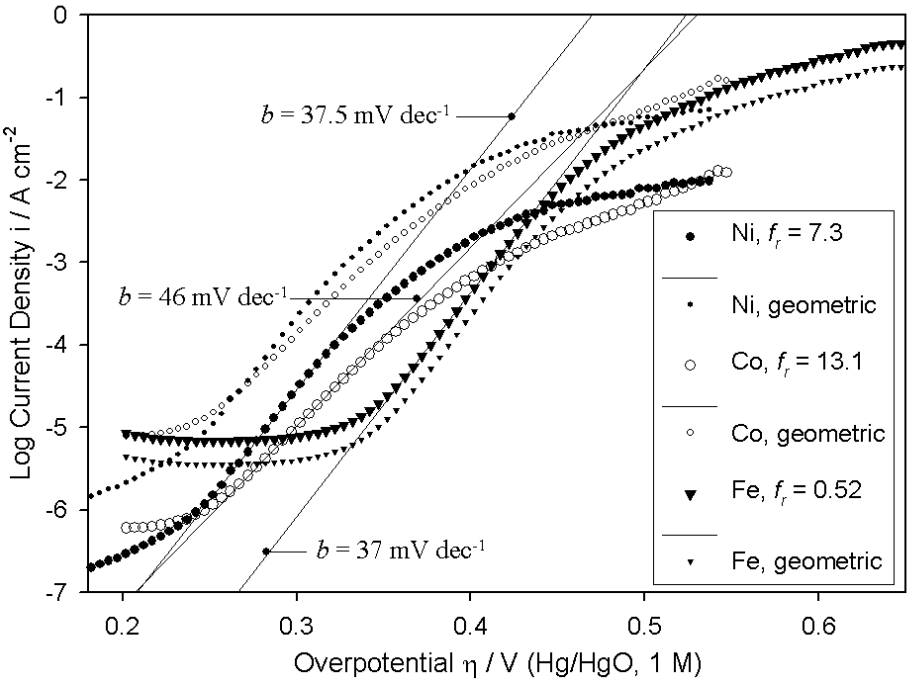

Figure 26. Comparison of *iR* corrected steady state polarisation curves recorded in 1.0 M NaOH solution at 25°C, for freshly prepared non-electrochemically pre-treated Ni, Co and Fe electrodes. As indicated in the legend each curve is presented for both the case where the current density values are based on the geometric electrode surface area and also the case where they have been normalised to the estimated active surface area.

Examination of Figs. 26 and 27, and the associated Tables 4 and 5, reveals that, for $\eta \leq 0.4$ V (i.e. the range of overpotentials associated with the entire length of the lower *b* straight line regions for the Ni and Co electrodes, and most of the length of this region for the Fe electrodes), the real surface area normalised steady state polarisation curves of the present work are indicative of the same OER catalytic activity series as observed by Miles et al.[161] and Scarr [191] – i.e. Ni > Co > Fe. The data presented in these figures also indicates that the degree of inferiority of the catalytic activity of the Fe electrodes, relative to the Co and Ni electrodes, is overstated by steady state polarisation curves based on geometric surface areas, at least in the case of the polycrystalline metallic electrodes utilised here. This arises of course, due to the fact that roughness factors of less than unity have been estimated, via the OH_{ads} desorption method, for the Fe electrodes, in comparison with factors significantly larger than unity yielded by the same technique for the Ni [1] and Co [2] electrodes. Indeed in the case of the pre-reduced electrodes (Fig. 18), at overpotentials in the approximate range of $0.25 \text{ V} \leq \eta \leq 0.32$ V, the steady state polarization curves normalized to the geometric surface area, indicate that the Co electrode is catalytically superior to the Ni electrode. However, normalisation of these data to the respective values of the active surface area, reveals that the aforementioned apparent conclusion is actually incorrect.

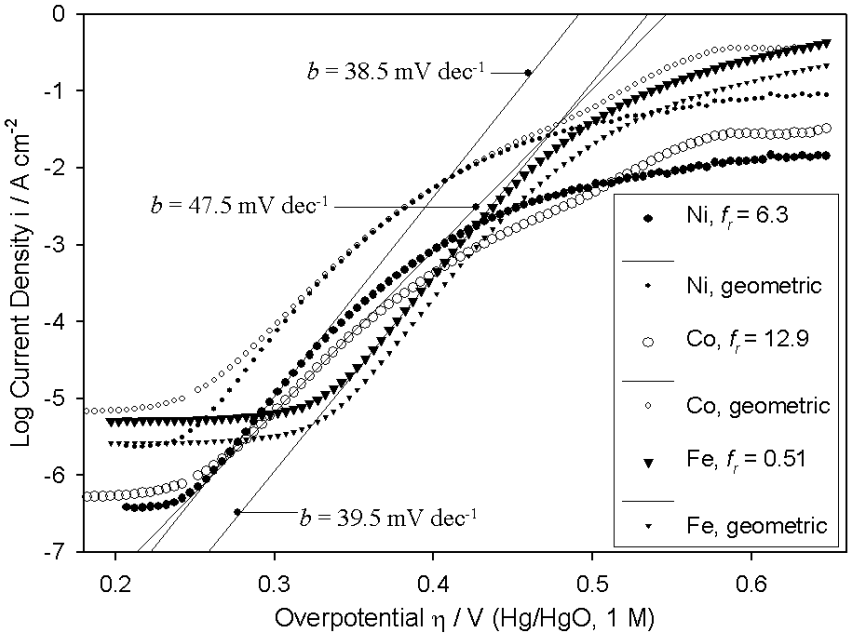

Figure 27. Comparison of *iR* corrected steady state polarisation curves recorded in 1.0 M NaOH solution at 25°C, for pre-reduced Ni, Co and Fe electrodes. As indicated in the legend each curve is presented for both the case where the current density values are based on the geometric electrode surface area and also the case where they have been normalised to the estimated active surface area.

Bockris and Otagawa [169] have reported the following OER steady state current density values, for various perovskite electrodes in 1.0 M NaOH (25°C) at η = 0.3V: $i = 1.3 \times 10^{-5}$ A cm^{-2} for a nickelate electrode ($f_r = 5.6 \times 10^3$) , $i = 1.4 \times 10^{-6}$ - 1.0×10^{-5} A cm^{-2} for various cobaltate anodes (f_r values of the order of $10^2 - 10^3$), $i = 5.0 \times 10^{-7}$ A cm^{-2} ($f_r = 6.0 \times 10^2$) for a $La_{0.7}Sr_{0.3}FeO_3$ ferrite electrode, and $i = 8.1 \times 10^{-7}$ A cm^{-2} ($f_r = 3.3 \times 10^3$) for a for a $La_{0.5}Sr_{0.5}FeO_3$ ferrite electrode. The quoted roughness factor values were estimated using the double layer capacitance ratio approach in conjunction with cyclic voltammetry measurements. Comparing the values of $i_{(\eta = 0.3V)}$ obtained by Bockris and Otagawa [169] for their perovskite electrodes with the values of $i_{(\eta = 0.303V)}$ observed in the present work and listed in Tables 4 and 5, it is apparent that there is agreement to within an order of magnitude between the values quoted for our oxidised polycrystalline metal electrodes and the perovskite electrodes (based on the corresponding transition metal) of the former authors. This order of magnitude agreement prevails despite the fact that the roughness factors of the perovskite electrodes are 2 – 3 orders of magnitude greater than the roughness factors of our electrodes. It might therefore be suggested that the OER occurs at *essentially the same type of active site* on an anodic oxide covered metal electrode surface, as on the corresponding perovskite electrode surface.

In his review on the OER, Kinoshita [6] commented that electrodes consisting of specifically pre-synthesised metal oxides (like the peroskite electrodes of Bockris and Otagawa [169]) generally display superior catalytic properties towards the reaction, compared to (anodic

oxide covered) metallic electrodes. However, most literature reports on the OER do not attempt to normalise observed steady state current densities to estimated real surface areas. With this point in mind, and considering the conclusions of the previous paragraph, it might be suggested, that the apparently superior OER performance of synthesised metal oxide electrodes, relative to the oxide formed anodically on polycrystalline electrodes of the same metal, arises principally due to the larger available active specific surface areas of the former type of anode, and not due to any intrinsically superior electrocatalytic properties of the synthesised oxides.

The concept of a volcano plot is often encountered in attempts to rationalise the relative electrocatalytic activities for a given reaction, of different electrode materials, in terms of a given physicochemical property [211]. Attempts to draw correlations between electrode physicochemical properties and OER catalytic performance is complicated by the fact that it is the metal oxide and not metal that catalyses oxygen evolution. Kinoshita [6] has reviewed the efforts of various workers who have tackled this problem and sought to formulate a coherant theory of electrocatalysis for the OER. Amongst these, perhaps the most complete and successful attempt to provide an interpretation of OER catalytic activity in terms of physicochemical parameters was provided by Bockris and Otagawa [169] in their study of the reaction at perovskite electrodes. For perovskites based on the first row transition metal M (general formula AMO_3, where A is a lanthanide), they found that there was an inverse linear relationship between the estimated M(III)-OH bond strength and $i_{(\eta = 0.3V)}$ – i.e. while the estimated bond strength increases in the order Ni < Co < Fe < Mn < Cr, the OER catalytic activity follows the reverse of this series. They rationalised this in terms of a rate determining step involving the desorption of the OH_{ads} species adsorbed in the initial discharge step – obviously the weaker the M-OH bond the greater the rate of desorption at a given overpotential. Bockris and Otagawa devised molecular orbital diagrams for the bonding of an OH entity to a $M(III)O_5$ species (which they proposed as a valid model for a transition metal site in the {001} plane of the perovskite unit cell) and concluded that the M-OH bond strength had an inverse dependence on the number of d electrons occupying antibonding orbitals (4 for Ni(III)-OH, 3 for Co(III)-OH etc).

While at first glance, the aforementioned concepts of Bockris and Otagawa [169] would appear to be in accord with the experimental observation [198] of an OER activity series of Ni > Co > Fe at overpotentials associated with a (deduced) rate determining OH desorption step, some caution is in order. The relationship between M-OH bond strength and OER catalytic activity, and the molecular orbital analysis referred to above, apply specifically to first row transition metal ions in the +3 oxidation state. While this is consistent with the RDS of the pathway that Lyons and Brandon have proposed for the OER at oxidised Ni substrates [200], it is clearly not the case for the RDS envisaged for iron [202] in which an Fe(VI)-OH chemical bond is broken. Similarly in the case of Co, Lyons and Brandon [198] contended that the rate limiting OH desorption step involves the breaking of a Co(IV)-OH rather than a Co(III)-OH bond. Nevertheless, if it is the case that the molecular orbital electron configurations for the Co(IV)-OH and Fe(IV)-OH bonds are the same as those proposed by Bockris and Otagawa [169] (see Figs. 14 and 20 in that reference) for Fe(III)-OH and V(III)-OH respectively, then the correlation envisaged by the same authors between the number of d electrons in antibonding orbitals and OER catalytic activity would also

hold for the electrodes of the present work, based on rate determining steps involving the breaking of Ni(III)-OH (4 antibonding electrons), Co(IV)-OH (2 antibonding electrons) and Fe(IV)-OH (1 antibonding electon) bonds. In conclusion we comment that the Lyons Brandon observation of similar (real surface area normalised) OER catalytic activities at passive oxide covered Co (catalytic site envisaged to be in the Co(IV) valance state) and Fe (catalytic site envisaged to be in the Fe(VI) valance state) electrodes, to those observed by Bockris and Otagawa [169] at their cobaltate and ferrite electrodes, may cast some doubt on the conviction of these authors (based on rather little experimental evidence) that M(III) sites are the OER active centres at the surface of electrodes of all perovskites. If this assumption regarding the common valance state of the catalytic ions at perovskite surfaces is not true, then the correlation of OER activity with the number of antibonding d-electrons becomes more complicated than that originally envisaged by Bockris [169](although it might well still be applicable).

5. CONCLUSIONS

We now summarise the principal conclusions arising from the present review of the formation, redox properties and electrocatalytic activity with respect to the OER of hydrous oxide coated electrodes of the non noble transition metals in aqueous alkaline solution. First, hydrous microdispersed oxides are readily prepared via the repetitive cyclic potential sweep method applied to the parent metal (Fe, Co, Ni) in aqueous alkaline solution. The latter method is very similar to that employed in the electropolymerization of Electronically Conducting Polymer (ECP) films such as poly(pyrrole) or poly(aniline). The oxide/solution interface has a duplex character, consisting of an inner, largely anhydrous compact oxide, and an outer, hydrated microdisperse oxide layer which exhibits significant electrocatalytic activity with respect to anodic oxygen evolution. Second, the charge storage/charge percolation properties of the hydrous oxide depend on electrochemical and environmental variables such as the lower and upper potential sweep limits, the potential sweep rate, the base concentration employed, the solution temperature, and the solution pH. Third, the acid/ base behaviour of anodically formed transition metal oxides is important when considering mechanism of both redox switching & oxygen evolution. Furthermore, hydrous oxides are more difficult to reduce than less hydrated compact materials, and this may well have a significant implication for the catalysis of the cathodic ORR.

With respect to the catalysis of the anodic OER process, the sole pathway, that can account for the entire set of experimental parameters observed for the various Co and Fe electrodes (see Table 3), is the *physisorbed hydrogen peroxide mechanism*. The second step of this pathway, which involves the breaking of a M-OH chemical bond, is considered to be rate limiting. The different values of b and m_{OH^-} observed for electrodes subjected to different pre-treatments, or for the same electrode at different overpotentials, arise due to changes in the fractional coverage θ of the reaction intermediates, and not due to changes in rate determining step.

A similar mechanistic pathway is likely to prevail for oxidised Ni anodes, except that the OH^- ion that reacts in the rate determining second step originates from the surface anionic complex

$[Ni(III)O_m(OH)_{n+1}]^{p-}$ (p=2m+n-3) rather than from the bulk solution . An alternative pathway involving the cyclical formation and decomposition of an unstable Ni(IV) entity cannot be ruled out on the basis of the experimental data. However a change in the catalytic metal ion oxidation state is not suggested by the data obtained for Co and Fe electrodes, and thus in the greater scheme of things, the Ni(III) physisorbed peroxide pathway would seem to be the most consistent solution to the problem of mechanistic determination for the OER at passive oxide covered Ni anodes. Unlike the Ni(IV) path, the RDS for the Ni(III) scheme involves the desorption of a chemisorbed OH entity, which is consistent with the possibly applicable OER electrocatalytic theory of Bockris and Otagawa [169].

In general it is important to understand that , giving consideration to the acidic nature of hydrated oxide surfaces at high pH, is extremely useful in understanding the OER at transition metal surfaces in aqueous alkaline media. Since in general, the catalytic centres for oxygen evolution reside on the surface of an oxide phase in contact with aqueous solution, the surface region of the oxide will inevitably become somewhat hydrated. In view of this, it is our belief that all workers in this area should consider the amphoteric nature of their oxide surfaces, regardless of how the oxide phase was prepared. It is, for example, to take the case of a Ni anode in alkaline solution, more realistic to represent the OER active site as $[Ni(III)O_m(OH)_n]^{p-}$ (where extra hydroxide ions have been coordinated from solution, owing to the acidic nature of the oxide in electrolytes of high pH), rather than the traditional practice of considering it to be a discrete NiOOH entity.

The observation, under particular circumstances, of Tafel slopes of 45 – 48 mV dec^{-1} ($b \cong 2.303(4RT/3F)$ at 25ºC) or ca. 240 mV dec^{-1} ($b \cong 2.303(4RT/F)$ at 25ºC) for passive oxide covered Fe and Co electrodes has been explained in terms of the existance of a second potential barrier, related to the field driven migration of charge carriers across the oxide layer, in series with the normal electrochemical charge transfer barrier at the oxide surface/solution interface. This model was devised many years ago – the new contribution provided by Lyons and Brandon [198] has been to identify the "barrier layer" with the inner compact anhydrous region of the passive oxide film.

Finally, normalisation of experimental $i(\eta)$ characteristics to estimated electrode active surface areas revealed an activity series for the OER (in terms of decreasing activity in the lower Tafel slope region of potential) of Ni > Co > Fe. As discussed in the previous section, this observation aligned with the fact that we envisage the RDS for all electrodes studied to involve the desorption of an OH entity, suggests that our experimental data conforms to the electrocatalytic theory of the OER devised by Bockris and Otagawa [47]. However we envisage that the central metal ion of the electrocatalytically active surface complexes exist in the Ni(III), Co(IV) and Fe(VI) valance states for oxidised Ni, Co and Fe anodes respectively, and not in a common oxidation state as was proposed by Bockris for perovskite electrodes based on these (and other first row transition metal) elements. In view of this, it is our conclusion that while the relatively simple model of Bockris and Otagawa [169] captures the essence of the dependence of OER activity on the transition metal of the anode oxide material, a further layer of sophistication is required to account for the fact that the oxidation state of the active metal ion probably varies from the oxide

of one element to another (within the same periodic table row).

ACKNOWLEDGEMENT
The Physical and Materials Electrochemistry Group TCD is grateful for the financial support of Enterprise Ireland Grant Number SC/2003/0049, IRCSET Grant Number SC/2002/0169 and the HEA-PRTLI Program. This publication has emanated in part from research conducted with the financial support of Science Foundation Ireland (SFI) under Grant Number SFI/10/IN.1/I2969.

References

1. G.W. Crabtree, M.S. Dresselhaus, M.V. Buchanan, *Physics Today*, December 2004, pp.39-44.
2. (a)K.Zeng, D. Zhang, *Prog. Ener., Comb. Sci.*, 36 (2010) 307. (b) H. Tributsch, *Int. J. Hyd. Ener.*, 33 (2008) 5911.
3. (a) S. Wasmus, A. Kuver, *J. Electroanal. Chem.*, 461(1999) 14-31. (b) D.P. Wilkinson, *J. Power Sources*, 155 (2006) 95-110. (c) V. Mehta, J. Smith Cooper, *J. Power Sources*, 114 (2003) 32-53.
4. M. Gattrell and B. MacDougall, in *Handbook of Fuel Cells- Fundamentals, Technology and Applications*, W. Vielsch, H.A. Gasteiger, A. Lamm (Eds), Vol.2 Electrocatalysis, Chapter 30, pp.443-464, Wiley, (2003).
5. The classic reference for early work in oxygen electrochemistry is: (a) J.P. Hoare, *The Electrochemistry of Oxygen*, Wiley Interscience, New York , 1968 ; (b) idem, in *Adv. Electrochem. Electrochem. Eng.*, P. Delehay (Ed), Vol.6, p.201, Wiley Interscience, New York, (1967).
6. K. Kinoshita, *Electrochemical Oxygen Technology*, Wiley, New York, 1992.
7. M.R. Tarasevich, A. Sadkowski and E. Yeager, Oxygen Electrochemistry, in *Comprehensive Treatise of Electrochemistry*, B.E. Conway, J.O'M. Bockris, E. Yeager, S.U.M. Khan and R.E. White (Eds), Plenum Press, New York, Vol.7, 1983, pp.301-398.
8. A.Damjanovic, Mechanistic analysis of oxygen electrode reactions, in *Modern Aspects of Electrochemistry*, B.E. Conway, J.O'M. Bockris (Eds.), Plenum Press, New York, Vol.5, 1969, Chapter 5, pp.369-483.
9. A.J. Appleby, *J. Electroanal. Chem.*,357 (1993) 117.
10. M.E.G. Lyons, S. Rebouillat, *Int. J. Electrochem. Sci.*, 4 (2009) 481.
11. (a)B.E. Conway, *J. Electroanal. Chem.*, 524/525 (2002) 4.
12. (a) H. Nagucki, T. Ohada, K. Uosaki, *Faraday Discuss*, 140 (2009)125. (b) C.A. Lucas, M. Cormack, M.E. Gallagher, A.Brownrigg, P. Thompson, B. Fowler, Y. Grunder, J. Roy,Y. Stamenkovi, N.M. Markovic, *Faraday Discuss.*, 140 (2009) 41.
13. M.T.M. Koper, *J. Electroanal. Chem.*, 574 (2001) 375. (b) M.T.M. Koper, *Faraday Discuss.*, 140 (2009) 11.
14. J.K. Norskov, J. Rossmeisl, L. Lindqvist, J.R. Kitchin, T. Bligaard, H. Jonsson, *J. Phys. Chem.B.*, 108 (2004) 17886.
15. J. Rossmeisl, A. Logadottir, J.K. Norskov, *Chem. Phys.*, 319 (2005) 178.
16. J. Rossmeisl, Z-W. Qu, H. Zhu, G-J. Kroes, J.K. Norskov, *J. Electroanal. Chem.*, 607 (2007) 83.
17. (a) M.E.G. Lyons, L.D. Burke, *J. Chem. Soc., Faraday Trans. I*, 83 (1987) 299; (b) M.E.G. Lyons, S. Floquet, *Phys.Chem. Chem. Phys.*, 13 (2011) 5314.
18. K. Kinoshita, *Electrochemical Oxygen Technology*, Wiley-Interscience, New York, 1992, chapter 2, pp. 78-99.
19. A.C.C. Tseung, S. Jasem, *Electrochim. Acta*., 22 (1977) 31.
20. (a) S.I. Cordorba, R.B. Carbonio, M. Lopez Teijelo, V.A. Macagno, *Electrochem. Acta*, 32 (1987) 749-755. (b) Y. Zhang, X. Cao, H. Yuan, W. Zhang, Z. Zhou, *Int. J. Hydrogen Energy*, 24 (1999)

529-536. (c) X. Wang, H. Luo, D.R. Zhou, H. Yang, P.J. Sebastian, S.A. Gamboa, *Int. J. Hydrogen Energy*, 29 (2004) 967-972.
21. (a) C. Iwakura, A. Honji, H. Tamura, *Electrochim. Acta*, 26 (1981) 1319-1326. (b) P. Rasiyah, A.C.C. Tseung, *J. Electrochem. Soc.,* 130 (1983) 365-368. (c) E.B. Castro, C.A. Gervasi, J.R. Vilche, *J. Appl. Electrochem.*, 28 (1998) 835-841. (d) S. Palmas, F. Ferrara, A. Vacca, M. Mascia, A.M. Polcaro, *Electrochim. Acta*, 53 (2007) 400-408.
22. (a) C.R. Davidson, G. Kissel, S. Srinivasan, *J. Electroanal. Chem*. 132 (1982) 129-135. (b) P. Rasiyah, A.C.C. Tseung, *J. Electrochem. Soc*.130 (1983) 2384-2386. (c) S. K. Tiwari, S. Samuel, R. N. Singh, G. Poillerat, J. F. Koenig, P. Chartiers, *Int. J. Hydrogen Energy* 20 (1995) 9-15. (d) C. Bocca, A. Barbucci, M. Delucchi, G. Cerisola, *Int. J. Hydrogen Energy* 24 (1999) 21-26.
23. (a) J.P Singh, N.K. Singh, R.N. Singh, *Int. J. Hydrogen Energy* 24 (1999) 433-439. (b) R.N. Singh, J.P.Singh, B.Lal, M.J.K. Thomas, S Bera, *Electrochim. Acta*, 51 (2006) 5515-5523.
24. (a) Y. Matsumoto, S. Yamada, T. Hishida, E. Sato, *J. Electrochem. Soc.* 127 (1980) 2360-2364. (b) J. O'M. Bockris, T. Otagawa, *J.Phys. Chem.* 87 (1983) 2960-2971. (c) C. Bocca, G. Cerisola, E. Magnone, A. Barbucci, *Int. J. Hydrogen Energy* 24 (1999) 699-707. (d) R.N. Singh, B. Lal, *Int. J. Hydrogen Energy* 27 (2002) 45-55.
25. (a) T. Kessler, J.R. Vilche, M. Ebert, K. Jüttner, W.J. Lorenz, *Chem. Eng. Technol.* 14 (1991) 263-269. (b) K.K. Lian, D.W. Kirk, S.J. Thorpe, *J. Electrochem. Soc.* 142 (1995) 3704-3712. (c) A.M. Fundo, L.M. Abrantes, *Russian J. Electrochem*. 42(2006) 1291-1297.
26. L.D. Burke, M.E.G. Lyons, *Mod. Asp. Electrochem*., 18 (1986) 169-248.
27. (a) A. Daghetti, G. Lodi, S. Trasatti, *Mater. Chem. Phys*., 8 (1983)1-90. (b) S. Trasatti, *Electrochim Acta.*, 36 (1991) 225.
28. R.J. Hunter, *Foundations of Colloid Science*, 2nd edition, Oxford University Press, 2005, Ch7 & Ch8, pp.305-434.
29. (a) S.D. James, *J. Electrochem. Soc.*, 116 (1969) 1681. (b) J. Balej, O. Spalek, *Coll. Czech. Chem. Commun*., 37 (1972) 499. (c) S. Shibita, *J. Electroanal. Chem*., 89 (1978) 37.
30. (a) L.D. Burke, M. McRann, *J. Electroanal. Chem.*, 125 (1981) 387.
31. (a) D.N. Buckley, L.D. Burke, *J. Chem. Soc. Faraday Trans. I.*, 71 (1975) 1447. (b) D.N. Buckley, L.D. Burke, J.K. Mulcahy, *J. Chem. Soc. Faraday Trans. I.*, 72 (1976) 1896.
32. D.F. Pickett, J.T. Malloy, *J. Electrochem. Soc.*, 125 (1978) 1026.
33. G.W. Nichols, *Trans. Electrochem. Soc.*, 62 (1932) 393.
34. (a) M. Winter, R.J. Brodd, *Chem. Rev*., 104 (2004) 4245 ; (b) A. Burke, *J. Power Sources*, 91 (2000) 37 ; (c) J.W. Long, B. Dunn, D.R. Rollison, H.S. White, *Chem. Rev*., 104 (2004) 4463.
35. (a) J. Jiang, A. Kucernak, *Electrochem. Acta*, 47 (2002) 2381 ; (b) S.C. Pang, M.A. Anderson, T.W. Chapman, *J. Electrochem. Soc.*, 147 (2000) 444. (c) O. Haas, E.J. Cairns, *Annu. Rep. Prog. Chem., Sect. C.*, 95 (1999) 163 ; (d) R. Kotz, M. Carlen, *Electrochim. Acta*, 45 (2000) 2483 ; (e) M. Jayalakshmi, K. Balasubramanian, *Int. J. Electrochem. Sci.*, 3 (2008) 1196.
36. (a) L.D. Burke, M.E.G. Lyons, *J. Electroanal. Chem.*, 198 (1986) 347. (b) L.D. Burke, E.J.M. O'Sullivan, *J. Electroanal. Chem*., 93 (1978) 11.
37. P.G. Pickup, V.I. Birss, *J.Electroanal. Chem*., 220 (1987) 83.
38. S.D. James, *J. Electrochem. Soc.*, 116 (1969) 1681.
39. J.W. Schultze, K.H. Vetter, *Electrochim. Acta*, 18 (1973) 889.
40. W.M. Sachtler, L.L.V. Reizen, *J. Res. Inst. Catal., Hokkaido Univ.*, 10 (1962) 87.
41. R. Woods in *Electroanal. Chem*., Vol. 9, Ed. A.J. Bard, Marcel Dekker, New York, 1976, Ch. 1.
42. L.D.Burke, E.J.M. O'Sullivan, *J. Electroanal. Chem.*, 117 (1981) 155.
43. L.D.Burke, J.K. Mulcahy, *J. Electroanal. Chem.*, 73 (1976) 207.
44. L.D.Burke, M.B.C.Roche, *J. Electroanal. Chem.*, 164 (1984) 315.
45. L.D.Burke, M.M. McCarthy, M.B.C.Roche, *J. Electroanal. Chem*., 167 (1984) 291.

46. M.P. Brandon, *Electrochemical Studies of the Oxygen Evolution Reaction at Passive Oxide Covered Ni, Co and Fe Electrodes in Aqueous Alkaline Solution*, Ph.D Thesis, University of Dublin, 2008.
47. (a) L. Ojefors, *J. Electrochem. Soc.*, 123 (1976)1691. (b) D.D. MacDonald and D. Owen, *J. Electrochem. Soc.*, 120 (1973) 317. (c) H. Neugebauer, G. Nauer, N. Brinda-Konopik and G. Gidaly, *J. Electroanal. Chem*., 122 (1981) 381. (d) F. Beck, R. Kaus and M. Oberst, *Electrochim. Acta*, 30 (1985) 173.
48. (a) R.S.S. Guzman, J.R. Vilche and A.J. Arvia, *Electrochim. Acta*, 24 (1979) 395. (b) S. Juanto, R.S.S. Guzman, J.O. Zerbino, J.R. Vilche and A.J. Arvia, *Electrochim. Acta*, 36 (1991) 1143. (c) G. Larramona and C. Gutierrez, *J. Electrochem. Soc.*, 136 (1989) 2171. (d) R. Šimpraga and B.E. Conway, *J. Electroanal. Chem.*, 313 (1991) 161. (e) S.T. Amaral, E.M.A. Martini and I.L. Muller, *Corros. Sci.*, **43 (**2001) 853. (f) S. Joiret, M. Keddam, X.R. Novoa, M.C. Perez, C. Rangel and H. Takenouti, *Cement & Concrete Composites*, 24 (2002) 7.
49. M.E.G. Lyons, M.P. Brandon, *Phys. Chem. Chem. Phys*., 11 (2009) 2203.
50. P.W. Schindler in Adsorption of Inorganics at Solid-Liquid Interfaces, M.A. Anderson and A.J. Rubin, Eds., Ann Arbor Science Publishers, Michigan, USA, 1981, Ch.1.
51. (a) J.O'M. Bockris, M. Genshaw, V. Brusic, *Symp. Faraday Soc.*, 4 (1970) 177. (b) J.O'M. Bockris, V. Brusic, H. Wroblowa, *Electrochim Acta*., 16 (1971) 1859. (c) H. Wroblowa, V. Brusic, J.O'M. Bockris, *J. Phys. Chem*., 75 (1971) 2823.
52. (a) R.D. Armstrong, I. Baurhoo, *J. Electroanal. Chem*., 34 (1972) 41. (b) R.D. Armstrong, I. Baurhoo, *J. Electroanal. Chem.*, 40 (1972) 325.
53. M.E.G.Lyons, *The Electrochemical Behaviour of some Hydrous and Thermally Prepared Transition Metal Oxides*, Ph.D Thesis, University College, Cork, 1983.
54. B. Kabinov, R. Burstein, A.N. Frumkin, *Disc. Faraday Soc*., 1 (1947) 259.
55. L.D. Burke and D.P. Whelan, *J. Electroanal. Chem.*, 162 (1984) 121.
56. (a) J. Bisquert, G. Garcia Belmonte, F. Fabregat Santiago, N.S. Ferriols, M. Yamashita, E.C. Pereira, *Electrochem. Commun.*, 2 (2000) 601. (b) A.J. Terezo, J. Bisquert, E.C. Pereira, G. Garcia-Belmonte, *J. Electroanal. Chem*., 508 (2001) 59.
57. (a) S. Sunde, I.A. Lervik, M. Tsypkin, L.E. Owe, *Electrochim. Acta*, 55 (2010) 7751. (b) L. Sziraki, L. Bobics, *Electrochim. Acta*, 47 (2002) 2189.
58. M.E.G. Lyons, *Electroactive Polymer Electrochemistry*, Plenum Press, New York, 1994, Chapter 2, pp.102-103.
59. N. Oyama, T. Ohsaka, *Prog. Polym. Sci.*, 20 (1995) 761.
60. (a) R. Etchenique, E.J. Calvo, *J. Electrochem. Soc.*, 148 (2001) A361.
61. (a) H.M. French, M.J. Henderson, A.R. Hillman, E. Vieil, *J. Electroanal. Chem.*, 500 (2001) 192. (b) M. Gonsalves, A.R. Hillman, *J. Electroanal. Chem*., 454 (1998) 183.
62. B.S.H. Royce, D. Voss, A. Bocarsly, *J. Phys. Chem*., 88 (1983) 325.
63. (a) J. Pawlisyzn, M.F. Weber, M.J. Dignam, A. Mandelis, R.D. Venter, S.M. Park, *Anal. Chem*., 58 (1986) 236, 239. (b) J. Pawlisyzn, *Anal. Chem*., 60 (1988) 1751.
64. R.E. Russo, D.R. McLarnon, J.D. Spear, E.J. Cairns, *J. Electrochem. Soc.*, 134 (1987) 2783.
65. A.Mandelis, B.S.H. Royce, *Appl. Opt*., 23 (1984) 2892.
66. C.A. Barbero, M.C. Miras, *J. Arg. Chem. Soc.*, 91 (2003) 1.
67. (a) G. Tremiliosi-Filho, L.H. Dall'Antonia, G. Jerkiewicz, *J. Electroanal. Chem*., 578 (2005) 1. (b) M. Tian, W.G. Pell, B.E. Conway, *Electrochim Acta*, 48 (2003) 2675. (c) G. Tremiliosi-Filho, L.H. Dall'Antonia, G. Jerkiewicz, *J. Electroanal. Chem*., 422 (1997) 149.
68. (a) M. Keddam, N. Portail, D. Trinh, V. Vivier, *ChemPhysChem*., 10 (2009) 3175. (b) G. Garcia, M.M. Bruno, G.A. Planes, J.L. Rodriguez, C.A. Barbero, E. Pastor, *Phys. Chem. Chem. Phys.*, 10 (2008) 6677.
69. R. Kotz, C. Barbero and O. Haas, *J. Electroanal. Chem*., 296 (1990) 37.
70. L.D. Burke, O.J. Murphy, *J. Electroanal. Chem.*, 109 (1980) 373.

71. D.E. Hall, *J. Electrochem. Soc.*, 130 (1983) 317.
72. J. McBreen, in *Handbook of Battery Materials*, J.O. Besenhard (Ed), Wiley-VCH, Weinheim, 2007, Chapter 6, pp.135-151.
73. A.Seghiouer, J. Chevalet, A. Barhoun., F. Lantelme, J. *Electroanal. Chem.* 442 (1998) 113.
74. (a) L.D. Burke, T.A.M. Twomey, *J. Electroanal. Chem.*, 162 (1984) 101. (b) L.D. Burke, T.A.M. Twomey, *J. Electroanal. Chem*., 167 (1984) 285.
75. W. Visscher, E. Barendrecht, *J. Appl. Electrochem.*, 10 (1980) 269.
76. L.M.M. de Souza, F.P. Kong, F.R. McLarnon, R.H. Muller, *Electrochim. Acta.*, 42 (1997) 1253.
77. R. Simpraga, B.E. Conway, *J. Electroanal. Chem*., 280 (1990) 341.
78. A.C. Makrides, *J. Electrochem. Soc.*, 113 (1966) 1158.
79. M. Okuyama, S. Haruyama, *Corros. Sci.*, 14 (1974) 1.
80. M.R. Gennero De Chialvo, A.C. Chialvo, *Electrochim. Acta*., 33 (1988) 825.
81. H. Bode, K. Dehmelt, J. Witte, *Electrochim. Acta*,11 (1966) 1079.
82. M. Wehrens-Dijksma, P.H.L. Notten, *Electrochim. Acta.*, 51 (2006) 3609.
83. R. Barnard, C.F. Randell, F.L. Tye, *J. Appl. Electrochem*., 10 (1980) 109.
84. S. Le Bihan, M. Figlarz, *J. Cryst. Growth*, 13/14 (1972) 458.
85. B. Mani, J.P. de Neufville, *J. Electrochem. Soc.*, 135 (1988) 801.
86. M.J. Madou, M.C.H. McKubre, *J. Electrochem. Soc.*, 130 (1983) 1056.
87. P.C. Milner, U.B. Thomas, *Adv. Electrochem. Electrochem.* Eng., C.W. Tobias, Ed., Wiley Interscience, New York, 1967, Vol. 5, Chapter 1.
88. H. Gerisher, *Physical Chemistry – An Advanced Treatise*, Vol. IX A, H. Eyring, D. Henderson, W. Jost, Eds., Academic Press, New York, 1970, Chapter 5.
89. C. Greaves, M.A. Thomas, *Acta Cryst*., B42 (1986) 51.
90. F.P. Kober, *J. Electrochem. Soc.*, 112 (1965) 1064
91. M.S. Kim, T.S. Hwang, K.B. Kim, *J. Electrochem. Soc.*, 144 (1997) 1537.
92. F.P. Kober, *J. Electrochem. Soc.*, 114 (1967) 215.
93. M.K. Carpenter, D.A. Corrigan, *Electrochem. Soc. Abstracts*, Atlanta Meeting, 1988, Abstract 490, p.700.
94. S.A. Aleshkevich, E.I. Golovchenko, V.P. Morozov, L.N. Sagoyan, *Sov. Electrochem*., 4 (1968) 530, 1117.
95. T. C. Liu, W.G. Pell, B.E. Conway, *Electrochim. Acta*, 44 (1999) 2829.
96. N. Sac-Epee, M.R. Palacin, A. Delahaye-Vidal, Y. Chabre, J.M. Tarascon, *J. Electrochem. Soc.*, 145 (1998) 1434.
97. G.W.D. Briggs, *Specialist Periodical Reports : Electrochemistry*, Chemical Society, London, 1974, Volume 4, Chapter 3.
98. M. Pourbaix, *Atlas of electrochemical equilibria in aqueous solutions*, Pergamon Press, London, 1965.
99. D.C. Silverman, *Corrosion*, 37 (1981) 546.
100. P.L. Bourgault, B.E. Conway, *Can. J. Chem*., 38 (1960) 1557.
101. P.L. Bourgault, B.E. Conway, *Can. J. Chem*., 40 (1962) 1690.
102. B.E.Conway, P.L. Bourgault, *Trans. Faraday Soc.*, 58 (1962) 593.
103. B.E.Conway, E. Gileadi, *Can. J. Chem.*, 40 (1962) 1933.
104. R. Barnard, C.F. Randell, F.L. Tye, *J. Electroanal. Chem*., 119 (1981) 17.
105. P. Bernard, C. Gabrielli, M. Keddam, H. Takenouti, J. Leonardi, P. Blanchard, *Electrochim. Acta*, 36 (1991) 743.
106. G.T. Cheek, W.E. O'Grady, *J. Electroanal. Chem.*, 421 (1997) 173.
107. G. Feuillade, R. Jacoud, *Electrochim. Acta*, 14 (1969) 1297.
108. N. Sac-Epee, M.R. Palacin, B. Beaudoin, A. Delahaye-Vidal, T. Jamin, Y. Chabre, J.M. Tarascon, *J. Electrochem. Soc.*, 144 (1997) 3896.
109. V. Srinivasan, B.C. Cornilsen, J.W. Weidner, *J. Solid State Electrochem.*, 9 (2005) 61.

110. (a) B.C. Cornilsen, P.J. Karjala, P.L. Loyselle, *J. Power Sources*, 22 (1988) 351. (b) B.C. Cornilsen, X. Shan, P.L. Loyselle, *J. Power Sources*, 29 (1990) 453.
111. M. Butel, L. Gautier, C. Delmas, *Solid State Ionics*, 122 (1999) 271.
112. P. Benson, G.W.D. Briggs, W.F.K. Wynne-Jones, *Electrochim. Acta*., 9 (1964) 275.
113. W.K. Behl, J.E. Toni, *J. Electroanal. Chem*., 31 (1971) 63.
114. D. Erts, E. Ahlberg, J. Asbjornsson, H. Olin, J. Prikulis, *J. Appl. Phys*., A66 (1998) S477.
115. T. Ohtsuka, N. Sato, J. Electroanal. Chem., 147 (1983) 167.
116. K.E. Heusler in *Passivity of Metals*, R.P. Frankenthal, J. Kruger, Eds., Electrochem. Soc., Princeton NJ, 1978, p.771.
117. A.Foelske, H.H. Strehblow, *Surf. Interface Anal.,* 34 (2002) 125.
118. R.P. Simpraga, *J. Electroanal. Chem.*,355 (1993) 79.
119. A.Bewick, C. Gutierrez, G. Larramora, *J. Electroanal. Chem.*, 333 (1992) 165.
120. G.W. Simmons, in *Passivity of Metals*, R.P. Frankenthal and J. Kruger, Eds., Electrochem. Soc., Princeton, NJ., 1978, p.899.
121. R.Simpraga, B.E. Conway, *J. Electroanal. Chem.*, 313 (1991) 161.
122. R. Simpraga, B.E. Conway, *J. Electroanal. Chem.*, 280 (1990) 341.
123. T.C. Liu, W.G. Pell, B.E. Conway, *Electrochim. Acta*., 44 (1999) 2829.
124. H. Gomez Meier, J.R. Vilche, A.J. Arvia, *J. Electroanal. Chem.*, 138 (1982) 367.
125. L.D. Burke, M.E.G. Lyons, O.J. Murphy, *J. Electroanal. Chem*., 132 (1982) 247.
126. L.D. Burke, M.M. Murphy, *J. Electrochem. Soc.*, 138 (1991) 88.
127. A.Laisa in *Handbook of Fuel Cells, Fundamentals, Technology and Applications*, Vol. 2, Electrocatalysis. W. Vielstich, A. Lamm, H.A. Gasteiger (Eds), Wiley, Chichester, 2003, Chapter 29, pp.
128. J.O'M. Bockris, S.U.M. Khan, *Surface Electrochemistry*, Plenum Press, New York, 1993, Section 3.23, pp. 319-349.
129. H. Wroblowa, M.L.B. Rao, A. Damjanovic, J.O'M. Bockris, *J. Electroanal. Chem.*, 15 (1967) 139.
130. J.O'M. Bockris, L.E. Oldfield, *Trans. Faraday Soc.*, 51 (1955) 249.
131. J.Z. Giner, *Z. Electrochem*., 63 (1959) 386.
132. J.O'M. Bockris, A.M.K.S. Huq, *Proc. Roy. Soc*., 273A (1956) 1733.
133. R. Parsons, *Trans. Faraday Soc.*, 47 (1951) 1332.
134. J.O'M. Bockris, S.U.M. Khan, *Surface Electrochemistry*, Plenum Press, New York, 1993, Section 3.5, pp. 218-223.
135. (a) A. Damjanovic, A. Dey, J.O'M. Bockris, *Electrochim. Acta*., 11 (1966) 791. (b) A. Damjanovic, M.A. Genshaw, J.O'M. Bockris, *J. Electrochem. Soc.*, 114 (1967) 466.
136. A.Damjanovic, in *Electrochemistry in Transition*, O.J. Murphy, S. Srinivasan, B.E. Conway, Eds., Plenum Press, New York, 1992, p.107.
137. K. Kinoshita, *Electrochemical Oxygen Technology*, Wiley, New York, 1992, Chapter 2.
138. M. Gattrell, B. McDougall, in *Handbook of Fuel Cells, Fundamentals Technology and Applications, Vol.2, Electrocatalysis*, W. Vielstich, A. Lamm, H.A. Gasteiger, Eds., John Wiley & Sons, Chichester, 2003, Chapter 30, pp.446-452.
139. A.J. Appleby, *J. Electroanal. Chem.*, 357 (1993) 117.
140. V.S. Bagotskii, L.N. Nekrasov, N.A. Shumilova, *Russ. Chem. Rev*., 34(10) (1965) 717.
141. A. Damjanovic, M.A. Genshaw, J.O'M. Bockris, *J. Chem. Phys.*, 45 (1966) 4057.
142. H.S. Wroblowa, Y.C. Pan, G. Razumney, *J. Electroanal. Chem.*, 69 (1976) 195.
143. A.J. Appleby, M. Savy, *J. Electroanal. Chem.*, 92 (1978) 15.
144. (a) V. Vesovic, N. Anastasijevic, R.R. Adzic, *J. Electroanal. Chem.*, 218 (1987) 53. (b) N.A. Anastasijevic, V. Vesovic, R.R. Adzic, *J. Electroanal. Chem*., 229 (1987) 305, 317.

145. (a) V.S. Bagotskii, V. Yu. Filinovskii, N.A. Shumilova, *Elektrokhimiya*, 4 (1968) 1129 ; (b) V.S. Bagotskii, M.R. Tarasevich, V. Yu. Filinovskii, *Elektrokhimiya*, 5 (1969) 1218 ; (c) M.R. Tarasevich, *Elektrokhimiya*, 4 (1968) 182.
146. F. Van der Brink, E. Barendrecht, W. Visscher, *J. Electrochem. Soc.*, 127 (1980) 2003.
147. P. Fischer, J. Heitbaum, *J. Electroanal. Chem.*, 112 (1980) 231.
148. D.S. Gnanamuthu, J.V. Petrocelli, *J. Electrochem. Soc.*, 114 (1967) 1036.
149. K.C. Pillai, J.O'M. Bockris, *J. Electrochem. Soc.*, 131 (1984) 568.
150. B. Viswanathan, Ch. Venkateswara Rao, U.V. Varadaraju, *Photo/Electrochemistry and Photobiology in the Environment, Energy and Fuel*, Research Signpost, Kerala, India, 2006, 43-101.
151. B. Sljukic, C.E. Banks, R.G. Compton, *J. Iranian Chem. Soc*., 2 (2005) 1.
152. (a) K.Tammeveski, K. Kontturi, R.J. Nichols, R.J. Potter, D.J. Schiffrin, *J. Electroanal. Chem*., 515 (2001) 101. (b) A. Sarapuu, K. Vaik, D.J. Schiffrin, K. Tammeveski, *J. Electroanal. Chem.*, 541 (2003) 23. (c) G. Jurmann, D.J. Schiffrin, K. Tammeveski, *Electrochim. Acta*, 53 (2007) 390. (d) S. Cere, M. Vazquez, S.R. de Sanchez, D.J. Schiffrin, *J. Electroanal. Chem.*, 505 (2001) 118.
153. C.E. Banks, G.G. Wildgoose, C.G.R. Heald, R.G. Compton, *J. Iranian Chem. Soc.*, 2 (2005) 60.
154. (a) F. Wang, S. Hu, *J. Electroanal. Chem.*, 580 (2005) 68.
155. (a) J. Xu, W. Huang, R.L. McCreery, *J. Electroanal. Chem.*, 410 (1996) 235. (b) H.H. Yang, R.L. McCreery, *J. Electrochem. Soc.*, 147 (2000) 3420. (c) J. Xu, W. Huang, R.L. McCreery, *J. Electroanal. Chem.*, 410 (1996) 235.
156. S.Maldonado, K.J. Stevenson, *J. Phys. Chem.B.*, 109 (2005) 4707.
157. K. Gong, F. Du, Z. Xia, M. Durstock, L. Dai, *Science*, 323 (2009) 760.
158. C.C. Chang, T.C. Wen, *Electrochim. Acta*, 52 (2006) 623.
159. P. Ruetschi, P. Delehay, *J. Chem. Phys.*, 23 (1955) 556.
160. A.C.C. Tseung, S. Jasem, *Electrochim. Acta*., 22 (1977) 31.
161. M.H. Miles, Y.H. Huang, S. Srinivasan, *J. Electrochem. Soc.*, 125 (1978) 1931.
162. S. Trasatti, G. Lodi, in *Electrodes of Conductive Metallic Oxides, Part B*, S. Trasatti Ed., Elsevier, New York, 1981, p.521.
163. L.D.Burke, D.P. Whelan, *J. Electroanal. Chem.*, 103 (1979) 179.
164. D.E. Hall, *J. Electrochem. Soc.*, 130 (1983) 317.
165. J.O'M. Bockris, *J. Chem. Phys*., 24 (1956)817.
166. C.A. Christiansen, *Z. Physik Chem.*, B33 (1936) 145. B37 (1937) 374.
167. B.E.Conway, E. Gileadi, *Trans. Faraday Soc*., 58 (1962) 2493.
168. P.L. Bourgault, B.E. Conway, *Can. J. Chem.*, 40 (1962) 1690.
169. (a) J.O'M. Bockris, T. Otagawa, *J. Phys. Chem*., 87 (1983) 2960. (b) J.O'M.Bockris, T. Otagawa, *J. Electrochem. Soc*., 131 (1984) 290.
170. A.I. Krasil'shchikov, *Zh. Fiz. Khim.*, 37(1963) 531.
171. T.P. Hoare, *Proc. 8th Meeting CITCE*, Madrid, 1956, Butterworths, London, 1958, p.439.
172. V.I. Birss, A. Damjanovic, *J. Electrochem. Soc*., 134 (1987) 113.
173. C. Iwakura, K. Fukuda, H. Tamura, *Electrochim. Acta*., 21 (1976) 501.
174. V.I. Birss, A. Damjanovic, P.G. Hudson, *J. Electrochem. Soc*., 133 (1986) 1621.
175. A.C. Ferreira, E.R. Gonzalez, E.A. Ticianelli, L.A. Avaca, B. Matvienko, *J. Appl. Electrochem.*, 18 (1988) 894.
176. P.W.T. Lu, S. Srinivasan, *J. Electrochem. Soc.*, 125 (1978) 1416.
177. L.D. Burke, M.E.G. Lyons, O.J. Murphy, *J. Electroanal. Chem*., 132 (1982) 247.
178. M.E.G. Lyons, L.D. Burke, *J. Electroanal. Chem.*, 170 (1984) 377.
179. S. Joiret, M. Keddam, X.R. Nova, M.C. Perez, C. Rangel, H. Takenouti, *Cement & Concrete Composites*, 24 (2002) 7.

180. S. Gottesfeld, S. Srinivasan, *J. Electroanal. Chem.*, 86 (1978) 89.
181. Y. Matsumoto, H. Manabe, E. Sato, *J. Electrochem. Soc.*, 127 (1980) 811.
182. Y. Matsumoto, S. Yamada, T. Nishida, E. Sato, *J. Electrochem. Soc.*, 127 (1980) 2360.
183. G. Wu, N. Li, D.R. Zhou, K. Mitsuo, B.Q. Xu, *J. Solid State Chem.*, 177 (2004) 3682.
184. X. Wang, H. Luo, H. Yang, P.J. Sebastian, S.A. Gamboa, *Int. J. Hyd. Energy.*, 29 (2004) 967.
185. Y. Zhang, X. Coa, H. Yuan, W. Zhang, Z. Zhou, *Int. J. Hyd. Energy.*, 24 (1999) 529.
186. A.Damjanovic, A. Dey, J.O'M. Bockris, *J. Electrochem. Soc.*, 113 (1966) 739.
187. N. Sato, G. Okamoto, *Electrochim. Acta.*, 10 (1965) 495.
188. P. Rasiyah, A.C.C. Tseung, D.B. Hybbert, *J. Electrochem. Soc.*, 129 (1982) 1724.
189. P. Rasiyah, A.C.C. Tseung, *J. Electrochem. Soc.*, 130 (1983) 2384.
190. H. Willems, A.G.C. Kobussen, J.H.W. De Wit and G.H.J. Broers, *J. Electroanal. Chem*, 170(1984) 227.
191. R.F. Scarr, *J. Electrochem. Soc.*, 116(1969) 1526.
192. K.I. Rozental, V.F. Vesolovskii, *Doklady Akad. Nauk. SSSR*, 111 (1956) 637.
193. R.N. Singh, J.F. Koenig, G. Poillerat, P. Chartier, *J. Appl. Electrochem.*, 20 (1990) 442.
194. R.N. Singh, J.F. Koenig, G. Poillerat, P. Chartier, *J. Electrochem. Soc.*, 137 (1990) 1408.
195. S.K. Tiwari, S. Samuel, R.N. Singh, G. Poillerat, J.F. Koenig, P. Chartier, *Int. J. Hyd. Energy*, 20 (1994) 9.
196. W. O'Grady, C. Iwakura, J. Huang, E. Yeager, in *Proceedings of the Symposium on Electrocatalysis*, M.W. Breiter, Ed., The Electrochemical Society, Pennington NJ, 1974, p.286.
197. E.J.M. O'Sullivan, L.D. Burke, *J. Electrochem. Soc.*, 137 (1990) 466.
198. M.E.G. Lyons, M.P. Brandon, *J. Electroanal. Chem.*, 641 (2010) 119.
199. M.E.G. Lyons, M.P. Brandon, *J. Electroanal. Chem.*, 631 (2009) 62.
200. M.E.G. Lyons, M.P. Brandon, *Int. J. Electrochem. Sci.*, 3 (2008) 1386.
201. M.E.G. Lyons, M.P. Brandon, *Int. J. Electrochem. Sci.*, 3 (2008) 1425.
202. M.E.G. Lyons, M.P. Brandon, *Int. J. Electrochem. Sci.*, 3 (2008) 1463.
203. J. Willsau, O. Wolter, J. Heitbaum, *J. Electroanal. Chem.*195 (1985) 299.
204. L.D. Burke, M.E.G. Lyons, D.P. Whelan, *J. Electroanal. Chem.*, 139 (1982) 131.
205. L.D. Burke, M.E. Lyons, E.J.M. O'Sullivan, D.P. Whelan, *J. Electroanal. Chem.*, 122 (1981) 403.
206. N. Sato, *Electrochemistry at Metal and Semiconductor Electrodes*, Elsevier, 1998, pp181-184.
207. L.D. Burke, M.M. Murphy, *J. Electrochem. Soc.*, 138 (1991) 88.
208. J.J. McDonald, B.E. Conway, *Proc. Roy. Soc.,London, Ser.A.*, 269 (1962) 419.
209. R.E. Meyer, *J. Electrochem. Soc.*, 107 (1960) 847.
210. B.E. Conway, L. Bai and M.A. Satter, *Int. J. Hydrogen Energy*, 12(1987) 607.
211. S Trasatti in *Handbook of Fuel Cells, Fundamentals Technology and Applications, Vol 2, Electrocatalysis*, W. Vielstich, A. Lamm and H.A. Gasteiger, Eds., John Wiley and Sons, Chichester, 2003, chapter 10.